Numerical modeling of the long-term poromechanical performance of deep geothermal energy systems

Saeed Vadiee

A Thesis

In

The Department

Of

Building, Civil, and Environmental Engineering

Presented in Partial Fulfillment of the Requirements

For the Degree of Master of Applied Science (Civil Engineering) at

Concordia University

Montréal, Québec, Canada

March 2025

© Saeed Vadiee, 2025

CONCORDIA UNIVERSITY

SCHOOL OF GRADUATE STUDIES

This is to certify that the thesis prepared

By: Saeed Vadiee

Entitled: Numerical modeling of the long-term poromechanical performance of deep geothermal energy systems

and submitted in partial fulfillment of the requirements for the degree of

Master of Applied Science (Civil Engineering)

complies with the regulations of the University and meets the accepted standards with respect to originality and quality.

Signed by the final Examining Committee:

_____ Chair

Dr. Adel Hanna

_____ Examiner

Dr. Adel Hanna

_____ Examiner

Dr. Ayhan Ince

_____ Thesis Supervisor

Dr. Biao Li

Approved by

_____

Dr. P.H. Chen Graduate Program Director

_____

Dr. Mourad Debbabi Dean of Faculty

Abstract

Numerical modeling of the long-term poromechanical performance of deep geothermal energy systems

Saeed Vadiee

In recent years, the technological development of carbon-free energy sources has gained increasing attention among communities. Among various clean energy sources, geothermal energy stands out as an environmentally friendly alternative that is not affected by weather fluctuations, like solar and wind energy, and does not generate harmful waste, unlike nuclear energy. Geothermal energy production involves extracting the naturally stored heat within the Earth's crust for direct use or electricity generation. This process requires drilling one or more boreholes into the targeted formation, where fluid is injected and circulated to extract heat from the subsurface.

A wide range of injection and production scenarios exist for geothermal energy systems. However, a common challenge across all scenarios is the need to accurately capture and understand geological structures, including faults, fractures, and other planes of weakness, and to quantify, both spatially and temporally, the dynamics of relevant physical processes and their interactions with the geological environment. Continuous fluid injection and production induce thermodynamic changes within the reservoir, leading to significant variations in pore pressure and temperature. These variations create local stress gradients in the porous rock, affecting reservoir performance. The transport properties of the porous medium, namely porosity and permeability, are highly sensitive to bulk and pore volume deformations, which can influence or even control overall reservoir productivity. Additionally, changes in stress conditions along geological discontinuities, such as fractures or faults, induced by geothermal operations, can compromise the mechanical stability of these structures. This may result in the propagation or closure of existing fractures or induce slip along fault planes, potentially leading to induced seismicity.

This study investigates the dynamics of pore pressure diffusion and thermal effects within a geothermal reservoir subjected to cold fluid injection. The incorporation of International Association for the Properties of Water and Steam (IAPWS) equations enables realistic simulations of heterogeneous pressure field distributions. The simulated system represents a doublet within a faulted zone, featuring two hydraulically stimulated fractures. The primary objective is to assess

the probability of fault reactivation under varying in-situ stress conditions over a 100-year geothermal injection and production period. The findings reveal that stress distribution patterns are primarily governed by thermal stresses along the fluid circulation pathway. Fluid velocity and temperature gradients significantly influence the reservoir's mechanical stability, while minimal pore pressure changes suggest that thermal stresses play a dominant role in fault behavior. The analysis indicates no potential for fault reactivation under various in-situ stress conditions, even over the anticipated production and injection period, as thermal effects continue to influence the surrounding rocks. Slip tendency values remain below the threshold for fault reactivation, considering the reduced mechanical properties defined by the Hoek-Brown failure criterion. These results suggest that the geothermal reservoir, subject to thermo-poromechanical effects, exhibits mechanical stability conducive to sustained injection and production activities.

Keywords: Fault reactivation potential, Deep geothermal Reservoir, Thermo-Hydro-Mechanical (THM) coupled analysis, finite element method

Acknowledgements

First and foremost, I would like to express my deepest gratitude to Allah for granting me health, resilience, and inspiration throughout my research journey. Allah has been the guiding light, filling my heart with strength and joy even during the darkest moments of this process.

I am profoundly grateful to my supervisor, Dr. Biao Li, for the opportunity to work on such pioneering research. His insight, dedication, and encouragement provided me with the necessary tools and motivation to conduct this study. This work would not have been possible without his invaluable guidance.

I would also like to thank all the current and former members of Prof. Biao Li's research team, Kian, Emad, Mohammad, and Sina. Their support and camaraderie helped foster a positive and collaborative environment, greatly enhancing my research experience. Their insights and shared knowledge have enriched this work in countless ways.

My sincere appreciation extends to Coreform for generously providing me with a two-year license for their Cubit meshing software, which played a key role in my research. I also acknowledge Compute Canada for access to their high-performance computing resources, which were instrumental in completing this project.

Finally, I would like to thank Concordia University for the funding support I received, which allowed me to focus fully on this research endeavor.

Table of contents

List of figures x

List of tables xii

Nomenclature xiii

List of symbols xiii

Abbreviations xiii

List of Roman Symbols xiii

List of Greek Symbols xiv

List of other Symbols xiv

List of Publications xv

1. Chapter 1: Introduction 1

1.1. Rationale 1

1.2. Objective 3

1.3. Major Goals and Questions Addressed in the Study 5

1.4. Workflow overview 5

1.5. Overview over the thesis 9

2. Chapter 2: Literature Review 11

2.1. Introduction 11

2.2. Overview on different geothermal systems 11

2.2.1. Open-Loop Systems 12

2.2.2. Closed-Loop Systems 13

2.2.3. Enhanced Geothermal Systems (EGS) 15

2.3. Working fluid 17

2.4. Numerical methods 18

2.4.1. Finite Element Method 19

2.4.2. Multiphysics Object-Oriented Simulation Environment (MOOSE) framework 19

2.5. Numerical Modeling of Heat Extraction in EGS: Well Configuration and Production Dynamics 21

2.6. Interactions among physical processes 23

2.6.1. Coupling among the different processes 23

2.6.2. Complexity of Porous Rocks and Fault Zones 27

2.7. Transport properties 27

2.8. Assessing fault reactivation potential 30

Preface to chapter 3 32

Geological setting and methodology 33

3. Chapter 3: Numerical modeling of the long-term poromechanical performance of a deep enhanced geothermal system in northern Québec 35

3.1. Abstract 35

3.2. Introduction 36

3.3. Mathematical formulation of Coupled THM processes in pressurized fractured geothermal reservoir 40

3.3.1. Fluid flow within porous media 41

3.3.2. Fluid Properties of ordinary water 43

3.3.3. Heat transport within porous media 46

3.3.4. Solid displacement 47

3.3.5. Porosity Evolution: 48

3.3.6. Permeability Evolution: 48

3.3.7. Fault reactivation potential 49

3.3.8. Strength of rock mass 50

3.3.9. Equivalent Mohr-Columb parameters 51

3.4. Geological setting and geomechanical characterizations 53
3.5. Finite element modeling 56
3.5.1. Numerical model description 57
3.5.2. Initial and boundary conditions 60
3.5.3. Stress field characterization 61
3.6. Results 62
3.6.1. Steady-state simulation results 62
3.6.2. Fault reactivation potential under prevailing in-situ stress conditions 63
3.6.3. Thermohydraulic processes in a geothermal doublet system 66
3.6.4. Dynamic evolution of slip tendency 68
3.7. Discussions 70
3.7.1. The impact of hydraulic properties 71
3.7.2. Evaluating slip tendency results against Mohr-Coulomb predictions 76
3.8. Conclusions 77
4. Chapter 4: Conclusions, limitations, and recommendations for future work 79
4.1. Additional Discussion 79
4.1.1. The role of hydraulic properties of the (re)injected fluid into the reservoir 79
4.2. Limitations 82
4.3. Concluding remarks 83
4.4. Recommendations for future work 85
References 87
Appendices 88
Appendix A: Full derivation of the main governing equations 88

List of figures

Fig. 1. Schematic Representation of open-loop geothermal systems 13

Fig. 2. Schematic representation of closed-loop geothermal systems 15

Fig. 3. Schematic representation of Enhanced Geothermal Systems..... 17

Fig. 4. Regions of IAPWS-IF97, modified after Cooper and Dooley (2007)..... 44

Fig. 5. Plot showing the laboratory data on the rock samples with fitted Hoek–Brown and Mohr-Coulomb models (typical pictures of pre-test and post-test paragneiss samples are embedded) . 56

Fig. 6. Graphs showing: (a) the 3D Geological Model, fault, and two hydraulically stimulated fractures, (b) the numerical mesh of the domain, generated using Delaunay triangulation (2D surfaces, i.e., fault, fractures) and Tetrahedralization (3D domain), and (c) the position of the principal stresses concerning the fault offset. 59

Fig. 7. Steady-state simulation results showing the initial pore pressure and temperature distributions within the reservoir 63

Fig. 8. Initial and evolution of slip tendency results calibrated after Miranda et al. (2023a) for the in-situ stress state in three possible stress state scenarios..... 65

Fig. 9. Graphs showing the response of the reservoir due to the operational activity: Panels (a) and (b) show the pore pressure distribution over the domain and fault face; Panels (c) and (d) illustrate the temperature distribution; panel (e) provides detailed information regarding the fluid flow and thermal dynamic of the geothermal reservoir after 100 years of continuous fluid injection with a 15 L/s injection rate. 68

Fig. 10. Initial and evolution of slip tendency results calibrated after Miranda et al. (2023a) for the in-situ stress state in three possible stress state scenarios..... 70

Fig. 11. Plots showing the evolution of pore pressure, temperature, fluid properties (Density and viscosity) of the most probable case over 100 years of operational activity. The injection fracture is located in -200 m, and the prodcution fracture is located in +200 meters. The injection and production fractures are located equidistantly from the fault plane which is located in 0 m in X direction. 73

Fig. 12. Graphs showing the slip tendency and stress distribution results for the cases with and without IAPWS formulation. 75

Fig. 13. Plots showing the pore pressure changes for the cases with and without IAPWS formulation. 76

Fig. 14. Mohr circle diagrams illustrating stress conditions during geothermal energy productions. 77

Fig. 15. Temperature and pressure evolutions with time at injection and prediction wells 81

List of tables

Table 1. Rock mass characterization: Relationship between rock mass quality for the intact and the fractured rock mass 54

Table 2. Material properties used for numerical modeling. 59

Table 3. The in-situ stress state at the potential geothermal site. 61

Nomenclature

List of symbols

Abbreviations

DGE	Deep geothermal systems
GSI	Geological strength index
ST	Slip tendency
THM	Thermal–Hydraulic–Mechanical
UCI	Uniaxial compressive strength

List of Roman Symbols

a	Material constant
c_f	Fluid heat capacity
c_s	Rock heat capacity
D	Disturbance factor
E_i	Young Modulus of intact rock
$\boldsymbol{g}$	Gravitational acceleration vector
G	Rock shear modulus
h	Aperture
K	Drained bulk modulus
K_f	Fluid bulk modulus
K_s	Solid bulk modulus
M_b	Biot modulus
m_i	Material constant
m_b	Material constant
n	Porosity
p_f	Fluid pressure
$P_{f,r}$	Reduced fluid pressure
p_f^*	Critical fluid pressure
$\boldsymbol{q_D}$	Darcy velocity vector
R	Specific gas constant of ordinary water
S	Material constant
S_0	Cohesion
T	Temperature
T_r	Reduced fluid temperature
T^*	Critical fluid temperature
$\boldsymbol{u}$	Displacement vector
v	Poisson's ratio
z	Depth

List of Greek Symbols

α	Biot's coefficient
β_b	Bulk volumetric thermal expansion coefficient
β_f	Fluid volumetric thermal expansion coefficient
β_s	Solid volumetric thermal expansion coefficient
ϵ	Strain tensor
$\dot{\epsilon}_{kk}$	Volumetric component of the total strain rate tensor
$\kappa_{x=y=z}$	Permeability tensor
λ_b	Bulk thermal conductivity
λ_f	Fluid thermal conductivity
λ_s	Rock thermal conductivity
μ_f	Fluid viscosity
μ_s	Coefficient of friction
ρ_b	Bulk Density
ρ_f	Fluid density
ρ_s	Rock density
$\bar{\sigma}'$	Mean effective stress
$\sigma_{3,max}$	Failure envelope range
σ_{ci}	Uniaxial compressive strength of intact rock
σ_n	Normal stress acting of plane of discontinuities (faults and fractures)
σ_n'	Effective normal stress acting of plane of discontinuities (faults and fractures)
$\sigma_{H,max}$	Maximum horizontal stress
$\sigma_{h,min}$	Minimum horizontal stress
σ_v	Vertical stress
φ	Friction angle

List of other Symbols

∇	Nabla operator
π	Reduced pressure
$\mathbb{I}$	Rank-two identity tensor

List of Publications

Refereed journal paper

- Saeed Vadiee, Biao Li, Jasmin Raymond, Mafalda M Miranda, "Numerical modeling of the long-term poromechanical performance of a deep enhanced geothermal system in northern Québec", Rock Mechanics Bulletin, Volume 4, Issue 1, 2025, 100170, ISSN 2773-2304, (Vadiee et al., 2025)

Conference proceedings papers and presentation:

- Saeed Vadiee*, Biao Li, "Thermo-Hydro-Mechanical Analysis of Fault Damage Zones for Deep Geothermal Systems: Implications for Reservoir Performance and Seismic Stability", 23rd Canadian Rock Mechanics Symposium, Montreal, August 2025 – Accepted, Presenter*.

- Saeed Vadiee, Biao Li, Jasmin Raymond, Mafalda M Miranda, "Thermal-Hydro-Mechanical Behavior of a Deep Enhanced Geothermal System in a Faulted Zone in Northern Québec, Canadian Geothermal Student Day, Quebec City, Quebec, September 2024, Presenter*.

- Saeed Vadiee, Biao Li, Jasmin Raymond, Mafalda M Miranda, "Thermal-Hydro-Mechanical Coupled Numerical Analysis of a Faulted Zone in a Québec's Potential Geothermal Engineering Site", 76th Annual Canadian Geotechnical Society Conference, GeoSaskatoon, Saskatchewan, October 2023, Presenter* (Vadiee et al., 2023).

Contribution of Authors

The sections encompassing this thesis showcase the author's distinctive contributions. This dissertation was conducted under the supervision of Dr. Biao Li, who provided guidance and support throughout the research process. The primary author, Saeed Vadiee, was responsible for all simulation work, implementation of models, and development of the research methodology, including data integration and analysis.

Two additional authors, Dr Jasmin Raymond and Dr Mafalda M Miranda from INRS university contributed to this research by carrying out laboratory testing and performing excavation work. Their specific role was to supply laboratory data pertaining to the geological area of study, which was essential in validating and informing the simulations and models developed in this work. All authors reviewed the final manuscript and approved of the content

1. Chapter 1: Introduction

1.1. Rationale

Deep geothermal operations offer a sustainable and renewable solution to growing global energy demands by harnessing the Earth's inherent heat stored in deep rock formations, presenting a potential to the energy landscape and contributing to significant reductions in greenhouse gas emissions. The global push towards decarbonization has increasing interest in geothermal energy, which provides a stable and reliable energy source compared to other source of renewable energy like solar and wind, which are heavily affected by the weather fluctuations. However, the effective and safe exploitation of geothermal resources hinges on a precise understanding and prediction of the complex, coupled Thermo-Hydro-Mechanical (THM) interactions that govern subsurface behavior (Cacace and Jacquey, 2017; Wilkins et al., 2021).

The dynamics of geothermal reservoirs are influenced by a convergence of interrelated physical processes, including thermal flux, fluid flow, and mechanical deformation. These processes become even more complex when considering the heterogeneous nature of geological formations, as well as the inherent spatial and temporal variability and uncertainties in subsurface conditions (Hudson and Harrison, 1997). At the microscopic level, geomaterials are composites of mineral phases that have developed over geological time under a range of tectonic and thermal conditions. This history results in a distinct arrangement of solid grains and microstructures, such as mineral interfaces, microcracks, and pore spaces, that form the rock's rigid skeleton. These micro-level features are crucial because they dictate how the rock responds to external forces and changes in thermodynamic and hydrodynamic conditions, contributing to nonlinear and transient behaviors.

On the macroscopic level, these microscopic complexities manifest as observable variations in the rock's overall mechanical and hydraulic properties. The rock mass, viewed as a three-phase system, comprises a solid skeleton with interconnected void spaces filled with fluid, gas, or a mixture of both. The fluid movement and pressure distribution within these voids interact with the solid framework, affecting the rock's stiffness and overall thermodynamic stability under different loading conditions. This macro-level behavior is shaped by the collective response of microstructural elements, giving rise to complex Multiphysics interactions that require sophisticated modeling techniques to capture accurately. The challenge, therefore, lies in bridging

the gap between the microscopic and macroscopic perspectives to develop models that can reliably predict subsurface behavior in geothermal reservoirs (Jacquey, 2017).

Field observations and laboratory experiments strongly indicate that the macroscopic behavior of rock is heavily influenced by microstructural defects, such as microcracks and fissures, and their degree of connectivity (Blöcher et al., 2009; Dautriat et al., 2009; Morlier, 1971; Mura, 1987). However, these observations and experiments typically capture the behavior of intact rock without fully accounting for the complex structures present in fractured domains or fault zones. These fault zones are surrounded by areas characterized by intensely jointed rock materials and dilatant breccias (damage zones), which may also have undergone chemical alterations (Faulkner et al., 2010).

While intact rock exhibits higher stiffness and strength, its behavior primarily depends on the solid skeleton, and failure typically occurs through this solid matrix. In contrast, rock masses display lower stiffness and strength due to their heterogeneous nature, influenced by natural discontinuities, such as faults, fractures, and joints. The behavior of rock masses is largely controlled by these discontinuities, and failure often occurs along pre-existing weak planes rather than through the intact rock itself. Thus, understanding the heterogeneous characteristics of geological systems, including faults and fractures, is crucial as they can dominate overall system behavior (Hoek, 1994a; E. Hoek and Brown, 1997; Hoek and Diederichs, 2006).

The internal structure of faults, particularly the extent of fault-inherited fracture nucleation and propagation within the damage zone, determines whether a fault acts as a conduit for fluid flow or as a barrier. This variability can locally modify groundwater dynamics and, through hydromechanical coupling, alter the in-situ stress field. Fractures, on the other hand, whether naturally occurring or artificially induced, often serve as preferential flow pathways, significantly influencing reservoir permeability and porosity. The density and interconnectivity of these fractures give rise to secondary permeability, profoundly affecting hydraulic conditions and fluid flow dynamics (Barton et al., 1997; Cherubini et al., 2013; Walder and Nur, 1984; Cacace et al., 2013). In geothermal reservoirs characterized by low porosity and low permeability, stimulation treatments are commonly employed to induce hydraulic fractures, enhancing fluid flow and increasing reservoir productivity. Thus, understanding the interactions between the host rock and

the induced fractures is critical for optimizing reservoir performance (Blöcher et al., 2018; Moeck et al., 2009b).

The second major motivation of this study concerns the thermodynamic properties of the working fluid. Geothermal operations induce variations in thermodynamic state of the system which result in changes in fluid properties, such as density and viscosity, due to variations in temperature and pressure fields. Oscillations in the heterogeneous fluid field can result in complex interactions that further influence reservoir behavior and productivity (Cooper and Dooley, 2007; Wagner et al., 2000).

Finally, the onset conditions and the evolution of processes in geothermal operations are intricately interlinked, making it essential to consider a Multiphysical approach that integrates thermal, hydraulic, and mechanical phenomena. Using numerical techniques, specifically the Finite Element Method (FEM), is crucial for this purpose, as it allows for the accurate simulation of these coupled processes under reservoir operations. By employing FEM, this study aims to predict reservoir behavior more reliably, accounting for the complex and dynamic interactions that govern the subsurface environment. This predictive capability is vital for enhancing the productivity and sustainability of geothermal reservoirs, while also mitigating the associated risks with their exploration, induced seismic activity, which can lead to jeopardizing the life of people and the project itself.

1.2. Objective

Deep geothermal operations aim to harvest the inherent heat stored naturally in deep rock formations and utilize it as a renewable source of energy, which can significantly contribute to reducing greenhouse gas emissions and transforming the energy consumption landscape. This naturally reserved heat can be extracted by drilling one or more boreholes into deep geological formations, through which a geothermal fluid is (re)injected and produced. The produced geothermal fluid can be later used to answer the heating or electricity demand of communities, promoting sustainable energy use.

However, in the majority of cases, the targeted geological horizon which might be a suitable source of energy lack natural permeability as these geological layers have gone through centuries of naturally occurring dynamic processing, including variations in formation processes,

environmental conditions, tectonic activity, changes in mineral composition, and the continues natura of the rock cycle. In these geological formations, the primary permeability of the domain is very low.

As the main factor affecting the productivity of the open-loop geothermal systems is convection (Movement of heat though working fluid), enhancing the permeability of the domain become of paramount importance. The permeability of the reservoir is usually enhanced by the creation of a secondary permeability via induced fracturing (Zimmermann et al., 2010; Genter et al., 2010). The induced fracturing is technique though which the natural fractures inside the rock formation get connected with each other, thus creating a fractured network along the path of fluid flow. These fractures form when the fluid pressure exceeds the minimum principal stress and tensile strength of the rock. The injected fluid is a mixture of water, chemicals, and proppants. This process of inducing the fracture network should be carried out multiple time though out the lifetime of the open-loop geothermal systems in order to keep the fracture network open and functional as over time, these fractures tend to close due to movement of fine grains, chemical reactions, and changes in in-situ stress state.

Despite the advantages of having deep geothermal systems, a number of concerns should be answered before proceeding with the operations of such systems. One of the primary concerns is the risk of induced seismicity in areas where natural plane of weaknesses, i.e., faulted zones, exists. The variations in in-situ stress caused by geothermal operations can cause the (re)activation of dormant fault zones or even can cause a new fault zone to be created. This process can induce seismic slip movement along the plane of rupture is faulted zones.

Given these complexities, it becomes crucial to quantify, both temporally and spatially, the dynamic interactions between the various physical processes and the geological environment in which they occur. Therefore, the principal aim of this thesis is to develop a flexible working framework that integrates laboratory and field data into numerical dynamic models, to predict the long-term poromechanical performance of faulted zones under geothermal production conditions. Specifically, this study aims to (1) investigate the impact of thermal and hydraulic factors on the mechanical stability of the reservoir, (2) analyze the influence of varying in-situ stress conditions on the potential for induced seismicity, and (3) propose a comprehensive framework for assessing and mitigating poromechanical risks during geothermal operations.

1.3. Major Goals and Questions Addressed in the Study

Building upon the concepts outlined earlier, the primary objective of this study is to develop a comprehensive workflow that enhances our understanding of the risks associated with geothermal energy exploitation. This requires integrating laboratory data with a robust Multiphysics approach to effectively model and predict the complex behaviors of geothermal reservoirs.

The central research questions guiding this study are as follows:

1. What are the dominant physical processes that influence or control the behavior of the fractured reservoir rocks?
2. How can the risks associated with geothermal operations be quantified, and what methodologies can be employed to mitigate these risks?
3. What role does slip tendency analysis play in assessing the stability of fractured rock domains, and how can this analysis be effectively applied?
4. How do the thermodynamic properties of the fluid phase influence slip tendency results, and what are the implications for risk assessment and management?
5. How can the current constitutive models be adapted to simulate large-scale, over extended period of time, Multiphysics-coupled processes using finite element modeling (FEM)?
6. In what way does incorporating the strength characteristics of fractured rock using an appropriate constitutive model, such as the Hoek-Brown criterion, impact simulation outcomes and predictions?

1.4. Workflow overview

The workflow outlined in this study integrates laboratory-derived experimental data on rock samples into a comprehensive, multicomponent physical framework known as GOLEM, developed by (Cacace and Jacquey, 2017). This framework enables a detailed description of the underlying physics and quantifies the interactions among various coupled processes.

As mentioned previously, intact rock typically exhibits higher stiffness and strength parameters compared to the rock mass. To model this effectively, the initial step involves using laboratory-scale data to establish the Hoek-Brown failure criterion, which serves to differentiate between the

behavior of intact rock and the rock mass. Following this, the Hoek-Brown model is approximated using the Mohr-Coulomb failure criterion. This approximation yields a revised set of cohesion and friction angle values, which are often lower than those for intact rock. These reductions are influenced by several factors, including the material constant, the Geological Strength Index (GSI), and the excavation method employed.

Despite this, the numerical simulator used in our study, based on the Drucker-Prager model, requires a further adaptation. To bridge the gap between the Mohr-Coulomb and Drucker-Prager failure criteria, series of triaxial tests are conducted using the GOLEM finite element method (FEM) simulator. The Mohr-Coulomb parameters derived earlier serve as input for these simulations, enabling the calibration of cohesion and friction angle values compatible with the Drucker-Prager model. The derived equivalent Drucker-Prager parameters approximate the Mohr-Coulomb behavior as closely as possible within the constraints of the Drucker-Prager model. This approach ensures that the final simulations accurately capture the original rock behavior while remaining consistent with the numerical modeling framework constraints.

Integrating data into numerical models presents a significant challenge when addressing increasingly realistic scenarios that feature complex geometries and data-based property relations. The technical difficulties extend beyond the processing of geological data, which often originates from diverse sources. The primary challenge for numerical applications lies in discretizing the continuous geological representations into a format suitable for efficient simulation. Most discretization tools, such as meshing software, often yield simplified and generic model representations constrained by the assumptions necessary to approximate the actual geological geometry.

To address these challenges in the present workflow and accurately represent the geological structure of the subsurface, we employed Coreform Cubit meshing software. Cubit enables the creation of a consistent discrete mesh that captures the intricacies of geological formations, including non-planar and intersecting interfaces. It also allows for the accurate modeling of formations separated by significant fault zones and fractures, ensuring that the mesh is well-suited for finite element method (FEM) simulations. This capability is crucial for modeling the complex behavior of the subsurface in a realistic and reliable manner.

The discretization must balance the need for capturing essential geological features with maintaining computational efficiency. Achieving this balance requires a comprehensive sensitivity analysis to ensure that the discretized domain is both accurate and manageable. Within this framework, geological features are represented hierarchically, the primary domain consists of the rock mass itself, while subdomains include faults, fractures, wells, and injection nodes, all integrated into a unified 3D model.

The rock mass is modeled using 3D elements, while fractures and faults are represented as 2D surfaces embedded within the 3D mesh. Wells are depicted as 1D elements, modeled as lines with interconnected nodes, and source nodes are defined as 0D elements, represented by individual nodes. Geological features such as fault zones can divide the rock mass into separate domains, each potentially having distinct material properties. In Coreform Cubit, these domains and subdomains are designated as material blocks, with material properties integrated through the input file in the GOLEM FEM framework. Moreover, the quality of the mesh, defined by factors like element shape, size distribution, and distortion of elements, significantly impacts simulation accuracy and numerical stability. Therefore, it is essential to evaluate the mesh quality using Coreform Cubit's capabilities to ensure a robust and reliable model.

The GOLEM FEM (Cacace and Jacquey, 2017) framework used in this study operates within the MOOSE (Multiphysics Object-Oriented Simulation Environment) platform (Gaston et al., 2009), which is designed to facilitate the simulation of complex Multiphysics problems. MOOSE employs a modular structure based on the finite element method (FEM), allowing for the flexible integration of different physical processes. Each aspect of the governing equations, such as thermal, hydraulic, and mechanical interactions, can be implemented in separate "Kernels," ensuring modularity and ease of customization. These Kernels are then coupled to simulate the full THM behavior of the system, providing a robust and efficient framework for handling nonlinear and coupled processes. By leveraging MOOSE's inherent capabilities, the numerical model can accurately reflect the complex subsurface dynamics of geothermal reservoirs, incorporating data-driven property relations and realistic geometrical representations.

In MOOSE based applications, such as GOLEM FEM framework, configuring and defining a simulation problem is accomplished through an input file. This file serves as the primary interface

for specifying all aspects of the simulation. Users define the physics of the problem by setting up governing equations, assigning material properties, and establishing boundary conditions. The input file also facilitates mesh setup by describing the geometry of the problem domain and determining the discretization details. Furthermore, the input file allows users to configure solvers, selecting and parameterizing the numerical methods required to solve the equations efficiently. Lastly, the input file specifies the desired output, detailing which results should be recorded and the format in which they should be presented.

MOOSE's input file system is highly extensible, allowing applications built on the MOOSE framework to introduce custom syntax and additional parameters tailored to their needs. This feature enables domain-specific language extensions while preserving a consistent structure across different applications. By leveraging this system, MOOSE provides a powerful and flexible method for defining complex Multiphysics simulations. This approach separates problem definition from the underlying C++ solver code, making the framework more user-friendly and facilitating code reuse. It empowers scientists and engineers to conduct sophisticated simulations without needing to delve into the complexities of modifying core code, thereby enhancing both usability and versatility across various scientific and engineering disciplines.

The MOOSE framework employs Kernels to define the physics governing the primary variables. Kernels are used to implement the partial differential equations that dictate the evolution of these primary quantities throughout the simulation domain. In contrast, Auxiliary Kernels handle the physics needed to compute the auxiliary variables. These Auxiliary Kernels utilize the results from the primary variables to derive additional quantities, ensuring a comprehensive description of the system's behavior.

This separation of primary and auxiliary variables within the input file allows for a more modular and organized approach to defining complex Multiphysics simulations. It ensures that the core physics of the problem is efficiently solved while also enabling the computation of supplementary quantities needed for a complete understanding of the modeled processes.

In the context of this thesis, the primary variables include thermal, hydraulic, and mechanical displacements. These primary variables represent the fundamental quantities that the simulation directly solves for, and their accurate computation is essential for modeling the physical processes

within the system. Auxiliary variables, on the other hand, are derived quantities computed based on the primary variables. These include parameters such as stress and strain distributions, fluid density and viscosity evolution, changes in porosity and permeability, and calculations like slip tendency. These auxiliary variables are essential for interpreting the physical state of the system and for understanding how primary variable interactions manifest in the overall behavior of the geothermal reservoir.

Additionally, it should be noted users must still carefully review the equations and understand the logic behind their derivation. This comprehension is essential to ensure that the correct Kernels are selected for the specific problem that needs to be addressed. Despite the MOOSE framework's capability to manage complex physics through its structured input file system, users require a certain level of proficiency in C++ for more advanced customizations. This is especially true when creating or modifying Kernels to handle unique physical processes that are not covered by the existing options. Understanding how to navigate and potentially extend the code base allows for greater flexibility and ensures that the simulation setup accurately reflects the desired physics.

1.5. Overview over the thesis

This thesis is prepared in accordance with the manuscript-based thesis format provided by Concordia University. The chapters detail how and to what extent the research questions posed earlier are addressed.

Chapter 2 presents a comprehensive literature review that forms the foundation of this research. It explores the theoretical and empirical basis for understanding the complex interactions in geothermal systems, laying the groundwork for the subsequent analyses.

Chapter 3 contains the manuscript titled *Numerical Modeling of the Long-Term Poromechanical Performance of a Deep Enhanced Geothermal System in Northern Québec*, prepared in accordance with the requirements of Rock Mechanics Bulletin Journal. This chapter examines the long-term behavior of a faulted zone in northern Québec under geothermal energy production. It details the large-scale, coupled Multiphysics modeling using the Finite Element Method (FEM), incorporating the strength characteristics of fractured rock and evaluating fault slip tendency. The chapter also highlights the impact of the thermodynamic properties of the fluid phase on simulation

outcomes, emphasizing the relevance of fluid-rock interactions in geothermal reservoir performance.

Chapter 4 offers the concluding remarks, summarizing the key findings and acknowledging the limitations of the study. Also, in this chapter, the future extensions which should be added to the current framework is presented.

Appendix I provides the mathematical formulations, underlying assumptions, and numerical implementation strategies adopted for modeling coupled Thermo-Hydro-Mechanical (THM) processes in porous rock formations throughout the thesis. It is important to note that the derivation of these equations is credited to (Cacace and Jacquey, 2017), and the numerical simulations were conducted using the MOOSE Framework. This appendix is included to clarify the derivation of the equations, which is crucial for understanding the role of each variable and the nature of the coupling among hydrothermal, thermomechanical, and hydromechanical processes. In the MOOSE Framework, each component of the governing equations is implemented in separate Kernels. Thus, understanding the equation terms enables users to identify the specific Kernels needed to achieve accurate and expected simulation results.

2. Chapter 2: Literature Review

2.1. Introduction

Canada's harsh environment and resource-intensive industries, including mining, forestry, oil and gas extraction, transportation, and electricity power plants, contribute to its high energy consumption. These issues are especially pronounced in the northern regions, where approximately 200,000 individuals live without access to Canada's main electrical grid. Currently, they heavily rely on fossil fuels for electricity generation and space heating, posing both environmental and economic concerns (Canada, 2016).

Geothermal energy presents a promising alternative for these regions, as it provides a stable, renewable energy source that can mitigate the environmental risks and economic burdens associated with fossil fuels. Geothermal energy is the heat naturally present within the Earth's crust. When a significant amount of hot water and steam accumulates in a porous, permeable rock structure below the surface, a geothermal reservoir is formed (Ganguly and Mohan Kumar, 2012). A typical geothermal system consists of three main elements, a heat source, a reservoir, and a working fluid that transfers the heat (Dickson and Fanelli, 2013).

However, as beneficial as geothermal systems are, a wide range of fundamental questions and uncertainties about physical processes must be addressed to develop an efficient and functional energy harvesting system.

Researchers have long focused on geothermal energy because it is a clean, renewable source with considerable environmental advantages, producing minimal pollutants or waste emissions. Thus, research has expanded in various directions, including geothermal resource exploration, modeling the characteristics of geothermal reservoirs, and developing technologies to extract energy. These models aim to predict the output of hot water and steam and estimate the long-term viability as well as sustainability potential of geothermal reservoirs.

2.2. Overview on different geothermal systems

Geothermal energy systems harness the Earth's natural heat, which can be utilized for electricity generation, heating, or cooling. Different geothermal systems are suited to various geological conditions and energy demands, each with unique operational characteristics and efficiencies. Below, we discuss several key geothermal systems, including open-loop, closed-loop, and

Enhanced Geothermal Systems (EGS). However, it is worth mentioning that the main focus on this study would be on the physical processes of deep enhanced geothermal systems and their impact on the surrounding rocks. In addition, we would explore the associated risks, mainly induced seismic activity, with such systems.

2.2.1. Open-Loop Systems

Open-loop geothermal systems harness Earth's natural heat by directly utilizing groundwater as both a heat source and a heat-transfer medium. These systems operate by drawing water from a reservoir through a production well, circulating it through a heat exchanger or power plant (see **Fig. 1**), and then either reinjecting it back into the ground or discharging it at the surface. This straightforward method leverages the stable year-round temperature of groundwater, making open-loop systems highly efficient for both heating and cooling in regions with abundant, clean groundwater and sufficient aquifer permeability.

The mechanics of open-loop systems involve a direct heat exchange. In heating mode, the system transfers thermal energy from the groundwater to a refrigerant in a heat pump, where it is compressed to increase its temperature. For cooling, the process reverses. Heat from the building is transferred to the cooler groundwater, effectively using the reservoir as a natural heat sink. This direct interaction with groundwater generally yields higher efficiency than closed-loop systems, and the reduced need for extensive drilling and piping can lower installation costs (Hawkins and Tester, 2018; Sharmin et al., 2023).

Despite these benefits, open-loop systems face several limitations. Their use is typically confined to areas with reliable groundwater sources, and they may be prone to issues like mineral scaling, corrosion, or fouling of system components due to water quality variations. Regulatory requirements for groundwater extraction and reinjection can complicate the systems monitoring, while environmental concerns, such as reservoir depletion or contamination, require careful design and operational management. Seasonal groundwater temperature changes can also impact system performance.

Environmental sustainability is paramount in open-loop systems. Effective designs should prioritize groundwater conservation, ideally using reinjection methods to maintain reservoir levels. Thermal plumes, created by sustained operation, must be monitored to prevent disruptions to the

aquifer's temperature balance and local ecosystems. Additionally, chemical treatments to prevent scaling or biofouling require strict control to avoid unintended groundwater contamination. Routine monitoring of water quality and temperature is essential to ensure sustainable operation and to detect potential environmental impacts early.

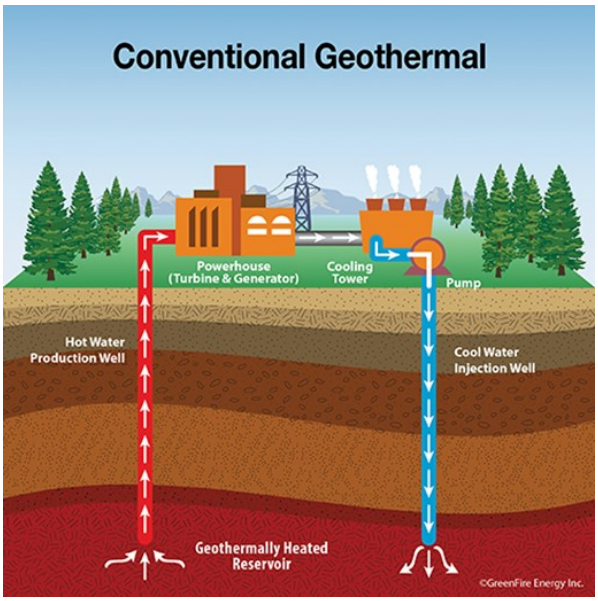

Fig. 1. Schematic Representation of open-loop geothermal systems

("GreenFire Energy - Developing Advanced Geothermal System," 2024)

2.2.2. Closed-Loop Systems

Closed-loop geothermal systems offer an innovative approach to harnessing the Earth's thermal energy by operating within a contained circuit that eliminates direct interaction with groundwater resources. These systems consist of a network of pipes, typically installed in vertical boreholes, repurposed oil and gas wells, or horizontal trenches, depending on local geological conditions and available space. The core component of the system is a heat-transfer fluid, often water or a water-antifreeze mixture, which circulates continuously within this sealed loop, transferring thermal energy from the Earth to the surface.

The principle behind closed-loop systems relies on the consistent temperature gradient found in the Earth's crust. As the heat-transfer fluid moves through the underground pipes, it absorbs heat

from the surrounding rock and soil. This heated fluid is then pumped to the surface, where a heat exchanger various extracts the thermal energy for applications, such as space heating, domestic hot water production, or electricity generation in larger installations. After the heat is extracted, the cooled fluid is recirculated back into the ground to reabsorb heat, completing the closed loop.

One of the major advantages of closed-loop systems is their versatility. These systems are especially beneficial in areas with limited water resources or low-permeability rock formations, where open-loop systems would be impractical or impossible. Since closed-loop systems do not rely on aquifers, they can be installed in a wide range of geological settings, broadening the potential for geothermal energy utilization.

Environmentally, closed-loop systems offer significant benefits. Unlike open-loop systems, they do not deplete or interact with groundwater supplies, addressing concerns about reservoir depletion and potential contamination. The sealed nature of the circulation loop also prevents issues like mineral scaling and corrosion, which often affect open-loop systems. This can result in reduced long-term maintenance needs and lower operational costs.

Despite these advantages, closed-loop geothermal systems do have limitations. Their heat transfer efficiency tends to be lower than that of open-loop systems, primarily because the heat exchange occurs indirectly through the pipe walls. This reduced efficiency may require more extensive installations, especially in regions with low geothermal gradients, leading to higher initial capital costs. Additionally, the installation process can be more invasive and time-consuming, particularly for vertical borehole systems that require deep drilling.

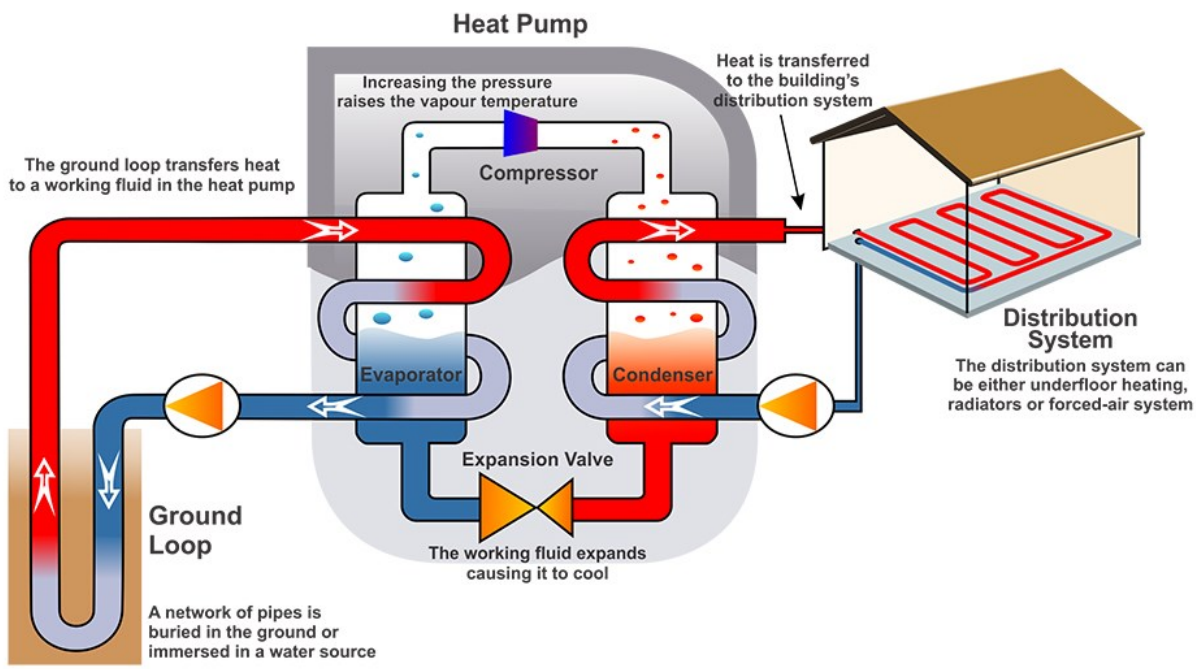

Fig. 2. Schematic representation of closed-loop geothermal systems (Climo et al., 2012)

2.2.3. Enhanced Geothermal Systems (EGS)

Enhanced Geothermal Systems (EGS) represent a transformative leap in geothermal energy technology, significantly expanding the potential to harness Earth's thermal resources beyond traditional hydrothermal reservoirs. EGS enables the extraction of geothermal energy from regions previously considered unsuitable due to insufficient permeability or water content, thereby broadening the geographical scope for geothermal power production.

The core principle of EGS involves creating or enhancing a subsurface heat exchanger in hot, dry rock (HDR) formations typically found at depths between 3 to 10 kilometers. This process, known as hydraulic stimulation (or hydro-shearing), injects high-pressure fluid into the target formation to create new fractures or expand existing ones. The resulting network of interconnected fractures significantly enhances the rock's permeability, allowing for fluid circulation and efficient heat extraction from the engineered reservoir.

EGS is typically designed as an open-loop system, comprising injection and production wells. Cool water is injected into the engineered reservoir through the injection wells, where it circulates through the fracture network, absorbing heat from the surrounding hot rock. The heated fluid is

then extracted through production wells for use in electricity generation at a power plant or for direct heat applications. After heat extraction, the cooled fluid is reinjected into the reservoir, maintaining system pressure and sustaining the heat extraction process in a continuous cycle.

One of the key advantages of EGS is its potential for widespread deployment in diverse geological settings. Unlike conventional geothermal systems, which are limited to specific tectonic or volcanic regions, EGS can theoretically be implemented wherever sufficiently hot rock exists at accessible depths. This opens vast new areas for geothermal energy production, potentially transforming it into a baseload renewable energy source in regions previously considered unsuitable for traditional geothermal development.

However, the challenges associated with reinjection in EGS are often more pronounced than in conventional systems. The risk of induced seismicity is generally higher due to the initial hydraulic stimulation and ongoing high-pressure fluid circulation in areas that may not be naturally permeable. While most induced seismic events are typically too small to be felt at the surface, larger events can occur, requiring robust seismic monitoring and risk assessment protocols. Thus, Careful monitoring and management of injection rates and pressures are crucial to minimize this risk.

In addition to micro seismic activity, thermal breakthrough can be a significant concern in EGS, as the engineered fracture networks might create preferential flow paths, potentially leading to rapid cooling of the production fluid. Chemical interactions between the injected fluid and the host rock can be more complex in EGS, potentially altering fracture permeability over time and affecting system performance. Additionally, fluid losses can be more significant in EGS, especially during the initial stimulation phase, requiring careful water resource management.

The efficiency of EGS is largely dependent on successfully creating and maintaining a subsurface heat exchanger or in other words the fractured network. Achieving optimal fracture networks that balance high permeability with controlled fluid pathways is a complex and ongoing challenge. Researchers are exploring a variety of stimulation techniques, including chemical treatments and thermal fracturing, to improve reservoir performance while minimizing environmental impacts.

The economic feasibility of EGS remains a challenge, primarily due to the high initial costs associated with deep drilling and reservoir stimulation. However, technological advancements in

drilling techniques, such as millimeter-wave drilling and plasma drilling, offer promising solutions to reduce these costs. Furthermore, the development of more efficient power conversion systems tailored to the temperature profiles of EGS reservoirs is improving system performance and overall economic viability.

Recent research in EGS is focused on improving reservoir characterization and modeling capabilities. Advanced geophysical imaging techniques, combined with sophisticated numerical simulations, are enhancing our ability to predict and optimize reservoir behavior over long-term operation. These tools are essential for site selection, system design, and operational management, ensuring the success of EGS projects.

While the environmental footprint of EGS is generally lower than that of fossil fuel-based energy sources, careful attention must be paid to factors such as land use, water consumption, and induced seismicity. Life cycle assessments and comprehensive environmental impact studies are increasingly being conducted to ensure that EGS projects are developed sustainably and responsibly.

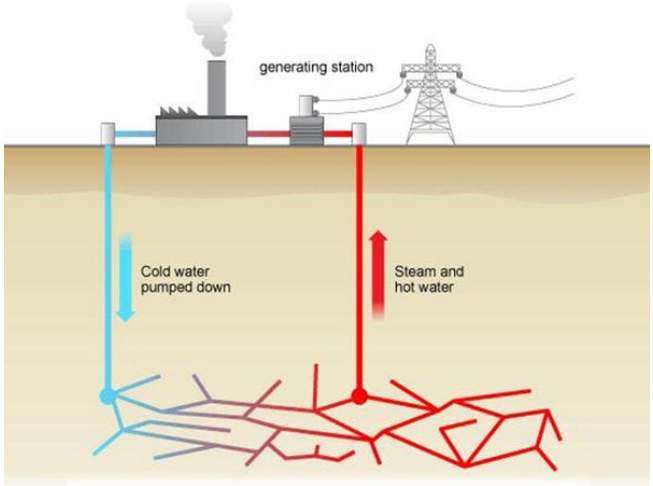

Fig. 3. Schematic representation of Enhanced Geothermal Systems (Design-Engine, 2015)

2.3. Working fluid

In geothermal systems, the working fluid can be different from the fluid saturating the porous media's pore space, depending on the type of system employed. In closed-loop systems, the working fluid circulates in a sealed network of pipes, separate from the natural groundwater or

fluids in the rock formation. This working fluid can be water, a water-antifreeze mixture, or a specialized heat transfer fluid, designed to efficiently capture and transport heat without interacting with the surrounding environment. In contrast, open-loop systems utilize the natural groundwater as both the working fluid and the pore fluid, extracting it from the reservoir, using it for heat transfer, and then reinjecting it back into the ground.

2.4. Numerical methods

Geological observations often arise from the complex, nonlinear interplay of multiple physical processes, such as groundwater flow, heat and solute mass transfer, rock deformation, and chemical feedback from fluid-matrix interactions (Stephansson et al., 2004). These interactions occur within geologically diverse environments, where heterogeneities like faults and fractures introduce additional layers of complexity. These factors span a wide range of temporal and spatial scales, interacting in highly nonlinear ways that make accurate modeling essential for predicting the behavior of various subsurface systems. Reliable representation of these processes is particularly crucial for applications in geothermal and fossil energy extraction, as well as for storage systems for CO_2, hydrogen, and heat, where the success of these infrastructures depends on understanding these interrelated dynamics.

The interconnected nature of thermo-hydro-mechanical (THM) processes in porous reservoirs often involves complex feedback mechanisms. For instance, pore pressure and temperature changes, such as those induced by cold fluid injection, are dynamically linked to the in-situ stress field. These couplings are influenced by the presence of faults and fractures, which affect fluid flow and heat transfer, thereby altering system behavior over time. Consequently, capturing the full extent of rock mass variations due to natural and anthropogenic factors requires an approach that goes beyond individual processes to examine their combined effects. This integrated perspective is especially important in reservoir applications, where understanding the behavior of complex, Multiphysics rock-fluid systems is essential for making accurate predictions about reservoir performance, productivity, and sustainability.

To achieve these insights, it is imperative to employ a robust conceptual model that accurately captures the physical processes occurring within naturally complex geological settings. Such models must integrate key elements of groundwater flow, heat and solute transfer, and mechanical

deformation, particularly in fractured, porous rock systems. These processes have a profound impact on critical properties like permeability and porosity, which in turn influence the productivity, recovery, and longevity of geothermal systems (Blöcher et al., 2010; Cacace et al., 2013; Raghavan and Chin, 2002; Walder and Nur, 1984).

2.4.1. Finite Element Method

The Finite Element Method (FEM) is particularly well-suited for modeling the complex thermo-hydro-mechanical (THM) processes in subsurface reservoirs, offering significant advantages over other numerical approaches. FEM's ability to discretize complex geometries with highly customizable mesh structures allows it to capture the intricate features of geological formations, such as faults, fractures, and heterogeneities, with a high degree of accuracy. By refining the mesh in regions with high gradients or complex boundaries, FEM provides localized detail where needed, improving the accuracy and reliability of simulation results.

Scalability is another key strength of FEM. The method efficiently handles large-scale simulations, making it suitable for applications that span a broad range of spatial and temporal scales, such as reservoir modeling. FEM's structured approach enables seamless scaling from fine to coarse mesh resolutions, optimizing computational resources based on the demands of each region in the model. This flexibility makes FEM highly effective for simulating both local processes, such as fluid-rock interactions in fault zones, and larger basin-scale phenomena, where precise representation of geological features is essential.

Additionally, FEM provides robust frameworks for integrating coupled physical processes. Unlike many other methods, FEM can easily handle Multiphysics interactions, thermal, hydraulic, and mechanical couplings, by allowing each physical process to be modeled with tailored parameters and boundary conditions. This adaptability is crucial for studying reservoirs where the dynamic interactions between temperature, fluid flow, and stress fields directly impact system behavior and sustainability. For these reasons, FEM is an ideal choice for simulating the complex, Multiphysics dynamics of subsurface reservoirs, offering both precision and scalability essential for predictive modeling.

2.4.2. Multiphysics Object-Oriented Simulation Environment (MOOSE) framework

The Multiphysics Object-Oriented Simulation Environment (MOOSE) framework (Gaston et al., 2009) offers several advantages over traditional commercial FEM software for modeling complex thermo-hydro-mechanical (THM) processes in reservoirs and other geosystems. Developed by Idaho National Laboratory, MOOSE is an open-source platform specifically designed to handle Multiphysics simulations, making it exceptionally well-suited for the highly coupled and nonlinear interactions present in reservoir modeling. Unlike many commercial software packages that may require complex workarounds or additional licensing to integrate multiple physical processes, MOOSE is built with Multiphysics coupling in mind. This integrated approach allows users to easily implement, customize, and expand simulations involving thermal, hydraulic, and mechanical interactions within a single cohesive system.

A notable advantage of MOOSE is its support for advanced meshing capabilities, including adaptive mesh refinement (AMR). In reservoir modeling, capturing localized phenomena such as fault zones or fracture networks can be crucial to accurately predicting system behavior. With AMR, MOOSE automatically refines the mesh in areas where higher resolution is needed, thereby improving accuracy without sacrificing computational efficiency. Many commercial FEM packages lack this level of flexibility or require additional costs for high-end meshing tools, making MOOSE a highly adaptable and cost-effective choice for complex geosystem simulations.

As an open-source platform, MOOSE offers unrestricted access to its source code, allowing users to adapt and extend the framework to meet specific research needs or constraints. This degree of customizability is rarely available in commercial software, where access to the underlying code is often restricted. Additionally, MOOSE benefits from a large and active community of researchers and developers who continually contribute to its growth by adding new modules, enhancing functionality, and sharing innovations. This collaborative ecosystem allows users to benefit from the latest advancements in simulation techniques, ensuring that MOOSE remains at the forefront of Multiphysics modeling.

MOOSE's nonlinear solver capabilities are another significant advantage for THM applications, which often involve highly nonlinear interactions between stress, deformation, fluid flow, and temperature. Equipped with state-of-the-art solver libraries like PETSc (Balay et al., 2022), MOOSE is optimized for handling complex, nonlinear systems, improving both stability and

computational efficiency in large-scale simulations. In many cases, this can lead to better performance and reliability compared to commercial FEM software, which may be less optimized for these types of coupled interactions.

Moreover, MOOSE is designed to leverage high-performance computing (HPC) infrastructure, allowing for highly scalable parallel processing. This capability is particularly beneficial for reservoir simulations, where large-scale models with intensive computational demands are often required. While some commercial software supports parallel computing, MOOSE's open framework provides the flexibility to customize parallel routines, making it well-suited for research environments that require both scalability and flexibility.

Lastly, MOOSE's open-source nature offers a distinct cost advantage, particularly for academic and research-based projects. In contrast to commercial FEM software, which can carry significant licensing fees, MOOSE provides a sustainable, accessible option for long-term research. This cost-effectiveness not only allows researchers to conduct extensive simulations without incurring prohibitive costs but also fosters innovation, encouraging users to explore advanced modeling techniques that might not be feasible within commercial constraints.

2.5. Numerical Modeling of Heat Extraction in EGS: Well Configuration and Production Dynamics

On of the main focuses of this research is on optimizing Enhanced Geothermal System (EGS) well configurations for sustained heat extraction. Three primary well layout schemes are commonly modeled, simulated, and analyzed in EGS studies, including the doublet (one injection and one production well), the triplet (one injector with two flanking production wells), and the five-spot (a central injector surrounded by four corner production wells). Given the extensive body of research on this subject, this review concentrates on recent and relevant studies.

Sanyal and Butler (2005) conducted a 30-year power generation simulation using a 3D hypothetical EGS model with a five-spot well arrangement. Their analysis focused on the impacts of fracture spacing, reservoir permeability, and well geometry on system performance. Their research showed that the cooling rate at production wells is not an adequate measure of project effectiveness. Instead, the net generation profile over time and reservoir heat recovery factor are more appropriate criteria. The study emphasizes that improving matrix-to-fracture heat transfer

area by reducing fracture spacing is more beneficial for heat recovery and net generation than merely enhancing permeability. Interestingly, their study suggests that net generation profiles can be optimized by reducing throughput without significantly impacting average generation over the project's lifetime. Furthermore, increased stimulation volume has been shown to positively correlate with generation levels without substantially altering the generation profile shape. Additionally, their research indicates that for a given stimulation state, there exists a linear correlation between average net generation and stimulated volume, independent of well geometry. Furthermore, the recovery factor demonstrates a reasonable correlation with stimulation volume, irrespective of well geometry, fracture spacing, and fracture domain permeability. Notably, except in cases of small, stimulated volumes, the recovery factor remains relatively constant (between 0.4 to 0.5) across various parameters.

(Zeng et al., 2013) examined a 2D conceptual EGS model featuring a horizontal doublet well layout, concluding that energy efficiency is primarily influenced by reservoir permeability and water production rates.

Building on this work, (Jiang et al., 2014) designed and simulated a 3D conceptual EGS with a triplet well configuration over a 40-year heat extraction period. Their findings indicated that this layout could maintain preferential flow within the reservoir and extend heat production performance by approximately 10 years compared to a doublet system. Chen and Jiang (2015) performed a comparative analysis of long-term performance across doublet, triplet, and five-spot well layouts. Their numerical results revealed that simply increasing the number of production wells does not necessarily enhance EGS performance, as some triplet configurations outperformed five-spot layouts, while others underperformed compared to doublet systems.

In a more recent study, (Chen and Jiang, 2016) conducted a detailed sensitivity analysis of the heat extraction process in a doublet well EGS, examining various design parameters. They discovered that EGS production temperature and lifespan are closely linked to the reservoir's flow patterns. Notably, they found that thermal compensation from surrounding rocks contributes minimally to heat transfer to the transmission fluid for operational periods shorter than 15 years.

Although many of these studies were based on hypothetical or conceptual EGS models, the insights gained have significantly advanced our understanding of EGS heat production performance optimization. This body of research has laid a foundation for future investigations in the field.

2.6. Interactions among physical processes

Researchers (Cacace and Jacquey, 2017; Heidari et al., 2023b, 2023a; Jacquey et al., 2016; Norouzi et al., 2024; Sojoudi et al., 2024; Vadiee et al., 2025, 2023) have aimed for a long time to address several fundamental questions that are critical for improving the understanding of the thermo-hydro-mechanical behavior of enhanced geothermal systems (EGS). The primary objective is to identify and model the physical processes that govern the interactions among fluid flow, heat transfer, and mechanical displacement, integrating them into a numerical simulator capable of making reliable predictions at larger scales. A key challenge lies in capturing the inherent complexity and heterogeneity of geological systems, particularly in terms of faults and fractures, within a dynamic modeling framework (Cacace and Jacquey, 2017; Wang et al., 2023). By incorporating these natural discontinuities, the model will allow for the quantification of their effects on the thermo-mechanical and hydraulic conditions of a reservoir, which are crucial for optimizing reservoir management strategies and predicting long-term performance (Berre et al., 2019; Dudun and Feng, 2024).

2.6.1. Coupling among the different processes

The coupling of thermal, hydraulic, and mechanical processes in porous reservoirs is highly intricate and can be classified into three primary types, encompassing hydromechanical, thermomechanical, and hydrothermal couplings. Each of these interactions plays a significant role in determining the overall behavior of the reservoir, and their interdependence must be carefully accounted for to achieve accurate simulations (Jacquey, 2017). These couplings not only influence the flow of fluids and thermal regime within the reservoir but also affect the mechanical integrity of the surrounding rock, particularly in the presence of faults and fractures, which introduce additional complexity into the system (Dudun and Feng, 2024; Ma et al., 2023).

2.6.1.1.Hydromechanical Coupling

Hydromechanical coupling refers to the interdependent relationship between fluid flow and mechanical deformation within porous media, particularly in the context of reservoir operations. This coupling involves two primary processes. The first is the effect of differential changes in pore pressure, which induce deformation of the solid skeleton of the reservoir rock. This fluid-to-solid interaction significantly influences the overall reservoir behavior, as changes in pore pressure can

alter the permeability and stability of the rock matrix. The second process involves the effect of variations in stress applied to the solid skeleton, which in turn causes changes in pore pressure. These stress-induced changes in pore pressure can impact fluid dynamics, influencing the flow of fluids through the porous matrix and affecting the efficiency of heat and fluid extraction. These interrelated phenomena are integral to the behavior of reservoirs during operational activities, such as fluid injection, extraction, and thermal loading (Moeck et al., 2009b). They have been extensively studied in laboratory settings, where experimental work has demonstrated their significance in governing reservoir performance. Studies by Blöcher et al. (2009) and Ghabezloo and Sulem (2009) provide valuable insights into the mechanisms of hydromechanical coupling and its impact on reservoir dynamics, including the changes in permeability and stress distribution within the rock matrix. Understanding these coupled processes is essential for accurately modeling reservoir behavior and optimizing the management of geothermal, oil, and gas reservoirs.

2.6.1.2.Thermomechanical Coupling:

In Thermomechanical coupling, changes in the thermal state of the rock induce volumetric deformation, which may manifest as either contraction or dilation depending on the direction of the temperature change (Geertsma, 1957; McTigue, 1986). This coupling is crucial in understanding how heat extraction or injection impacts the reservoir rock's mechanical behavior, particularly in the context of geothermal operations. Thermal expansion or contraction of the rock matrix can lead to changes in the reservoir's stress and porosity, which in turn affect fluid flow and heat transfer efficiency.

Additionally, shear deformation, often observed during significant slip events along fault planes, can result in increased thermal energy in the form of shear heating. This phenomenon occurs when frictional forces during fault slip convert mechanical energy into heat, raising the temperature of the surrounding rock. While thermo-mechanical coupling in the form of volumetric deformation is essential for understanding the behavior of reservoirs during operational campaigns, shear heating is often more relevant in the context of geological processes such as the origin and evolution of sedimentary basins. This form of coupling interacts with broader crustal and mantle dynamics, playing a role in the thermal history and tectonic evolution of regions (Souche et al., 2013). Understanding both forms of thermal coupling is key to improving reservoir management strategies, as they influence both the mechanical and thermal properties of the rock over time.

2.6.1.3.Hydrothermal Coupling

Hydrothermal coupling refers to the transfer of heat via fluid movement, a process that has been extensively studied both at the reservoir scale and within the broader basinial system (Blöcher et al., 2010; Cherubini et al., 2014). A less-explored aspect of this coupling is the feedback effect, wherein changes in temperature conditions directly influence the resulting pore pressure field. Thermal pressurization, which refers to the increase in pore pressure due to temperature changes, has typically been considered a secondary effect, often investigated under controlled laboratory conditions (Ghabezloo and Sulem, 2009). However, in the context of reservoir management, this feedback can have significant implications for reservoir behavior, especially in high-temperature environments where fluid dynamics and pressure variations are more pronounced.

The complexity of hydrothermal coupling is further compounded by the nonlinear interactions between geological structures, material properties, and state variables. Variations in in-situ conditions, such as the hydraulic, thermal, and mechanical states of the reservoir, directly influence transport properties like porosity and permeability (Blöcher et al., 2014; Fatt and Davis, 1952; Walder and Nur, 1984). For instance, changes in pore fluid pressure due to injection or production activities can alter the structure of the porous matrix. Injection-induced pore pressure can expand the porous space, thereby increasing porosity, whereas production-induced reductions in pore pressure may reduce porosity. Additionally, temperature fluctuations can induce volumetric deformation, affecting stress distribution within the matrix and further influencing the reservoir's transport properties (Ghabezloo et al., 2009; Zimmerman, 2000).

Moreover, variations in the thermodynamic state of the system can alter the properties of the fluid within the pores, potentially leading to buoyant components in the flow. Changes in temperature, pore pressure, or mineral composition may induce anomalies in fluid density and viscosity, which can disrupt the flow dynamics and give rise to unstable convective flow patterns (Elder, 1967). These dynamic changes can significantly affect reservoir productivity, as they influence fluid movement, heat transfer efficiency, and overall reservoir performance. Therefore, understanding hydrothermal coupling and its influence on the reservoir's thermodynamic and mechanical state is critical for optimizing reservoir management and improving the sustainability of geothermal energy production.

2.6.1.4.Impact of Coupled Processes on EGS Heat Production

(McDermott et al., 2006) studied the impact of different coupled processes, hydro-mechanical and thermo-mechanical, on the EGS heat production performance. His research indicated that the production rate is minimum when the fluid properties in the fractured reservoir are functions of only the fluid pressure and temperature while the rock mechanical properties are kept constant, that is, without considering the hydro-elastic or thermo-elastic interactions between the rock and fluid. Hence, a lower limit of the EGS thermal energy production rate may be estimated in the case that the physical properties of rock are constant in the system. Therefore, in our conceptual EGS reservoir model, we can reasonably assume that after the made-made fractures have been created by stimulation, the mechanical properties of the fractured reservoir remain unchanged during the period of heat production process.

The neglect of hydro-elastic and thermo-elastic interactions in Enhanced Geothermal Systems (EGS) modeling represents a significant simplification that can lead to underestimation of system performance. These coupled processes play a crucial role in the dynamic behavior of geothermal reservoirs. Hydro-elastic interactions, which involve the coupling between fluid flow and rock deformation, can alter fracture apertures and pore spaces as fluid pressure changes, potentially enhancing permeability and fluid flow. Concurrently, thermo-elastic interactions, arising from temperature-induced rock deformation, can create thermal stresses that may open new fractures or widen existing ones, further improving fluid circulation and heat transfer efficiency. The combined effect of these interactions often results in an increased surface area for heat exchange between the rock and circulating fluid, leading to more efficient heat transfer and improved overall system performance.

The dynamic nature of these interactions creates a complex, evolving reservoir system where properties change over time. Stress-dependent porosity, a key factor in fractured rock reservoirs, is significantly influenced by variations in effective stress due to fluid pressure and temperature changes. As thermal drawdown progresses, thermo-elastic effects can become more pronounced, potentially creating new flow channels and improving long-term heat extraction efficiency. The evolution of the fracture network, driven by both hydro-elastic and thermo-elastic processes, may lead to the reactivation of pre-existing fractures or the creation of new ones, potentially accessing previously untapped heat sources within the reservoir.

Models that neglect these interactions may underestimate the long-term performance of EGS, failing to capture potential improvements in heat extraction efficiency over time. While including these coupled processes in simulations provides more accurate predictions, it also significantly increases model complexity. Advanced numerical simulations employing thermo-hydro-mechanical (THM) coupling are often required to accurately capture these intricate processes. Despite the challenges in modeling, considering hydro-elastic and thermo-elastic interactions is crucial for a comprehensive understanding of EGS behavior and for optimizing long-term energy production strategies.

2.6.2. Complexity of Porous Rocks and Fault Zones

In homogeneous porous media, the interaction among natural physical processes are governed by the averaged material's porosity, permeability, and mechanical properties (Magri et al., 2015). On the other hand, fractured porous media introduces additional complexity to account for fracture geometry, fracture apertures, and fracture-matrix interactions (Dudun and Feng, 2024; Ma et al., 2023). While the fundamental principles of THM processes remain the same, the presence of fractures introduces non-linear behavior, dominating the overall response of the system to thermal, hydraulic, and mechanical forces. Fractures generally have higher permeability than the surrounding porous matrix acting as preferential pathways for fluid flow and heat transfer, significantly altering the dynamics of the system (Frampton, 2014).

Accurate modeling of fractured porous media is a complex task that necessitates a robust numerical system (Berre et al., 2019; Dudun and Feng, 2024) and an unstructured approach for generating high-quality mesh (Cacace and Blöcher, 2015). The robust numerical system is crucial for capturing the intricate physical processes, including fluid flow, heat transfer, and mechanical deformations, that occur within fractured porous media. Concurrently, the quality of the mesh used in the simulations significantly impacts the accuracy of the results. An unstructured approach to mesh generation ensures that the complex geometries of the fractures and the heterogeneities of the porous media are accurately represented. Techniques such as adaptive mesh refinement can be used to refine the mesh in regions of interest, thereby capturing the important features of the system.

2.7. Transport properties

Understanding the processes that control the transport properties of saturated porous media holds significant importance for various applications, including geothermal power production, energy storage, and hydrocarbon exploration. Variations in porosity and permeability, both spatially and temporally, play a crucial role in determining reservoir productivity and recovery (Blöcher et al., 2010; Raghavan and Chin, 2002; Walder and Nur, 1984). Alterations in pore pressure, temperature, and stress distributions, induced by fluid injection or production, can lead to changes in porosity and permeability. These alterations can be effectively described using the theories of poroelasticity and thermoelasticity (Bernabe, 1986, 1986; Han and Dusseault, 2003). Correlations between pore pressure and temperature changes, such as those resulting from the injection of cold fluid, and the in-situ stress field within a reservoir create strong and non-linear couplings between thermo-hydro-mechanical physical processes (Cacace and Jacquey, 2017). Quantifying these phenomena at the reservoir scale proves challenging due to technical limitations of available methods and tools. Therefore, a common approach in geomechanics is to conduct experiments in the laboratory under simple and controlled reference conditions to observe and quantify the phenomena of interest. Based on these experimental results, researchers can calibrate and incorporate this information into mathematical formulations for conducting numerical simulations at the reservoir scale.

Jacquey et al. (2015) provided a comprehensive description of porosity evolution resulting from hydro-mechanical coupling. This theory is firmly grounded in a robust theoretical foundation for poroelasticity (Biot, 1973; Biot and Willis, 1957; Zimmerman, 1990). They demonstrated that the increase in porosity diffuses from the injection fracture, as pore pressure is solely controlled by diffusion. Building upon this work, (Jacquey et al., 2016), outlined an approach for evaluating porosity considering thermo-hydro-mechanical (THM) coupling, following the theory of coupled thermo-poroelasticity (Ghabezloo et al., 2009; Ghabezloo and Sulem, 2009; McTigue, 1986; Zimmerman, 2000). They showed that thermoelastic effects dominate over porosity change, as the temperature distribution is not only controlled by diffusion but also by thermal advection, which is the most effective process around the injection. Consequently, the absolute increase in porosity due to thermoelastic effects is not localized solely at the injection point.

Understanding the processes that govern the transport properties of saturated porous media is essential for a variety of applications, such as geothermal power production, energy storage, and hydrocarbon exploration. Key properties like porosity and permeability vary across spatial and temporal scales, directly influencing reservoir productivity, recovery rates, and overall efficiency (Blöcher et al., 2010, p. 2012, 2010; Cacace et al., 2013; Raghavan and Chin, 2002). Changes in pore pressure, temperature, and stress distributions, whether from fluid injection, production activities, or natural occurrences, can alter porosity and permeability within the reservoir. These dynamic changes are effectively modeled through poroelastic and thermoelastic theories, which describe the mechanical behavior of fluid-saturated porous media under varying pressure and thermal conditions (Bernabe, 1986; Fatt and Davis, 1952; Han and Dusseault, 2003).

The complex, non-linear interactions between thermo-hydro-mechanical (THM) processes in a reservoir are further intensified by correlations between pore pressure, temperature fluctuations, and in-situ stress fields. These interdependencies are especially evident in scenarios involving the injection of cold fluids, where the induced changes in pore pressure and temperature propagate through the reservoir, resulting in strong couplings among THM processes (Cacace and Jacquey, 2017). Accurately quantifying these phenomena at the reservoir scale; however, poses significant challenges due to the technical limitations of existing observational and measurement tools. As a result, geomechanics researchers often rely on controlled laboratory experiments to simulate these conditions in a simplified environment, enabling the observation and quantification of key processes. Laboratory data are then used to calibrate mathematical models that can predict reservoir behavior on a larger scale through numerical simulations.

Jacquey et al. (2015) offered an extensive framework for understanding porosity evolution in response to hydro-mechanical coupling, drawing from a solid theoretical basis in poroelasticity (Biot, 1956; Biot and Willis, 1957; Zimmerman, 1990). Their work demonstrated that porosity increase disperses away from the injection point as pore pressure diffuses throughout the reservoir. Building on this, Jacquey et al. (2016) expanded the model to incorporate THM coupling, based on the theory of thermo-poroelasticity (Ghabezloo et al., 2009; Ghabezloo and Sulem, 2009; McTigue, 1986; Zimmerman, 2000). This approach revealed that thermoelastic effects can dominate the porosity change patterns within the reservoir, especially when thermal advection, rather than mere diffusion, affects temperature distribution around the injection site. Consequently,

the resulting porosity increase due to thermoelastic effects is not limited to the immediate vicinity of the injection point but disperses more broadly, highlighting the need to account for complex THM interactions when simulating reservoir behavior.

This integration of hydro-mechanical and thermo-hydro-mechanical couplings provides a refined framework for predicting porosity and permeability changes, thus enhancing our understanding of reservoir performance under various operational scenarios.

2.8. Assessing fault reactivation potential

The assessment of fault reactivation potential due to human activities holds paramount significance in the development of successful enhanced geothermal systems (EGS). This potential signifies the likelihood that alterations in the in-situ stress state, induced by human activities, might initiate seismic activity in previously dormant faults.

Induced seismicity can arise from various man-made activities (Theoretical Soil Mechanics (1943), By Karl Terzaghi, n.d.) , including reservoir-induced seismicity due to reservoir loading and fluid pressure effects (Talwani and Acree, 1985) , mining-induced seismicity, and seismicity related to fluid injection and withdrawal processes, such as those in oil and gas operations (Suckale, 2009) , wastewater disposal (Ellsworth, 2013) , Carbon Capture and Storage (CCS) (Zoback and Gorelick, 2012), and geothermal energy development (Zang et al., 2014).

In man-made geothermal reservoirs, hydraulic stimulation treatments are utilized to improve permeability. A common consequence of these treatments is a continuous increase in pore pressure, which has the potential to trigger seismic events. Understanding and managing these factors are essential to ensure the safe and efficient development of EGS projects.

These induced fractures, coupled with micro-seismic events, play a pivotal role in creating additional fractured flow paths, thereby boosting permeability and, subsequently, productivity. Hence, precise mapping of induced seismicity hypocenters, with high accuracy (in the order of tens of meters), allows for the visualization and estimation of the geometry and dimensions of the fracture network formed at depth during hydraulic stimulation of geothermal reservoirs (Fehler et al., 2001). However, induced seismicity is also recognized as a potential hazard, leading to the suspension of several international projects due to public concerns, as observed in places like Basel (Giardini, 2009; Häring et al., 2008) and St Gallen (Obermann et al., 2015), in Switzerland.

Within the context of the EU project GEISER, Zang et al. (2014) conducted a comprehensive analysis of induced seismicity related to geothermal operations in various tectonic settings. This study compared the seismic response to fluid injection across different European and global EGS sites with data from wastewater disposal, hydraulic fracturing, and ultra-deep fluid injection. The comparative analysis demonstrated that EGS stimulation, involving smaller fluid volumes compared to wastewater disposal wells, generally resulted in smaller maximum magnitudes. In reservoirs with multiple stimulation wells, seismicity was typically not triggered until the stress level of the previous stimulation was surpassed, following the well-known Kaiser Effect (Lavrov, 2003).

During EGS stimulation, larger magnitude events often occurred after shut-in at greater distances from the injection well. Regardless of geological differences, the probability of such events increased with the volume of injected fluids. Distinguishing between long-term injection operations (such as reservoir impoundment), wastewater disposal, and short-term fluid injection operations is crucial. Notably, short-term injections and EGS stimulations have shown a higher likelihood of producing larger events compared to hydraulic fracturing in oil and gas operations (Blöcher et al., 2018).

Preface to chapter 3

When investigating the risks associated with fractured porous media, it becomes evident that the injection of cold fluid into a hot reservoir would cause changes in the natural stress state of the reservoir. Cooler fluid injection into a hotter reservoir can cause thermal contraction in the rocks around the injection well. This contraction tends to move along the path of fluid flow and could potentially change the stress state of the rocks. Additionally, the cooler injected fluid could alter the properties of the reservoir fluid properties, such as viscosity and density, further impacting the pressure and stress distribution in the reservoir.

These changes in fluid properties and rock behavior due to fluid pressure and temperature differences can significantly impact the performance of a reservoir during production. They can affect the flow of fluids in the reservoir, the pressure distribution, the stress state, and even the stability of the reservoir. Therefore, it's important to consider these effects when performing reservoir simulations or making predictions about reservoir performance.

Several studies have investigated the effects of reservoir stimulation and short-term fluid injection and production on subsurface formations (Blöcher et al., 2018; Kivi et al., 2022; Moeck et al., 2009a). Their results demonstrate that in the short term, pore pressure changes on pre-existing faults or planes of discontinuities can significantly reduce the effective normal stress, thereby increasing the likelihood of rapid and larger seismic events.

However, the long-term effects of fluid injection and production on fault behavior are not well understood. While some studies (Blöcher et al., 2018; Jacquey et al., 2016) suggest that stress variations may play a role in the long term, there is currently a lack of comprehensive investigations on the performance of fault zones under prolonged thermal disturbances caused by cold fluid injection.

The potential effects of thermal contraction or expansion on the behavior of large ductile shear zones or other fault systems have not been extensively explored in the provided sources. Further research is needed to understand the interplay between pore pressure changes, thermal effects, and the long-term stability and deformation patterns of fault zones subjected to continuous fluid (re)injection and production operations.

Geological setting and methodology

In this study, we focus on a geothermal reservoir located in the northern part of Quebec, an area not connected to the main electrical grid of Canada and heavily reliant on fossil fuels for electricity and heat generation. A deep geothermal reservoir would provide an environmentally friendly source of energy for this region (Heidari et al., 2023a; Miranda et al., 2021). Our research is a preliminary study aimed at assessing the feasibility and the associated risks of seismic events of operating such a reservoir.

To achieve this, the geothermal model presented in this paper aims to simulate the thermal, hydraulic, and mechanical behavior of the reservoir during its operational phases, encompassing injection and production activities over an anticipated reservoir lifespan of approximately 100 years. The operational activities under investigation involve specific processes related to the (re)injection of cold water and the extraction of heated water. By simulating these processes over a century, we aim to assess the long-term sustainability of the reservoir and anticipate potential risks associated with such projects.

To quantify the intricate dynamics of pore pressure diffusion and thermal effects within a geothermal reservoir induced by the injection of cold fluid, we utilize a fully coupled Thermal-Hydro-Mechanical Finite Element Method (THM FEM) package named GOLEM (Cacace and Jacquey, 2017). Our focus is on understanding the influence of these mechanisms on fault slip tendency. GOLEM is built upon the Multiphysics Object Oriented Simulation Environment (MOOSE) framework, an object-oriented C++ finite element framework developed by the Idaho National Laboratory (Gaston et al., 2009), which enables a comprehensive simulation of coupled THM processes.

Within GOLEM, faults and fractures are conceptualized as lower-dimensional elements (2D), specifically single-nodded entities with zero thickness, embedded within the porous matrix (3D) filled with fluid. The length of the discrete faults and fractures serves as a representative measure of the Representative Elementary Volume (REV) of the porous matrix, enabling the application of a continuum framework to depict the porous medium.

Utilizing single-nodded finite elements ensures the continuity of gradients in both pore pressure and temperature across the fracture width while assuming the absence of shear and normal strain acting on the fault and fracture plane. Consequently, local fracture mechanics are neglected, and

fractures are solely considered to have distinct hydraulic and thermal behavior concerning the porous domain.

Moreover, the model accounts for the effects of micro-defects such as fissures and micro-cracks on the thermal, hydraulic, and mechanical behavior of the porous rock. These micro-defects predominantly influence the evolution of material properties in the system, including parameters like porosity and permeability.

Additionally, as stated earlier, we consider the fluid properties (i.e., Density and Viscosity) to be a function of pore pressure and temperature according to the IAPWS formulation (Huber et al., 2009; Wagner et al., 2000). This approach is crucial as it accounts for the variations in fluid properties under different subsurface conditions, which can significantly impact the thermal, hydraulic, and mechanical behavior of the geothermal reservoir. By incorporating these fluid property variations, our model can more accurately resemble the in-situ conditions and capture the complex interplay between the fluid and the porous rock matrix. This advancement in the modeling approach enhances the reliability and accuracy of our simulations, enabling a more comprehensive understanding of the reservoir dynamics.

3. Chapter 3: Numerical modeling of the long-term poromechanical performance of a deep enhanced geothermal system in northern Québec[1]

3.1. Abstract

This study numerically investigates the thermo-poromechanical effects in a Canadian geothermal reservoir caused by long-term fluid production and injection. Using finite element modeling, it explores pore pressure diffusion and thermal dynamics, incorporating both the geological structure of the rock mass and faults. The simulations utilize the IAPWS (International Association for the Properties of Water and Steam) equations to model fluid density and viscosity, ensuring realistic representations of heterogeneous pressure fields. The system replicates a doublet configuration within a faulted zone, featuring two hydraulically stimulated fractures. The primary aim is to assess the likelihood of fault reactivation under varying in-situ stress conditions over a 100-year geothermal operation. Results show that stress distribution is largely influenced by thermal stresses along the fluid circulation pathway, with fluid velocity and temperature gradients affecting reservoir stability. Minimal pore pressure changes highlight the dominant role of thermal stresses in controlling fault behavior. The analysis indicates no potential for fault reactivation, as slip tendency values remain below the critical threshold, even when accounting for reduced mechanical properties using the Hoek-Brown criterion. Thermal effects continue to influence the surrounding rock throughout the operational period, suggesting that the reservoir maintains mechanical stability conducive to sustained geothermal production and injection. These findings provide valuable insights into the long-term safety and behavior of geothermal reservoirs, offering important implications for future geothermal energy development and management strategies.

Keywords: Fault reactivation potential, Deep geothermal Reservoir, Thermo-Hydro-Mechanical (THM) coupled analysis, finite element method

[1] A version of this manuscript has been published in *Rock Mechanics Bulletin.* (Vadiee et al., 2025)

3.2. Introduction

Canada's remote northern communities, particularly those in subarctic and arctic regions, face significant energy challenges. These remote communities, which constitute a small but notable portion of the country's population, are heavily reliant on fossil fuels for both electricity generation and heating. Due to factors such as geographical isolation, harsh climate conditions, and limited infrastructure, the cost of energy production in these areas is substantially higher than in the more densely populated southern regions of the country (Sojoudi et al., 2024). Deep geothermal energy (DGE) has emerged as a promising strategic technology to enhance energy security in these off-grid communities, specifically, villages located in northern part of Quebec (Gascuel et al., 2024; Heidari et al., 2023b; Miranda et al., 2021; Sojoudi et al., 2024). The northern parts, characterized by its subarctic climate and high energy costs primarily due to diesel-based heating, presents a unique opportunity for geothermal development (Majorowicz and Minea, 2015). As global initiatives to reduce carbon emissions and mitigate climate change intensify, DGE systems offer a compelling alternative for heat and electricity generation in remote areas. In Northern Quebec, where the average heat flow density is relatively low, deep drilling to depths of several kilometers may be required to achieve temperatures suitable for power generation (around 80°C) (Majorowicz and Minea, 2015). While such depths present economic challenges, areas with higher-than-average heat flow and enhanced permeability could make geothermal energy extraction feasible. However, the path to sustainable geothermal development is not without challenges. A primary concern is the risk of induced seismic activity (Foulger et al., 2018; Li et al., 2024; Parisio et al., 2019). Induced seismicity refers to seismic events triggered by human activities that alter the earth's inherent stress conditions which can be caused by various anthropogenic activities, including, fluid injection and withdrawal associated with geothermal operations (Ellsworth, 2013; Zang et al., 2014; Zoback and Gorelick, 2012), underground storage of heat, hydrogen, carbon dioxide, or other fluids, and other subsurface activities that perturb the local stress field (Suckale, 2009). The potential for induced seismicity necessitates careful site selection, continuous monitoring, and adaptive management strategies in geothermal energy development projects, particularly in regions like Northern Quebec where the geological conditions may present unique challenges.

One of the primary causes of induced seismicity is the high-pressure injection of fluids during geothermal plant operations which can reactivate dormant faults or create new ones, leading to

seismic events (Buijze et al., 2017; Ellsworth, 2013; Grigoli et al., 2018). This risk is particularly significant because fluid injection can increase pore pressure within faults, thereby altering the stress conditions and potentially triggering seismic activity. Although these induced seismic events are typically of smaller magnitude compared to natural earthquakes, they can still be significant enough to cause concern, especially in populated areas. This seismic risk necessitates rigorous geological surveys and robust monitoring systems to mitigate potential hazards.

To better understand and predict the behavior of geosystems under various environmental and operational conditions, such as in geothermal reservoirs and hydrocarbon extraction, studying the complex interplay of thermal, hydraulic, and mechanical phenomena that naturally occur within porous media is crucial (Cacace and Jacquey, 2017; Heidari et al., 2023b; Li et al., 2018). These coupled Thermo-Hydro-Mechanical (THM) processes are particularly important in the context of homogeneous and fractured porous media (Chen, 2024; Cui and Wong, 2022). The development of Partial Differential Equations (PDEs) for these classes of porous media has been instrumental in advancing our understanding of these systems (Magri et al., 2015). Compared to homogenous porous media where the interaction among natural physical properties is governed by averaged material's porosity, permeability, and mechanical properties (Magri et al., 2015), fractured porous media introduces additional complexity to account for fracture geometry, fracture apertures, and fracture-matrix interactions (Dudun and Feng, 2024; Ma et al., 2023). While the fundamental principles of THM processes remain the same, the presence of fractures introduces non-linear behavior, dominating the overall response of the system to thermal, hydraulic, and mechanical forces. Fractures generally have higher permeability than the surrounding porous matrix acting as preferential pathways for fluid flow and heat transfer, significantly altering the dynamics of the system (Frampton, 2014).

Accurate modeling of fractured porous media is a complex task that necessitates a robust numerical system (Berre et al., 2019; Dudun and Feng, 2024) and an unstructured approach for generating high-quality mesh (Cacace and Blöcher, 2015). The robust numerical system is crucial for capturing the intricate physical processes, including fluid flow, heat transfer, and mechanical deformations, that occur within fractured porous media. Concurrently, the quality of the mesh used in the simulations significantly impacts the accuracy of the results. An unstructured approach to mesh generation ensures that the complex geometries of the fractures and the heterogeneities of

the porous media are accurately represented. Techniques such as adaptive mesh refinement can be used to refine the mesh in regions of interest, thereby capturing the important features of the system.

When investigating the risks associated with fractured porous media, it becomes evident that the injection of cold fluid into a hot reservoir would cause changes in the natural stress state of the reservoir. Cooler fluid injection into a hotter reservoir can cause thermal contraction in the rocks around the injection well. This contraction tends to move along the path of fluid flow and could potentially change the stress state of the rocks. Additionally, the cooler injected fluid could alter the properties of the reservoir fluid properties, such as viscosity and density, further impacting the pressure and stress distribution in the reservoir. These changes in fluid properties and rock behavior due to fluid pressure and temperature differences can significantly impact the performance of a reservoir during production. They can affect the flow of fluids in the reservoir, the pressure distribution, the stress state, and even the stability of the reservoir. Therefore, it's important to consider these effects when performing reservoir simulations or making predictions about reservoir performance.

Several studies have investigated the effects of reservoir stimulation and short-term fluid injection on subsurface formations (Blöcher et al., 2018; Kivi et al., 2022; Moeck et al., 2009a). Their results demonstrate that in the short term, pore pressure changes on pre-existing faults or planes of discontinuities can significantly reduce the effective normal stress, thereby increasing the likelihood of rapid and larger seismic events. However, the long-term effects of fluid injection and production on fault behavior are not well understood. While some studies (Blöcher et al., 2018; Jacquey et al., 2016) suggest that stress variations may play a role in the long term, there is currently a lack of comprehensive investigations on the performance of the fractured porous media in the vicinity of the fault zones under prolonged thermal disturbances caused by cold fluid injection. The potential effects of thermal contraction or expansion on the behavior of large ductile shear zones or other fault systems have not been extensively explored in the provided sources. Further research is needed to understand the interplay between pore pressure changes, thermal effects, and the long-term stability and deformation patterns of fault zones subjected to continuous fluid injection and production operations.

In this preliminary study, we aim to assess the feasibility and the associated risks of seismic events of operating a geothermal reservoir in Northern Quebec. We utilize the International Association for the Properties of Water and Steam (IAPWS-IF97) formulations (Huber et al., 2009; Wagner et al., 2000) for region 1, where water predominantly exists in a liquid state (Parisio et al., 2019), to accurately represent the thermodynamic properties of the fluid phase. Here, fluid density and viscosity are treated as functions of fluid temperature and fluid pressure. This approach accounts for changes in fluid density within the fractures relative to the fluid flow within the reservoir. The adoption of IAPWS-IF97 offers several advantages over ad-hoc methods, including uniformity across diverse calculations and applications, adherence to established thermodynamic principles and experimental observations and ensuring reliability in calculated fluid properties. Additionally, fluid flow and pressure in a system depend on fracture apertures, which are influenced by the local mechanical stress field and fluid pressure. Thermal conduction through the rock and fluid, along with advection and convective heat transfer in the fluid, can affect the fluid-rock interaction. Changes in fluid density and viscosity can influence these thermal effects, potentially impacting the efficiency of operations such as hydraulic fracturing (Berre et al., 2019; Wang et al., 2022).

Furthermore, fractures can cause local stress concentration points and areas of large pressure gradients, leading to changes in the mechanical behavior of the material (Berre et al., 2019; Tsang, 2024). Changes in fluid density and viscosity can influence these stress concentrations and pressure gradients, affecting the overall behavior of the system.

The aim of this study is twofold. First, we present a comprehensive framework for analyzing efficient geothermal energy extraction systems and predicting the long-term sustainability of reservoirs over an extended 100-year operational period. The strength of our simulation lies in its ability to model long-term reservoir behavior effectively with relatively low computational cost, a significant advantage over existing studies that focus on shorter time scales or smaller-scale simulations. Our large-scale simulation incorporates a fault and two hydraulically fractured regions, each with distinct material properties, allowing for a more accurate representation of the domain. This approach captures the unique characteristics of fractures and faults, which act as preferential pathways for fluid flow and heat transfer.

Secondly, our work focuses on the long-term thermal effects on slip tendency, an aspect that has not been extensively studied in previous research for our region of interest. This consideration is

crucial for assessing the risk of induced seismicity and fault reactivation during geothermal operations. Furthermore, we incorporate the reduced mechanical properties suggested by the Hoek-Brown failure criterion (Hoek and Brown, 1997; Hoek and Brown, 2019; Hoek and Diederichs, 2006) to account for the presence of micro-defects, fractures, and bedding folds in rocks. This approach is particularly relevant for accurately representing the strength and deformability of jointed rock masses, which is essential for predicting the mechanical behavior of the reservoir.

By combining these key features, our work presents a comprehensive framework for analyzing efficient geothermal energy extraction systems, predicting long-term reservoir sustainability, and assessing the risk of induced seismicity. The incorporation of fractures, faults, and reduced mechanical properties, along with the consideration of thermal effects on slip tendency, sets our work apart from existing studies.

3.3. Mathematical formulation of Coupled THM processes in pressurized fractured geothermal reservoir

To evaluate the thermal, hydraulic, and mechanical response resulting from a projected 100-year production and injection period at the geothermal test site in northern Quebec, a numerical investigation of the reservoir has been conducted. This investigation involves the modeling of implicitly coupled and nonlinear thermal-hydraulic-mechanical (THM) processes within a fractured porous reservoir. In this study, we utilize the GOLEM simulator (Cacace and Jacquey, 2017), which is built upon the flexible, object-oriented MOOSE framework (Gaston et al., 2009).

Within this framework, faults and fractures are conceptualized as two-dimensional (2D) entities with zero thickness embedded in a three-dimensional (3D) porous matrix. This porous matrix is assumed to be saturated with fluid. Such an approach is advantageous as it allows the fractures and faults to be represented as discrete entities that interact with the surrounding porous medium.

The finite-element discretization employed in this study is based on the weak form of the system of partial differential equations governing fluid flow, mechanical deformation, and energy balance. The weak form allows for the transformation of these differential equations into an integral form, facilitating their numerical solution. To represent the porous matrix, Cacace and Jacquey (2017) consider a representative elementary volume (REV) in which the length of discrete fractures and

faults is significantly smaller than the dimensions of the REV itself. This approach allows for the homogenization of the fractured porous medium, enabling the effective properties of the matrix to be defined in terms of averaged parameters. In this framework, fractures are embedded within the REV, and their interactions with the surrounding porous matrix are captured through effective permeability and porosity values. The coupling between fractures and the porous matrix is addressed by incorporating fracture-specific characteristics such as aperture and orientation, which influence fluid flow and heat transport.

By adopting this methodology, the GOLEM simulator accounts for both the heterogeneity of the porous matrix and the discrete nature of fractures, allowing for a more accurate representation of the THM processes within the reservoir. The REV-based modeling also facilitates a more computationally efficient solution compared to explicitly resolving each fracture individually, thus enabling the simulation of complex scenarios over extended production and injection periods.

Mathematically, (Cacace and Jacquey, 2017) consider a closed domain of volume $\Omega \subset R^n$ bounded by a boundary $\Gamma \subset R^{(n-1)}$. Given the high aspect ratio characteristic of fractures, these features are modeled as lower-dimensional elements of volume $\Omega_f \subset R^{(n-1)}$ and surface area $\Gamma \subset R^{(n-2)}$.

The following section briefly outlines the governing equations for groundwater flow, heat transport, and rock deformation. These equations are derived from the principles of mass balance, energy balance, and momentum balance, respectively. Further details on their numerical implementation can be found in Cacace and Jacquey (2017).

3.3.1. Fluid flow within porous media

The governing equation for the fluid pressure is derived from the principle of conservation of mass and is expressed as below:

$$\frac{1}{M_b}\frac{\partial p_f}{\partial t} - \alpha\beta_b\frac{\partial T}{\partial t} + \alpha\dot{\epsilon}_{kk} + (1-\alpha)\dot{\epsilon}_{kk}^{*p} + \nabla\cdot\boldsymbol{q}_D + \boldsymbol{q}_D\cdot\left(\frac{1}{K_f}\nabla p_f - \beta_f\nabla T\right) + \boldsymbol{v}_s\cdot\left(\frac{1}{M_b}\nabla p_f - \beta_b\nabla T - \frac{1}{K_s}\nabla\bar{\sigma}'\right) = 0 \quad (1)$$

In this equation, the first term captures the rate of change of pore fluid pressure (p_f) over time, scaled by the specific storage, indicating how temporal variations in pressure influence fluid flow

within the porous medium. Here, $1/M_b$ represents the specific storage of the porous medium, defined as $\frac{n}{K_f} + \frac{(\sigma - n)}{K_s}$, where K_f, K_s and n denote fluid bulk modulus, solid bulk modulus, and porosity, respectively.

The second term ($\alpha\beta_b \frac{\partial T}{\partial t}$) illustrates the impact of temperature changes on the pore pressure field through thermal expansion or contraction, highlighting the thermal influence on fluid dynamics. This term represents the conductive heat transfer processes. The coefficient $\alpha = 1 - K/K_s$ represents the Biot coefficient, where K denotes the drained bulk modulus of the porous medium. The term $\beta_b = n\beta_f + (1 - n)\beta_s$ stands for the bulk volumetric thermal expansion coefficient, where $\beta_f = -\frac{1}{\rho_f} \left(\frac{\partial \rho_f}{\partial T}\right)_{p_f}$ and β_s are the fluid and solid grain's volumetric thermal expansion coefficient, respectively.

The third term ($\alpha\dot{\epsilon}_{kk}$) captures the mechanical influence on the fluid flow, showing how volumetric changes in the porous medium affect the pressure. Here, the term $\dot{\epsilon}_{kk} = \nabla \cdot \dot{\boldsymbol{u}} = \nabla \cdot \boldsymbol{v_s}$ represents the volumetric strain rate, where $\boldsymbol{v_s}$ is the velocity of solid matrix. The Biot coefficient (α) scales this term to relate the mechanical deformation to changes in fluid pressure.

The fourth term ($(1 - \alpha)\dot{\epsilon}_{kk}^{*p}$) accounts for the plastic strain rate, emphasizing how the inelastic behavior of the medium contributes to changes in the fluid pressure. It highlights the distinction between the effects of elastic and plastic deformation on pore pressure evolution.

The fifth term ($\nabla \cdot \boldsymbol{q}_D$) relates to the Darcy velocity, defined as $\boldsymbol{q}_D = -\frac{\boldsymbol{\kappa}}{\mu_f} \cdot \left(\nabla p_f - \rho_f \boldsymbol{g}\right)$, where $\boldsymbol{\kappa}$ signifies permeability tensor, μ_f is fluid viscosity, ρ_f is fluid density, and $\boldsymbol{g}$ is the gravitational acceleration vector. This expression governs the fluid transport within the porous medium, describing how fluid flow is driven by pressure gradients and gravitational forces. In other words, this term represents the diffusive transport in the context of pressure differences.

The sixth term ($\boldsymbol{q}_D \cdot \left(\frac{1}{K_f}\nabla p_f - \beta_f \nabla T\right)$) describes nonlinear advective effects caused by the interaction of fluid velocity with the pressure gradient and temperature gradient, indicating how fluid movement influences the distribution of pressure and temperature in the system. This term relates to convection, representing the advective effect of the solid matrix velocity on the gradients

of pore pressure, temperature, and mean effective stress. The seventh term ($\boldsymbol{v}_s \cdot \left(\frac{1}{M_b}\nabla p_f - \beta_b \nabla T - \frac{1}{K_s}\nabla \bar{\sigma}'\right)$) represents the advective effect of the solid matrix velocity on the gradients of pore pressure, temperature, and mean effective stress ($\bar{\sigma}'$), indicating how the solid-phase motion affects the transport and distribution of these quantities.

Beyond delineating the governing equation for fluid flow within porous media, precise estimation of fluid properties holds paramount importance across a spectrum of engineering applications, ranging from power generation to chemical processing. To facilitate this, the IAPWS-IF97 formulation, established by the International Association for the Properties of Water and Steam (IAPWS) (Wagner et al., 2000), furnishes a standardized methodology for computing the thermodynamic characteristics of ordinary water and steam.

3.3.2. Fluid Properties of ordinary water

The International Association for the Properties of Water and Steam (IAPWS) formulation defines the thermodynamic properties of water by dividing them into five distinct regions, each designed to accurately represent different temperature and pressure ranges. **Fig. 4** illustrates the five regions within the entire range of validity of the IAPWS-IF97 formulation. While the boundaries between most regions can be directly inferred from the figure, the specific demarcation between regions 2 and 3 requires additional consideration.

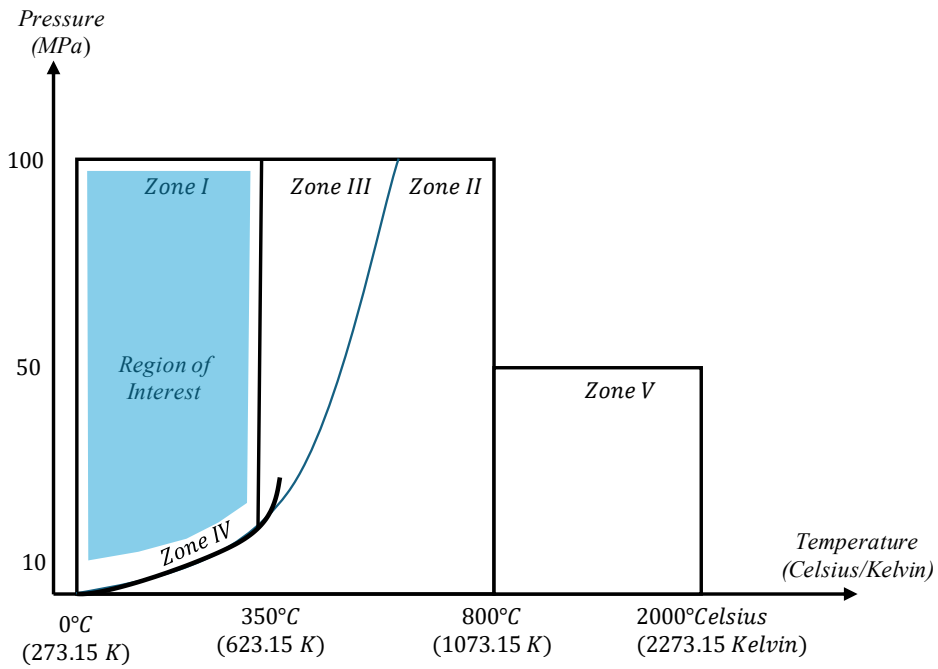

Fig. 4. Regions of IAPWS-IF97, modified after Cooper and Dooley (2007).

For our analysis, we assessed the temperature and pressure profiles obtained from the geothermal test site and determined that the in-situ conditions fall within region 1 of the IAPWS-IF97 framework. This region represents liquid water and spans temperatures from 0°C (273.15 K) to 350°C (623.15 K) and pressures up to 100 MPa. Region 1 is characterized using a formulation based on the Gibbs free energy equation, which provides a reliable basis for thermodynamic calculations under these conditions.

In region 1, the Gibbs equation of state stands as a fundamental cornerstone in the study of thermodynamic properties, offering a concise representation of a fluid's behavior in terms of its pressure, temperature, and specific volume. In the context of ordinary water, this equation takes on a dimensionless form, expressed in terms of reduced variables $p_{f,r}$ and $T_{f,r}$, also known as dimensionless input parameters. Here, $p_{f,r} = p_f/p_f^*$ represents the reduced pressure and $T_{f,r} = T_f^*/T_f$ signifies the inverse of reduced temperature, each scaled relative to reference values typically derived from critical properties. P_f and T_f denote the actual pressure and temperature of the fluid, while $p_f^* = 16.53\ MPa$ and $T_f^* = 1112.85°C\ (1386\ K)$ stand as the reference pressure and temperature of ordinary water, respectively.

The equation,

$$\gamma(p_{f,r}, T_{f,r}) = \sum_{i=1}^{34} n_i (7.1 - p_{f,r})^{I_i} (T_{f,r} - 1.222)^{J_i} \quad (2)$$

captures the dimensionless Gibbs free energy, $\gamma(p_{f,r}, T_{f,r})$, as a function of reduced pressure ($p_{f,r}$) and inverse of reduced temperature ($T_{f,r}$). Here, n_i, I_i and J_i represents coefficients derived from empirical data, and their values are available in (Wagner et al., 2000) and (Cooper and Dooley, 2007). These coefficients encapsulate the intricate thermodynamic behavior of ordinary water across various pressure and temperature regimes. The calculation of the Gibbs free energy entails the summation of terms over the provided coefficients, each term influenced by powers of $(7.1 - p_{f,r})$ and $(T_{f,r} - 1.222)$, thereby encapsulating the complex interplay of ordinary water's molecular interactions under differing conditions. The resultant dimensionless Gibbs free energy serves as a pivotal quantity, facilitating the derivation of numerous thermodynamic properties such as density, enthalpy, viscosity, and entropy.

3.3.2.1.Fluid Density

For the single-phase liquid region, denoted as region 1, the formulation is based on the dimensionless Gibbs free energy as the fundamental equation of state. By employing the following relation, the density of fluid can be determined:

$$\rho_f = \frac{P_f^*}{RT_f(\gamma'_{p_{f,r}})} \quad (3)$$

where P_f^* is the reference fluid pressure, T_f is the actual temperature in kelvin, $R = 0.461526\ kJ\ kg^{-1}\ K^{-1}$ is the specific gas constant of ordinary water, and $\gamma'_{p_{f,r}}$ is the derivative of Dimensionless Gibbs free energy with respect to reduced pressure ($p_{f,r}$):

$$\gamma_{p_{f,r}} = \left(\frac{\partial \gamma}{\partial p_{f,r}}\right)_{T_{f,r}} = \sum_{1}^{34} \left[-n_i I_i (7.1 - p_{f,r})^{I_i - 1} (T_{f,r} - 1.222)^{J_i}\right] \quad (4)$$

In essence, the IAPWS-97 formulation (Cooper and Dooley, 2007; Wagner et al., 2000) incorporates the temperature and pressure dependence of density through the fundamental dimensionless Gibbs free energy equation, which is an empirical polynomial fit to a wide range of experimental data. This allows accurate modeling of density over the entire liquid region.

3.3.2.2.Fluid properties (Viscosity)

The IAPWS-97 formulation (Huber et al., 2009) provides a means to accurately calculate the viscosity of ordinary water substances in the single-phase liquid region, denoted as region 1. Viscosity is an important transport property that governs the flow behavior and energy dissipation in fluid systems. Viscosity of ordinary water is represented by the following equation:

$$\bar{\mu} = \bar{\mu}_0(\bar{T}) \times \bar{\mu}_1(\bar{T}, \bar{\rho}) \times \bar{\mu}_2(\bar{T}, \bar{\rho}) \tag{5}$$

Here, $\bar{\mu}_0$ represent the viscosity in the dilute-gas limit and is given by:

$$\bar{\mu}_0(\bar{T}) = \frac{100\sqrt{\bar{T}}}{\sum_{i=0}^{3} \frac{H_i}{\bar{T}^i}} \tag{6}$$

The term, $\bar{\mu}_1$ accounts for the contribution to viscosity due to finite density and is expressed as:

$$\bar{\mu}_1(\bar{T}, \bar{\rho}) = \exp\left[\bar{\rho} \sum_{i=0}^{5} \left(\frac{1}{\bar{T}} - 1\right)^i \sum_{j=0}^{6} H_{ij}(\bar{\rho} - 1)^j\right] \tag{7}$$

Finally, $\bar{\mu}_2$ represents the critical enhancement of viscosity, which is significant only in a very small region in density and temperature around the critical point of the fluid.

The critical enhancement function, $\overline{\mu_2}$, is defined as:

$$\overline{\mu_2} = \exp\,(x_\mu Y) \tag{8}$$

For more information regarding the fluid viscosity calculation and the coefficient values, readers are referred to (Huber et al., 2009).

3.3.3. Heat transport within porous media

The partial differential equation (PDE), governing heat transfer, is derived from the energy balance equation for the fluid-rock mixture, assuming local thermodynamic equilibrium among two phases. This equilibrium implies that all phases (solid, liquid) within a small volume of the system are at the same temperature, with instantaneous heat transfer between them. Consequently, under this assumption, the contributions of different phases can be superposed or added together, as each phase is presumed to be in equilibrium with the others, enabling the study of their individual behaviors separately and then in combination. When the system is in local thermodynamic equilibrium and the phase contributions are superposed, terms related to phase changes (e.g., melting, evaporation) cancel out in the combined equations for the individual phases.

The governing equation takes the following form:

$$T\frac{\partial(\rho c)_{\mathrm{b}}}{\partial t}+(\rho c)_{\mathrm{b}}\frac{\partial T}{\partial t}+T_0\beta_{\mathrm{b}}\dot{\epsilon}_{kk}^{\mathrm{e}}+\nabla\cdot(\rho_{\mathrm{f}}c_{\mathrm{f}}\boldsymbol{q}_{\mathrm{D}}T-\lambda_{\mathrm{b}}\nabla T)-\dot{H}=0 \tag{9}$$

The first term on the left-hand side accounts for secondary, non-Boussinesq dissipative effects associated with the pressure-temperature dependence of bulk storage. This term can be rewritten considering only variable fluid and solid density as follows:

$$T\frac{\partial(\rho c)_{\mathrm{b}}}{\partial t}=(1-n)c_{\mathrm{s}}T\left(\frac{\rho_{\mathrm{s}}}{K_{\mathrm{s}}}\frac{\partial p_{\mathrm{f}}}{\partial t}-\rho_{\mathrm{s}}\beta_{\mathrm{s}}\frac{\partial T}{\partial t}\right)+nc_{\mathrm{f}}T\left(\frac{\rho_{\mathrm{f}}}{K_{\mathrm{f}}}\frac{\partial p_{\mathrm{f}}}{\partial t}-\rho_{\mathrm{f}}\beta_{\mathrm{f}}\frac{\partial T}{\partial t}\right) \tag{10}$$

The third term of the **Eq. 9** within the energy balance equation ($T_0\beta_{\mathrm{b}}\dot{\epsilon}_{kk}^{\mathrm{e}}$) denotes the thermoelastic dissipation rate term, reflecting the heat generated through thermoelastic deformation within the solid matrix of the porous medium. Thermoelastic deformation pertains to alterations in the shape and dimensions of a solid matrix resulting from temperature fluctuations. When subjected to temperature changes, a solid matrix undergoes expansion or contraction, leading to changes in volume that produce heat, a phenomenon termed thermoelastic dissipation. In the context of the provided equation, T_0 represents a reference temperature, β_s signifies the thermal expansion coefficient of the solid matrix, and $\dot{\epsilon}_{kk}^{\mathrm{e}}$ denotes the volumetric strain rate due to effective stress. The product of these factors yields the heat generated due to thermoelastic deformation.

Additionally, $(\rho c)_b = n\rho_f c_f + (1-n)\rho_s c_s$ represents the bulk-specific heat of the porous medium, T_0 denotes the absolute temperature of the stress-free porous medium, $\lambda_b = n\lambda_f + (1-n)\lambda_s$ stands for the bulk thermal conductivity, and $\dot{H}$ signifies the rate of energy production.

3.3.4. Solid displacement

The governing equation that explains the mechanical behavior of fluid-saturated porous media results from momentum balance in terms of effective Cauchy stress tensor and is represented as:

$$\nabla\cdot\left(\boldsymbol{\sigma}'-\alpha p_f\mathbb{I}\right)+\rho_b\boldsymbol{g}=0 \tag{11}$$

where $\boldsymbol{\sigma}'=\boldsymbol{\sigma}+\alpha p_f\mathbb{I}$ is the effective stress tensor, $\mathbb{I}$ represents the rank-two identity tensor, $\rho_b = n\rho_f + (1-n)\rho_s$ denotes the bulk density of the fluid-solid mixture, and α is the Biot coefficient. The first term represents the forces due to the effective stress in the medium, the second term represents the forces due to fluid pressure, and the third term represents the body forces.

The deformation of a solid skeleton is described in terms of thermo-poroelastic response (Biot's consociations theory) and dissipative plastic behavior. To simplify the presentation of the constitutive mechanical model, only small strain conditions ($\boldsymbol{\epsilon} = \frac{1}{2}(\nabla \boldsymbol{u} + \nabla^T \boldsymbol{u}) = \nabla^s \boldsymbol{u}$) have been considered.

Following Biot's theory, the (effective) stresses are related to total strain via the following relationship:

$$\dot{\boldsymbol{\sigma}}' = \mathbb{C}: (\dot{\epsilon}) \tag{12}$$

where $\mathbb{C}$ is the rank-four elastic stiffness tensor defined as $\mathbb{C} = \mathbb{C}_{ijkl} = \gamma \delta_{ij} \delta_{kl} + 2G \delta_{ik} \delta_{jl}$, and λ and G are the first (volumetric) and second (shear) Lamé moduli, respectively. Also, the total strain is defined as the sum of elastic strain (ϵ^e) and eigenstrain components of the total tensor (ϵ^*).

3.3.5. Porosity Evolution:

The equation for the evolution of porosity (n) is given by:

$$\frac{\partial n}{\partial t} = \frac{(\alpha - n)}{K_s} \frac{\partial p_f}{\partial t} - \beta_n \frac{\partial T}{\partial t} + (\alpha - n)\dot{\epsilon}_{kk} + (1 - \alpha)\dot{\epsilon}_{kk}^{*p} + \boldsymbol{v}_s \cdot \left(\frac{(\alpha - n)}{K_s} \nabla p_f - (1 - n)\beta_s \nabla T - \frac{1}{K_s} \nabla \bar{\sigma}' - \nabla n \right) \tag{13}$$

This equation captures how the porosity of a porous medium evolves over time due to fluid pressure influence (first term), thermal effects (second term), mechanical deformation (third term), and a second order term that represents the advective transport of porosity changes influenced by fluid flow. It combines the effects of gradients in pore fluid pressure, temperature, effective stress, and porosity itself, as influenced by the solid phase velocity ($\boldsymbol{v_s}$).

3.3.6. Permeability Evolution:

Rock permeability evolution follows a classical Kozeny–Carman-like relation, incorporating information about pore and grain geometries:

$$\mathrm{K} = A \frac{n_i^3}{(1 - n_i)^2} \tag{14}$$

Here, the subscript i refer to each numerical strep, $A = \frac{\boldsymbol{k_0}\,(1-n_0)^2}{(n_0)^3}$ is a constant factor calculated based on the initial permeability tensor, $\boldsymbol{\kappa_0}$, and initial porosity, n_0. In the introduced porosity-permeability relationship, permeability is assumed to depend only on the porosity of the sample. Changes in the shape of pores and the evolution of their interconnectivity have been neglected.

3.3.7. Fault reactivation potential

In pressurized reservoirs, the in-situ stress state undergoes alteration which can potentially lead to induced seismicity. These fluctuations in stress level are due to the injection of cold fluid into a hot reservoir, which induces variations in fluid pressure and temperature and eventually can lead to the reactivation of the pre-existing fault zones or fracture planes. This reactivation of faults and fracture planes during geothermal operations largely depends on the initial stress conditions acting on these planes of weakness (Blöcher et al., 2018).

To evaluate the reactivation potential of any planes of weakness, including faults, fractures, and bedding planes, under ambient stress forces conditions, a slip tendency analysis (ST analysis) is commonly conducted. This analysis hinges on the concept that the fault or fracture reactivation is governed by the ratio of the resolved shear stress to the effective normal stress on the fault surface. Hence, *ST* is mathematically defined as the ratio between the absolute magnitudes of resolved shear and effective normal stresses acting on the fault plane (Morris et al., 1996).

$$ST = \frac{\|\tau\|}{\|\sigma_n - \alpha p_f\|} = \frac{\|\tau\|}{\|\sigma_n'\|} \tag{15}$$

where τ represents the magnitude of the resolved shear stress, σ_n signifies the normal stress acting on the plane of structural weakness, p_f indicates the fluid pressure within the reservoir, α stands for the effective stress coefficient, often referred to as Biot's poroelastic coefficient, and σ_n' represent the effective normal stress acting on the fault's plane. In this simulation, the coefficient α is treated as a constant with a fixed value of 0.8086.

Slip is likely to occur when the resolved shear stress responsible for initiating movement equals or exceeds the cohesive strength and the coefficient of static friction (μ_s). This phenomenon is described by the Mohr-Coulomb failure criterion (Labuz and Zang, 2012) as:

$$\tau \geq S_0 + \mu_s \cdot \sigma_n' \tag{16}$$

$$ST \geq \frac{S_0}{\sigma_n'} + \mu_s \tag{17}$$

where S_0 represents the cohesion parameter of the fault, and μ_s denotes the coefficient of friction associated with the fault. Jaeger (2012) assumes that when the shear fracture develops, the rock possesses no cohesion across the fracture plane. In this case, where the cohesion (S_0) is zero, slip occurs when the slip tendency (ST) is greater than or equal to the coefficient of static friction (μ_s):

$$ST \geq \mu_s \tag{18}$$

In the experimental work conducted by Byerlee (1978), the coefficient of friction (μ_s) was determined to be greater than or equal to 0.85 for confining pressures up to $200\ MPa$. At higher confining pressure conditions, μ_s was found to be greater than or equal to 0.6. Once the slip tendency is determined, it becomes possible to calculate the extent to which the fault can withstand an increase in fluid pressure before failure occurs. This information is crucial in understanding the fault's stability and predicting potential seismic activity associated with geothermal operations.

3.3.8. Strength of rock mass

The strength parameters and mechanical characteristics of paragneiss rock were estimated using the Hoek–Brown classification for rock masses (Hoek and Brown, 2019). Hoek et al. (2000) suggest the following empirical failure criterion between the maximum and the minimum principal stresses at failure:

$$\sigma_1 = \sigma_3 + \sigma_{ci}\left(m_b \frac{\sigma_3}{\sigma_{c,i}} + s\right)^a \tag{19}$$

Key parameters considered the uniaxial compressive strength $\sigma_{c,i}$ of the intact rock, which is the strength of the intact rock at ambient pressure, alongside material constants s, m_b, and a, contingent upon rock mass traits, and σ_1 and σ_3 are the major and minor principal stresses at failure, respectively. The s value accounts for rock mass disturbance due to fractures and weathering, while m_b reflects the geometrical configuration of intact rock mass fragments. Hoek and Brown (1997) advised to utilize the findings from a minimum of five triaxial compression tests performed on intact samples with a diameter of approximately 50 mm.

$$m_b = m_i\ e^{\left[\frac{GSI-100}{(28-14D)}\right]} \tag{20}$$

$$s = e^{\left[\frac{GSI-100}{(9-3D)}\right]} \tag{21}$$

$$a = \frac{1}{2} + \frac{1}{6}\left(e^{-\frac{GSI}{15}} - e^{-\frac{20}{3}}\right) \tag{22}$$

In the provided equations, the term D signifies a dimensionless disturbance factor linked to damage resulting from excavation blasting or stress relaxation, ranging from 0 to 1, as determined by Hoek and Brown (2019). GSI, denoting Geological Strength Index, represents a dimensionless value characterizing the rock mass strength based on intact rock properties, typically derived from exposed rock formations. For intact rock, the material constant s and a are 1 and 0.5, respectively, and $m_b = m_i$.

The generalized Hoek and Diederichs (2006) equation employs the intact rock modulus of deformation (E_i), Geological strength index(GSI), and disturbance factor (D) to calculate the reduced rock mass modulus of deformation (E_{rm}). It is conventionally understood that intact rock possesses higher elastic moduli compared to the rock mass. This distinction stems from the assumption that intact rock constitutes a continuous and homogeneous material with fewer inherent defects or weaknesses, unlike rock mass with diminished strength. They recommended using the following equation for estimating the deformation modulus of rock masses:

$$E_{rm} = E_i\left[0.02 + \frac{1-\frac{D}{2}}{1+e^{\left[\frac{60+15D-GSI}{11}\right]}}\right] \tag{23}$$

3.3.9. Equivalent Mohr-Columb parameters

In this study, the generalized Hoek–Brown criterion was employed for the analysis of underground enhanced geothermal systems. In this specific context, it is advantageous to articulate the rock mass strength in terms of principal effective stresses. This approach enables a direct comparison with the principal effective stresses induced in the reservoir, thereby simplifying the evaluation of the potential for overstressing and failure, by the means of injecting higher volumes of geothermal fluid. Notably, effective stress accounts for the pore water pressure within the rock mass, resulting in a more precise depiction of the stresses that influence rock mass stability.

To establish the corresponding Mohr failure envelope, Hoek (1994b) proposed a numerical approach in which the general solution of Balmer (1952) was employed to generate pairs of σ_n and τ from the generalized Hoek-Brown criterion.

$$\sigma_n = \sigma_3 + \frac{\sigma_1 - \sigma_3}{\partial\sigma_1/\partial\sigma_3 + 1} \tag{24}$$

$$\tau = (\sigma_n - \sigma_3)\sqrt{\partial\sigma_1/\partial\sigma_3} \tag{25}$$

Hoek (1994b) proposed the utilization of equivalent strength properties with constant values, contrasting with instantaneous properties that fluctuate with stress levels. This approach provides a more stable and reliable foundation for analyzing the material's behavior under different stress conditions. He advocated for determining the equivalent cohesion (c^{eq}) and the equivalent friction angle (ϕ^{eq}) by fitting a linear Coulomb failure envelope to pairs of normal stress (σ_n) and shear stress (τ) determined by **Eq. 24**, and **25**. The relation is defined as:

$$\tau = c^{eq} + \sigma_n \tan(\phi^{eq}) \tag{26}$$

$$c^{eq} = \frac{\sigma_{c,i}[(1+2a)s+(1-a)m_b\sigma_{3n}](s+m_b\sigma_{3n})^{a-1}}{(1+a)(2+a)\sqrt{1+[6am_b(s+m_b\sigma_{3n})^{a-1}]/[(1+a)(2+a)]}} \tag{27}$$

$$\phi^{eq} = \sin^{-1}[\frac{6am_b(s+m_b\sigma_{3n})^{a-1}}{2(1+a)(2+a)+6am_b(s+m_b\sigma_{3n})^{a-1}}] \tag{28}$$

$$\sigma_{3n} = \frac{\sigma_{3,max}}{\sigma_{c,i}} \tag{29}$$

The equivalent Coulomb failure criterion provides an equivalent unconfined compressive strength (σ_c^{eq}) expressed by:

$$\sigma_c^{eq} = \frac{2c^{eq}\cos(\phi^{eq})}{1-\sin(\phi^{eq})} \tag{30}$$

Hoek and Brown (1997) recognized that the critical aspect in determining the equivalent cohesion and friction angle lies in selecting the suitable range of stresses over which the curve-fitting process should be conducted.

In this study, to determine the Hoek-Brown parameters for intact rock, including the uniaxial compressive strength (σ_{ci}) and the material constant (m_i), a series of triaxial compression tests as well as uniaxial compression tests were carried on 9 rock samples collected from the field.

Based on the carried laboratory results, it was determined that $\sigma_{3,max}$ for our geothermal reservoir test site is 71 MPa. The parameter $\sigma_{3,max}$ represents the upper limit of confining stress beyond which the correspondence between the Hoek-Brown and Mohr-Coulomb failure criteria is no

longer considered valid. This parameter is crucial for ensuring that the failure criterion is appropriately applied within a realistic stress range specific to the rock mass under investigation. The selection of $\sigma_{3,max}$ has a significant impact on the derived strength parameters. If excessively high values of $\sigma_{3,max}$ are used, it may result in an overestimation of the equivalent effective cohesion and an underestimation of the equivalent effective friction angle. This discrepancy can lead to inaccuracies in the assessment of the rock mass behavior under different loading conditions. Therefore, it is essential that the chosen $\sigma_{3,max}$ reflects the actual stress conditions expected within the rock mass for the specific engineering application, thereby maintaining the validity of the applied failure criterion.

3.4. Geological setting and geomechanical characterizations

This study focuses on a geothermal reservoir located in Northern Quebec, specifically within the remote region of Nunavik. This area is not connected to the main electrical grid of Canada and relies heavily on fossil fuels for electricity and heat generation. A deep geothermal reservoir could provide a sustainable and environmentally friendly energy source, reducing the dependency on diesel and supporting the energy needs of these isolated communities. The geological setting of the study area is characterized by the Lac Pingiajjulik fault, a significant geological feature that influences the geothermal potential of the region. Recent geological surveys have identified the Lac Pingiajjulik fault as a large ductile shear zone. This zone behaves differently from conventional brittle zones, typically exhibiting low permeability. However, small-scale fractures crosscutting the shear zone may enhance permeability, which is crucial for geothermal fluid flow. Previous studies, including those by Miranda et al., (2023b), have primarily focused on characterizing the fracture network at surface and near-surface levels using outcrop, well core, and satellite image data. These studies indicate an average fracture density of 1.35 fractures/m near the fault at surface levels, suggesting significant fracturing immediately adjacent to the fault. Well core data from Miranda et al., (2023b) revealed more widely spaced fractures at depth, indicating a potential decrease in fracture intensity with depth, although the specific depth range was not specified. Additionally, the fracture distribution is not entirely random; rather, it is spread in various directions and lengths near the fault zone, suggesting that an interconnected fractured network might exist. The lack of direct depth profile data suggests that fracture intensity is likely highest around the Lac Pingiajjulik fault trace at surface levels and decreases both laterally and

potentially with depth. This assumption aligns with the understanding of ductile shear zones, which typically exhibit reduced permeability due to intense shearing and plastic flow of rocks under high strain rates and temperatures.

Rock integrity attributes, such as disturbance, grain size, and shape, were obtained from rocks retrieved from the geothermal test site, and the mechanical properties of the rocks were obtained from NRCan's CanmetENERGY-Ottawa laboratory. Lab data and previous studies indicate that paragneiss and diorite are the primary lithologies at the desired depth where the geothermal reservoir will be located. **Table 1** illustrates the relationship between rock mass quality and material constants. This table serves as a reference for understanding the interconnection between the quality of rock mass and the specific material constants defined in the Hoek–Brown failure criterion.

Table 1. Rock mass characterization: Relationship between rock mass quality for the intact and the fractured rock mass

Hoek-Brown Classification	Intact Rock (From Lab)	Reduced Strength
Uniaxial compressive strength of intact rock, σ_{ci} (MPa)	218.876	41.154
Geological Strength Index (GSI) $(-)$	100	70
m_i $(-)$	22.615	$(-)$
D $(-)$	0	0
m_b $(-)$	22.615	7.746
s $(-)$	1	0.0357
a $(-)$	0.5	0.501
Failure envelope range, σ_{3max} (MPa)	71	71
Mohr-Coulomb: Cohesion, S_0 (MPa)	31.97	12.189

Mohr-Coulomb: Friction angle, φ $(Degree)$	55.18	48.92
Tensile Strength, σ_t (MPa)	9.6	1.008
Modules of Deformation, E (MPa)	$\mathrm{E_i} = 67000$	$\mathrm{E_{rm}} = 49000$

Nine laboratory samples were collected from the geothermal test site and the mechanical properties of the rock core specimens were determined by the triaxial and uniaxial compression tests. The outcomes of the tests on the intact rock samples were then graphically represented (with red x marker) in the principal stress space (σ_1, σ_3 space), as illustrated in **Fig. 5**. The intercept, σ_{ci}, and the slope of the failure envelope, m_i, were determined through the analysis of the principal stress plot. This analysis allowed us to understand the relationship between the principal stresses and the failure of the samples. Subsequently, a linear envelope was fitted over the non-linear Hoek-Brown envelope across the designated stress range using linear regression algorithm. This procedure allowed us to derive equivalent cohesion and friction angle values, which are essential components for establishing the Mohr-Coulomb failure criterion. The stress range was carefully selected to represent the expected in-situ stress conditions of the geothermal reservoir, ensuring the relevance of the derived parameters.

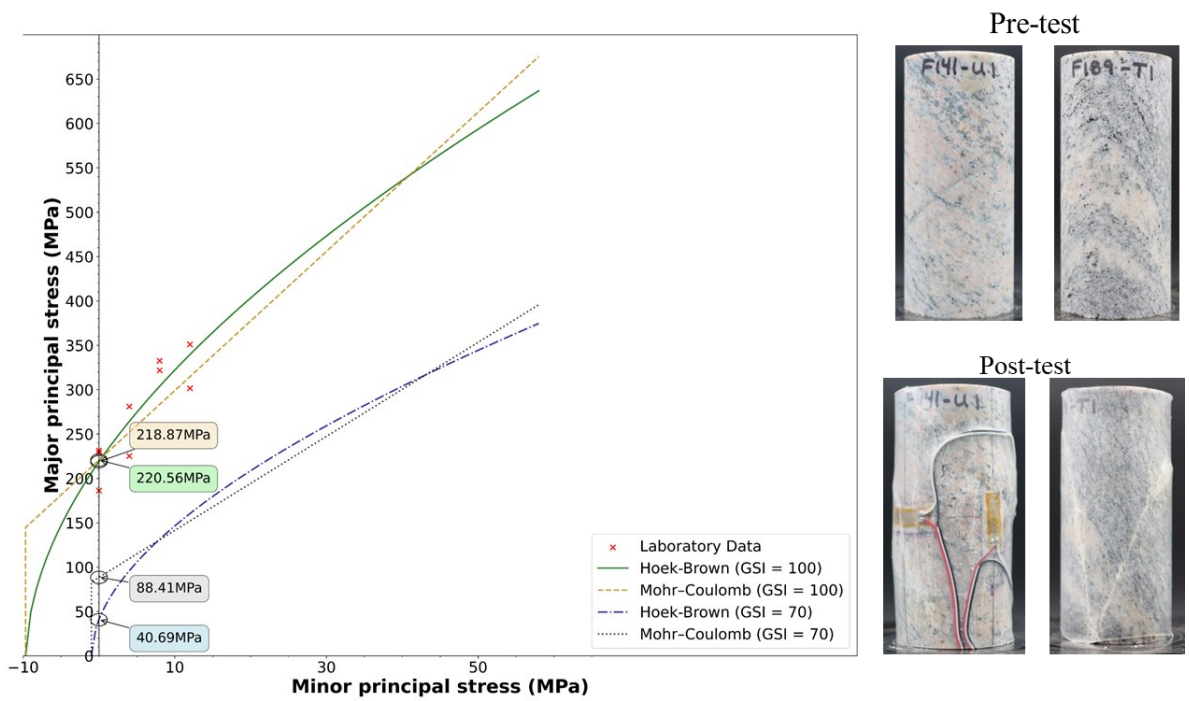

Fig. 5. Plot showing the laboratory data on the rock samples with fitted Hoek–Brown and Mohr-Coulomb models (typical pictures of pre-test and post-test paragneiss samples are embedded)

Fig. 5 presents the initial unconfined compressive strength (σ_c) for the rock sample as well as the equivalent unconfined compression strength (σ_c^{eq}) for both intact rock (with a Geological Strength Index, GSI, of 100) and the rock with Geological strength index, GSI, of 70. The value of GSI was determined based on the core logs and field characterization results by Miranda et al., (2023).

From **Fig. 5**, it can be observed that as the maximum confining stress $(\sigma_{3,max})$ increases, both the equivalent cohesion (c^{eq}) and the equivalent unconfined compressive strength (σ_c^{eq}) also increase. In contrast, the equivalent friction angle (ϕ^{eq}) decreases. Interestingly, the unconfined compressive strength derived from the equivalent Coulomb criterion ($\sigma_c^{eq} = 88.41\ MPa$) is generally higher than that obtained from the Hoek–Brown criterion ($\sigma_c = 40.69\ MPa$). This discrepancy becomes more pronounced with increasing $\sigma_{3,max}$.

3.5. Finite element modeling

The geothermal model presented in this paper aims to simulate the thermal, hydraulic, and mechanical behavior of the reservoir during its operational phases, encompassing injection and production activities over an anticipated lifespan of approximately 100 years. The model utilizes

the Thermal-Hydro-Mechanical Finite Element Method (THM FEM) package named GOLEM (Cacace and Jacquey, 2017), which is built upon the MOOSE framework (Gaston et al., 2009). This approach allows for a comprehensive simulation of coupled THM processes, focusing on understanding the influence of these mechanisms on fault slip tendency and reservoir dynamics. By integrating these geological insights and modeling techniques, our research provides a preliminary assessment of the feasibility and associated risks of operating a geothermal reservoir in this unique geological setting.

3.5.1. Numerical model description

The model geometry includes a reservoir domain measuring 8 kilometers in both width (x direction) and length (y direction), and 3 kilometers in depth (8 km × 8 km × 3 km). The targeted reservoir is positioned 4 km below the ground surface. It should be noted that, the effective domain which is significantly affected by fluid injection and production is considerably smaller, measuring 2 km in x, 2 km in y, and 1 km in depth. This focused area is where the most substantial changes and interactions are expected to occur. The larger surrounding domain allows for a more accurate representation of stress redistribution and fluid pressure diffusion beyond the immediate vicinity of the wells. Within this domain, a natural fault with a dip angle of 45 degrees and significant slip depth, extending 3 kilometers, is incorporated. Additionally, the model includes a doublet system comprising injection well and a production well. In a doublet system, the cold water is pumped from the injection well, and the hot water is restored through the production well. Reinjecting the cooled fluid helps sustain reservoir pressure and prevents pressure depletion, enabling longer-term sustainable extraction of the geothermal resource. Maintaining stable pore pressures is important for minimizing the risk of injection-induced seismicity (Buijze et al., 2017). However, it should be noted that even low-pressure fluid circulation can still induce stress changes in rocks and potentially trigger fault slip and seismic events (Kivi et al., 2022).

Two hydraulically induced fractures are integrated into the system, representing the outcomes of prior hydraulic simulation aimed at enhancing reservoir productivity. These fractures are oriented orthogonally to the minimum horizontal stress and are represented as squares with edges measuring 200 meters. Positioned equidistantly from the fault on each side, the fractures are set at a distance of 200 meters from the fault, with their centers located at specific coordinates within the model domain. The injection fracture is centered at (-200 m, 0 m, -4000 m) in the (x, y, z)

coordinate system, while the production fracture is centered at (200 m, 0 m, -4000 m). To simulate the fluid injection and production, a source node has been assigned at the midpoint of each fracture. The fluid injection and production rate are imposed at the injection and production nodes and are maintained at a constant rate of $15\mathrm{L/s}$ (or $1296\ \mathrm{m}^3/\mathrm{Day}$) during a century of continuous injection and production. The injection rate of $15\ \mathrm{L/s}$ was selected based on the maximum sustainable freshwater extraction capacity in the study area provided by local authorities and INRS university. This rate represents the optimal balance between maximizing injection volume and ensuring long-term sustainability of local freshwater resources.

The domain is meshed using the commercial software, Coreform Cubit. The 3D mesh consists of 3,376,445 tetrahedral elements (refer to **Fig. 6(b)**). The meshing procedure entails first meshing the internal features (e.g., faults, fractures, and source points) within the domain, followed by meshing the surrounding units. This method ensures that the mesh around the internal features automatically becomes finer, enhancing the resolution in critical areas. Additionally, a mesh sensitivity analysis was conducted, which demonstrated that further refinement of the mesh beyond this level did not significantly alter the simulation results. This confirms that the chosen mesh density provides sufficient resolution for accurate modeling of the system behavior

The geological formations, well geometries, induced fractures, and faults are visually depicted in **Fig. 6(a)**, and their material properties are listed in **Table 2.** The spatial arrangement of the principal stresses relative to the fault's location is illustrated in **Fig 6(c)** as provided by Miranda et al. (2023a), which elucidates a strike-slip faulting regime at the geothermal test site. In this simulation, the z-axis aligns with the principal vertical stress (σ_v), while the x and y-axes align with the minimum principal horizontal stress ($\sigma_{h,min}$) and maximum principal horizontal stress ($\sigma_{H,max}$), respectively.

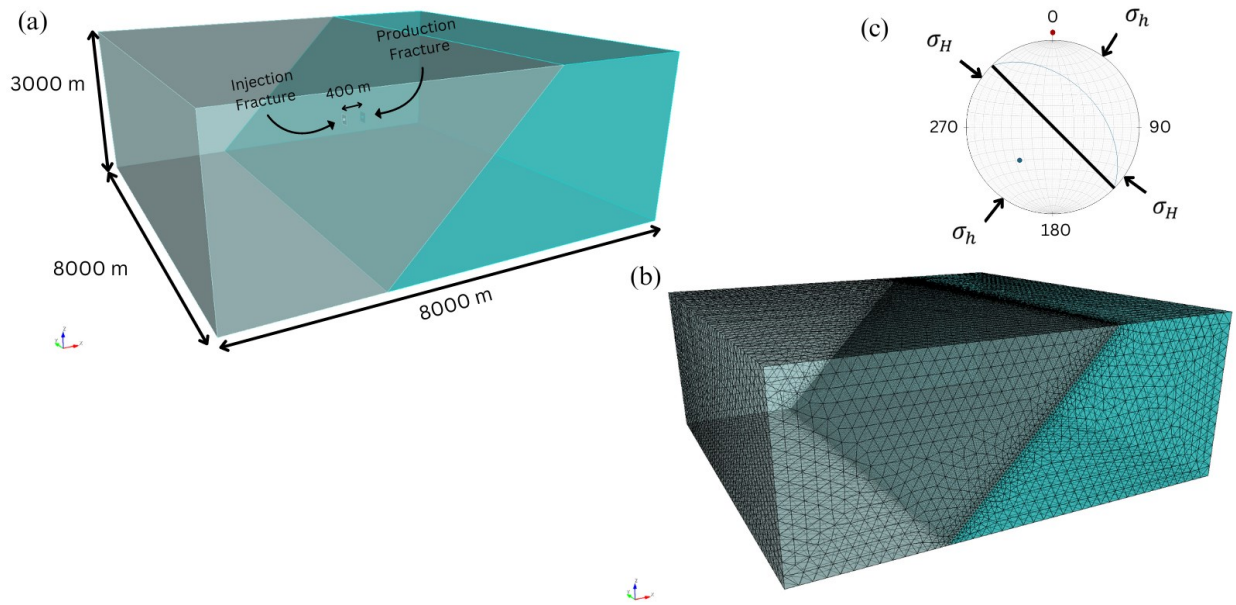

Fig. 6. Graphs showing: (a) the 3D Geological Model, fault, and two hydraulically stimulated fractures, (b) the numerical mesh of the domain, generated using Delaunay triangulation (2D surfaces, i.e., fault, fractures) and Tetrahedralization (3D domain), and (c) the position of the principal stresses concerning the fault offset.

Table 2. Material properties used for numerical modeling.

Property name	Reservoir Rock	Fault	Fracture
Initial Porosity, n $(-)$	0.06	1	1
Initial Permeability, $k_{x=y=z}$ (m^2)	1×10^{-15}	1×10^{-12}	1×10^{-8}
Fluid modulus, $\boldsymbol{K_f}$ (MPa)	1774	2500	2500
Initial Fluid viscosity, μ_f $(Pa\,S)$	3×10^{-4}	3×10^{-4}	3×10^{-4}
Initial Fluid density, ρ_f $(kg\ m^{-3})$	1080	1080	1080
Fluid heat capacity, c_f $(J\ kg^{-1}\ K^{-1})$	4180	4180	4180
Fluid thermal conductivity, λ_f $(W\ m^{-1}\ K^{-1})$	0.65	0.65	0.65

Rock density, ρ_s $(kg\ m^{-3})$	2672	–	–
Rock heat capacity, c_s $(J\ kg^{-1}\ K^{-1})$	898	–	–
Rock thermal conductivity, λ_s $(W\ m^{-1}\ K^{-1})$	2.6	–	–
Aperture, h (m)	–	1.0×10^{-2}	1.0×10^{-2}
Reduced Modulus of Deformation, E_{rm} (MPa)	49000	–	–
Poisson's ratio, v $(-)$	0.25	–	–
Rock bulk modulus, k_s (MPa)	44670	–	–
Rock shear modulus, G (MPa)	26800	–	–
Cohesion (MPa)			
Friction Angle (Degree)			

3.5.2. Initial and boundary conditions

In terms of the boundary conditions, hydrostatic pressure and geothermal gradient are applied to all six sides of the domain, representing a closed system where there is no mass (fluid) or heat exchange with the surroundings. The pore pressure and temperature boundary conditions are set using a generalization of the Dirichlet boundary condition which imposes a spatially dependent value on a particular set of degrees of freedom (DOFs) defined by the boundary parameter. For pore pressure, the value for this boundary condition is defined as the product of fluid density, gravitational acceleration, and depth. For temperature, the value is defined as the temperature gradient multiplied by depth. As for the displacement boundary conditions, null displacement conditions are applied normal to the vertical, top, and bottom boundaries.

Displacement, temperature, and pore pressure boundary conditions are applied before the system is solved, at the beginning of the timestep. This means that the value of the variable is enforced directly, and the degree of freedom (DOF) associated with that variable is removed from the equations, reducing the number of equations to solve. Moreover, in terms of the injection temperature's boundary condition, a Dirichlet boundary condition of 30 degrees Celsius is applied at the injection source node.

As for the initial conditions of the domain, the fluid pressure was estimated as hydrostatic pressure ($P_p = 1080\ (kg/m^3) \times 9.8\ (m^2) \times z\ (m)$). Similarly, the initial temperature is estimated as the product of the thermal gradient and the depth ($T = 20.9^{\circ}c \times z$).

Furthermore, it is pertinent to note that the regional stress field is applied as background stress to replicate a strike-slip faulting regime in the simulation. Three distinct in-situ stress states provided by (Miranda et al., 2023) are employed for calibration purposes, encompassing principal stress values and their respective orientations. These details are summarized in **Table 3**.

Table 3. The in-situ stress state at the potential geothermal site.

Principal stresses	$\boldsymbol{\sigma_v}$ $\boldsymbol{MPa\ km^{-1}}$	$\boldsymbol{\sigma_{H,max}}$ $\boldsymbol{MPa\ km^{-1}}$	$\boldsymbol{\sigma_{h,min}}$ $\boldsymbol{MPa\ km^{-1}}$	Stress Regime
Case I	27	45.25	26.5	Strike-Slip
Case II	24.25	38	21	Strike-Slip
Case III	34.5	53.25	30.25	Strike-Slip
Stress Orientation		$N215°E$	$N305°E$	

3.5.3. Stress field characterization

The propensity for slip or reactivation along pre-existing fractures and faults is fundamentally governed by the characteristics of the ambient stress field, which can be quantified by two dimensionless ratios, R and K involving the principal stress magnitudes (σ_1, σ_2 and σ_3).

R is defined as the $(\sigma_1 - \sigma_2)/(\sigma_1 - \sigma_3)$, and K is defined as the $(\sigma_1\sigma_3)/(\sigma_2^2)$. Here σ_1, σ_2, and σ_3 are the maximum, intermediate, and minimum principal stresses.

The stress ratio R, ranging from 0 to 1, classifies the stress regime based on the relative stress differences. When $R = 0$, it indicates either a radial compression ($\sigma_2 = \sigma_3$) or radial extension $\sigma_1 = \sigma_2$) regime. When $R = 1$, it represents a plane strain regime ($\sigma_2 = (\sigma_1 + \sigma_3)/2$). Intermediate values of R represent transitional stress states. This parameter is particularly useful in distinguishing between different faulting regimes: values close to 0 or 1 often indicate normal or reverse faulting, while intermediate values are associated with strike-slip faulting (Zoback, 2010). The stress difference ratio K governs the orientations of surfaces most prone to slip for a given stress state. When $K > 1$, surfaces prone to slip tend to form a girdle around the σ_1 axis. When $K < 1$, they tend to cluster around the σ_2 axis. When $K = 1$, there's no preferred orientation. This parameter is crucial in predicting the likely orientation of new fractures or the reactivation of existing faults (Morris et al., 1996).

Together, these ratios provide a quantitative framework for characterizing stress fields and relating them to the distribution of fractures, faults, and other geological structures expected to form or reactivate under those conditions. It's important to note that in a geothermal reservoir, these parameters can vary with depth and may change over time due to fluid extraction or injection, thermal effects, and induced seismicity (Ghassemi, 2012).

3.6. Results

3.6.1. Steady-state simulation results

Prior to initiating the transient simulation to model reservoir operational activities, a steady-state simulation was conducted to establish the baseline conditions of the reservoir unaffected by external influences, fluid injection and production. This initial simulation was performed under identical boundary conditions as described previously, without incorporating operational activity. Its primary purpose was to stabilize and ensure the consistency of fluid properties, notably density,

and viscosity, which are functions of primary variables as per IAPWS-IF97 (Huber et al., 2009; Wagner et al., 2000). This step was crucial to mitigate potential fluctuations or oscillations in the simulation results that may arise due to numerical instabilities or inconsistencies in the initial conditions. The steady-state simulation results display the initial pore pressure and temperature distributions within the reservoir (**Fig. 7**). These results serve as the initial input for the subsequent transient simulation, providing a stable and consistent starting point for modeling the reservoir's behavior under operational conditions.

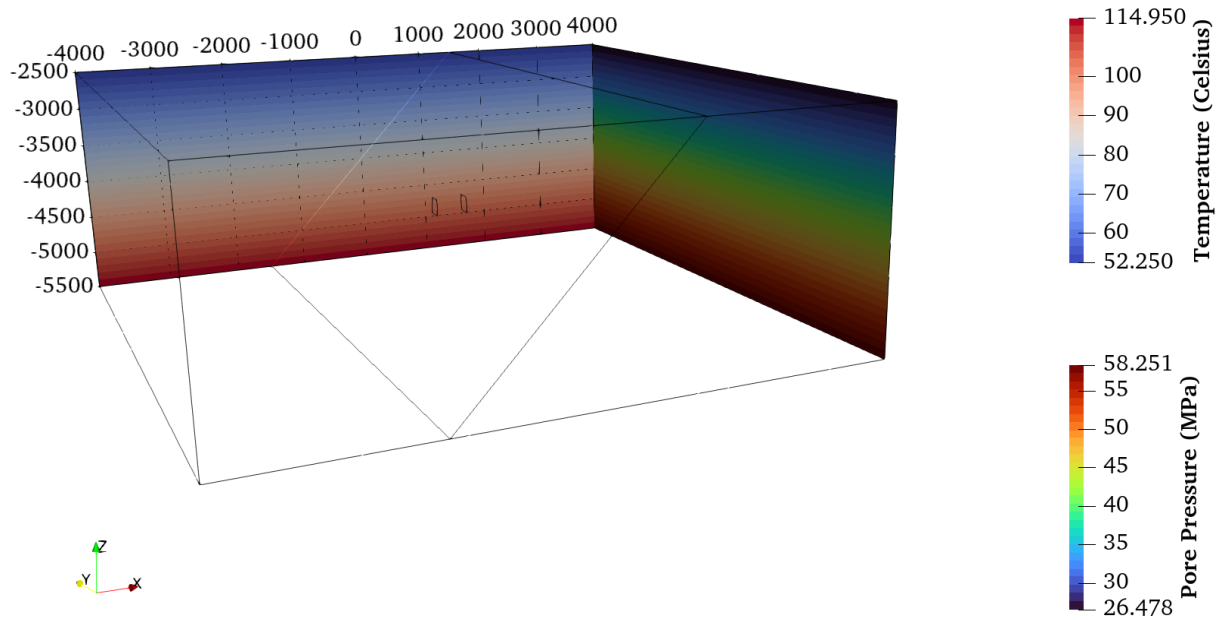

Fig. 7. Steady-state simulation results showing the initial pore pressure and temperature distributions within the reservoir

3.6.2. Fault reactivation potential under prevailing in-situ stress conditions

The initial slip tendency measures the likelihood or potential for a fault to slip under a given stress field, without the influence of fluid injection or production from the reservoir. This measure serves as a baseline for assessing the natural state and stability of the fault system prior to any external interventions. As outlined in section 3.5.2, three potential stress states were considered for the in-situ stress conditions. **Fig. 8** provide a comprehensive overview of the initial slip tendency, resolved shear stress, and normal stress for each respective case.

In the most favorable in-situ stress state, where the vertical stress (σ_v) is $-24.25\ MPa\ \ km^{-1}$, the maximum horizontal stress ($\sigma_{H,max}$) is $-38\ MPa\ km^{-1}$, and the minimum horizontal stress ($\sigma_{h,min}$) is $-21\ MPa\ km^{-1}$, the highest initial slip tendency, 0.132, is recorded (see **Fig. 8(c)**). This observation may be attributed to the heightened resolved shear stress acting on the fault plane (refer to **Fig. 8(f)**). Concurrently, the relatively lower normal stress, compared to other stress state scenarios, acting upon the fault plane, (refer to **Fig. 8(i)**), further elevating the initial slip tendency.

In this stress state, the R value is measured as 0.809 which represents a transitional stress regime between strike-slip and radial extension. The stress difference ratio $K = 1.357 > 1$ suggests that surfaces prone to slip or failure will tend to align in a girdle geometry around the $\sigma_{H,max}$ (Maximum principal stress) axis direction, promoting the development of fractures or faults at oblique angles to the maximum horizontal stress direction.

Conversely, in the most adverse in-situ stress state, where, $\sigma_v = -34.5\ MPa.km^{-1}, \sigma_{H,max} = -53.25\ MPa.km^{-1}$ and $\sigma_{h,min} = -30.25\ MPa.km^{-1}$, the initial slip tendency records lower (refer to **Fig. 8(b)**) compared to the former case. This could potentially be attributed to the augmented normal stress, compared to the former stress state scenario, exerted upon the fault plane (see **Fig. 8(h)**), counteracting the effect of higher resolved shear stress (**Fig. 8(e)**). In this stress state, the initial slip tendency value measured on the fault surface is 0.1, reflecting a lower potential for fault reactivation.

For this stress state, the value of R is determined as 0.815, representing a transitional regime between strike-slip and radial extension. The stress difference ratio $K = 1.353 > 1$ indicates that high slip tendency surfaces will concentrate around the $\sigma_{H,max}$ axis.

Finally, in the most plausible in-situ stress state scenario, characterized by $\sigma_v = -27\ MPa\ \ km^{-1}$, $\sigma_{H,max} = -45.25\ MPa\ km^{-1}$ and $\sigma_{h,min} = -26.5\ MPa\ km^{-1}$, a significantly lower resolved shear stress is determined (see **Fig. 8(d)**), yielding the lowest recorded value of slip tendency on the fault plane, 0.029 (refer to **Fig. 8(a)**), indicating the least potential for fault reactivation under prevailing in situ stress conditions.

In this stress state, the value of $R = 0.973$ indicates a strike-slip/transcurrent faulting regime. The high "R" value close to 1 signifies a highly anisotropic stress field typical of strike-slip

environments. The stress difference ratio $K = 1.645 > 1$ suggests that the distribution of surfaces with high slip tendency will tend to form a girdle or band around the $\sigma_{H,max}$ axis.

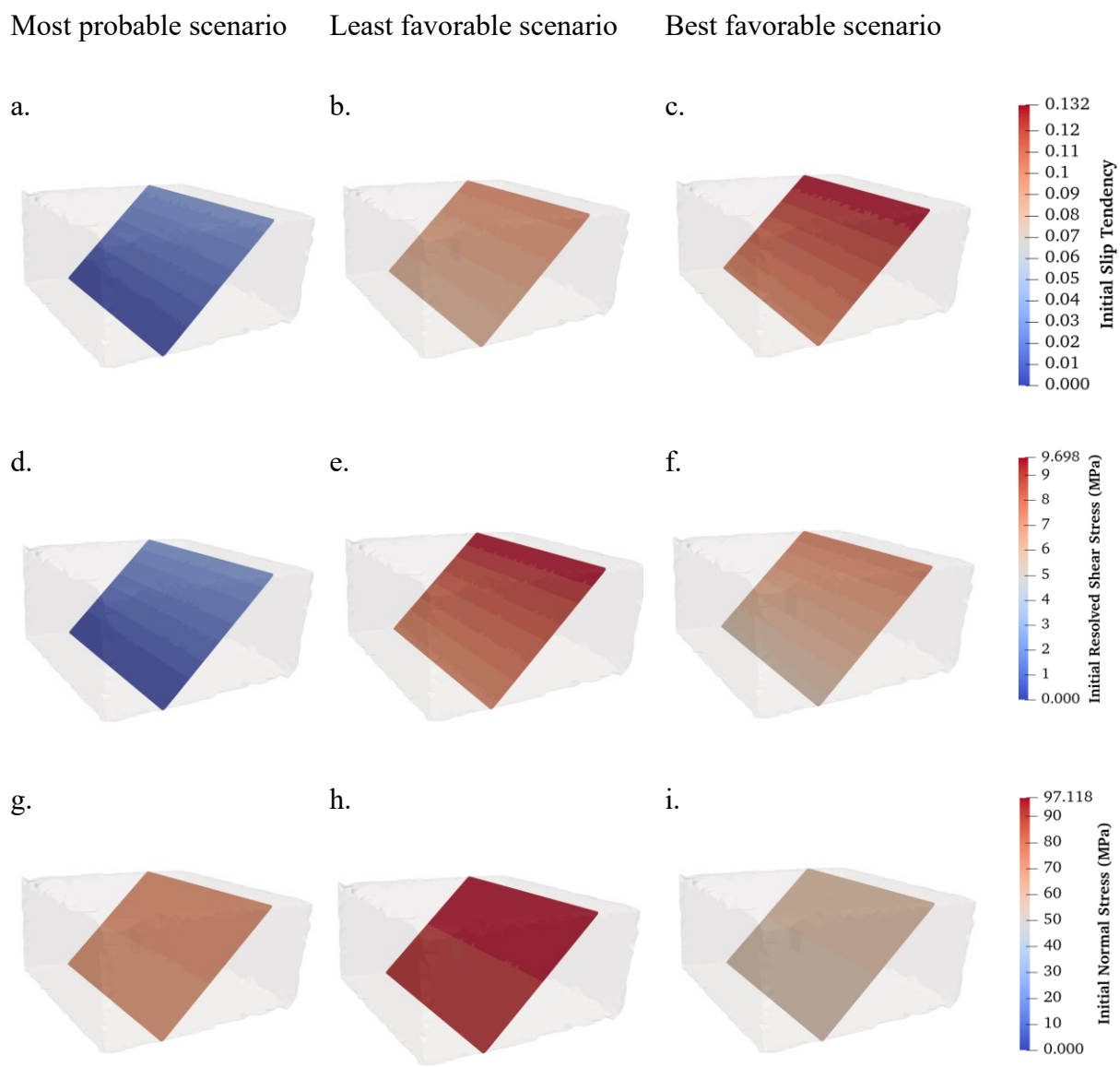

Fig. 8. Initial and evolution of slip tendency results calibrated after Miranda et al. (2023a) for the in-situ stress state in three possible stress state scenarios

These findings indicate the significant influence of stress anisotropy on fault reactivation potential. Accurately characterizing in-situ stress conditions is crucial for anticipating and mitigating

geomechanical challenges in geothermal reservoir operations, particularly in fractured porous media. While the initial slip tendency provides a baseline assessment of fault reactivation potential under the given in-situ stress conditions, it is important to recognize that reservoir operations can dynamically alter these conditions. Changes in pore pressure and temperature induced by fluid injection or extraction can significantly modify the effective stress state, potentially increasing or decreasing the slip tendency. Therefore, continuous monitoring and analysis of evolving stress conditions are essential for mitigating the risk of fault reactivation and ensuring the safe and sustainable operation of the geothermal reservoir. The subsequent sections will explore the complex interplay between these variables and the evolution of slip tendency due to external forces.

3.6.3. Thermohydraulic processes in a geothermal doublet system

The introduction of cold fluid into the hot reservoir matrix initiates thermo-mechanical and hydro-mechanical effects that significantly alter pore pressure and reservoir dynamics, as illustrated in **Fig. 9**. Over the operational period, substantial variations in these parameters are observed, reflecting the complex interplay of thermal and hydraulic processes within the reservoir.

Pore pressure dynamics show notable changes across the reservoir (**Fig. 9(a)**). Near the injection well, an increase of approximately 11.048 MPa is observed, highlighting the substantial impact of fluid injection on the reservoir's stress state. This pressure increase gradually dissipates with distance from the injection point, creating a pressure gradient that drives fluid flow through the reservoir. On fault surface, an increase of 5.585 MPa pore pressure is measured (**Fig. 9(b))**, highlighting the substantial impact that the fluid injection might have on the fault's stability. This increase is critical as it can influence fault stability and potentially lead to reactivation under certain conditions

Temperature distribution within the reservoir undergoes significant alterations due to the injection of cold fluid (**Fig. 9(c)**). As cooling front propagates from the injection well, a temperature decreases of up to 52°C is observed in the immediate vicinity of the injection point. This cooling effect extends progressively through the reservoir over time, influencing both the thermal regime and the associated thermo-mechanical stresses. The extent and rate of cooling vary spatially, with areas closer to the injection well experiencing more rapid and pronounced temperature changes.

Additionally, a progressive cooling effect is observed along the fault plane, with a temperature decrease of 52°C (**Fig. 9(d)**), affecting the thermal regime of the reservoir and contributing to thermo-mechanical stress changes that can alter the fault's mechanical behavior.

The interaction between injected cold fluid and the hot reservoir environment generates complex fluid flow patterns, as evidenced in **Fig. 9(e)**. After 100 years of operational activity, pronounced convection cells are observed near the injection and production wells, with cooler fluid descending from the injection point and warmer fluid rising towards the production well. These convective patterns significantly influence fluid migration and heat transfer within the reservoir. The continuous injection process introduces a non-equilibrium pressure regime, resulting in the formation of a pressure front that advance through the reservoir.

a.

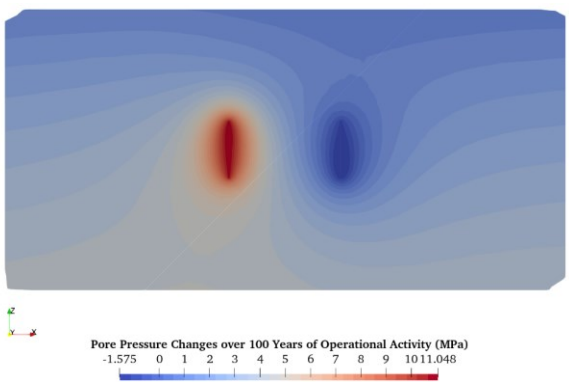

b.

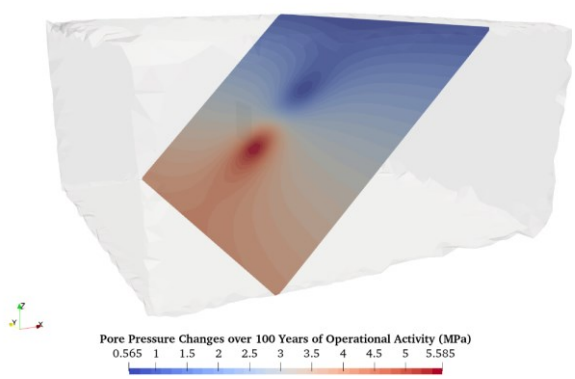

c.

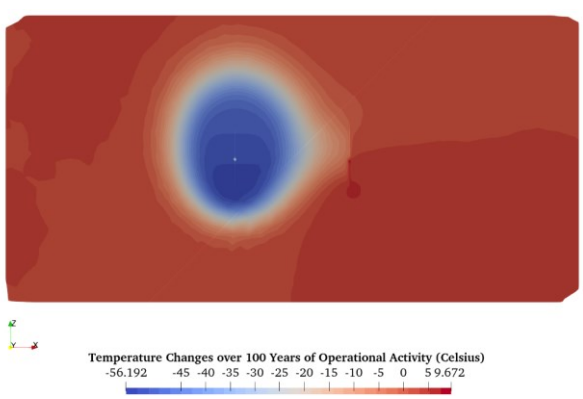

d.

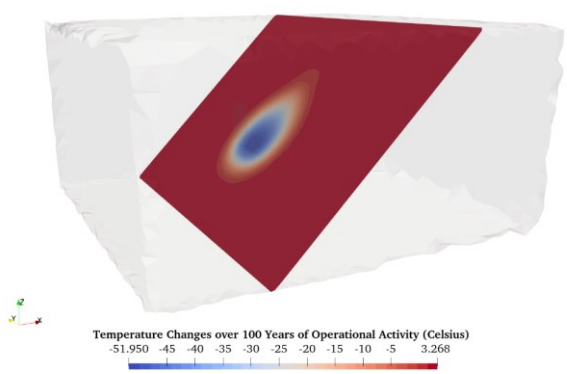

e.

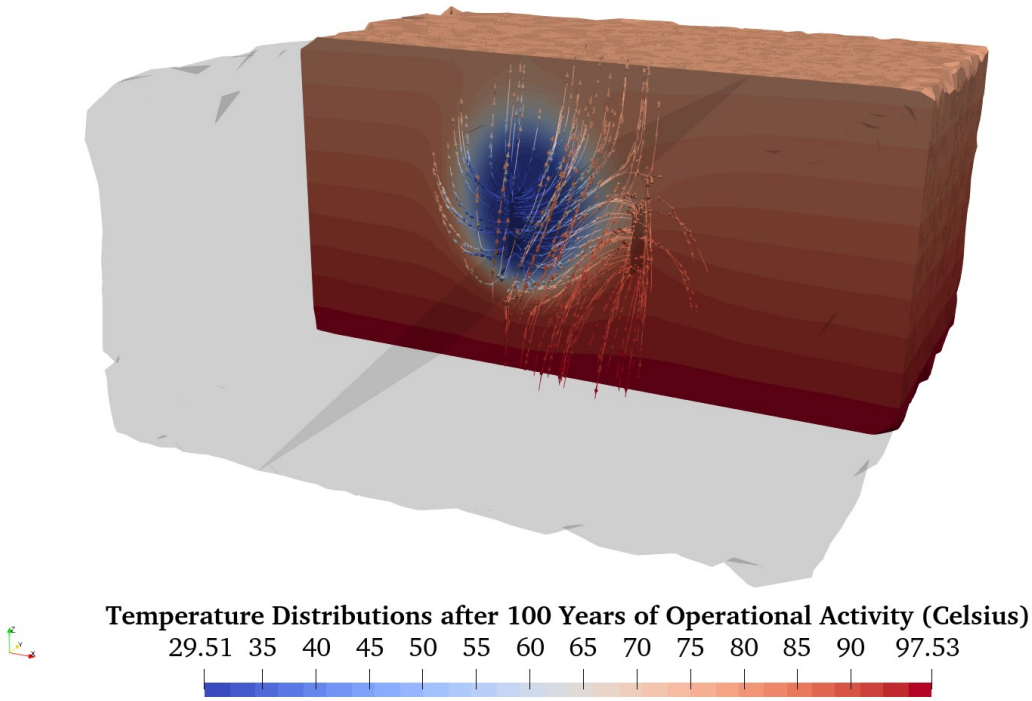

Fig. 9. Graphs showing the response of the reservoir due to the operational activity: Panels (a) and (b) show the pore pressure distribution over the domain and fault face; Panels (c) and (d) illustrate the temperature distribution; panel (e) provides detailed information regarding the fluid flow and thermal dynamic of the geothermal reservoir after 100 years of continuous fluid injection with a 15 L/s injection rate.

3.6.4. Dynamic evolution of slip tendency

Over the course of a century of operational activity, both resolved shear stress and normal stress exhibit dynamic changes, as illustrated in **Fig. 10**. These changes lead to significant variations in slip tendency, potentially influencing fault stability. The maximum value of initial slip tendency values prior to operational activities on the fault plane were 0.029 for the most plausible stress state scenario, 0.132 for the most favorable stress-state scenario, and 0.1 for the most adverse stress-state scenario. Throughout the operational period, these values underwent notable changes. In the most plausible stress state scenario, the increase in slip tendency measured on the faut plane was 0.152, occurring after 100 years of operational activity. Similar patterns were observed in the most favorable and adverse stress state scenarios, with maximum increases of 0.339 and 0.117, respectively. These changes in slip tendency are influenced by several factors, including the orientation of the faults relative to the principal stress directions and their proximity to the advancing cooling front. As the cooled front propagates towards the production well, a significant

reduction in the effective normal stress and an increase in resolved shear stress acting on the fault plane is observed (**Fig. 10**). This reduction in effective normal stress can be attributed to the cooling effect of the injected cold water on the surrounding rock, which induces contraction and consequently reduces the normal stress exerted on the fault. In the most plausible stress state scenario, we observe an increase in resolved shear stress on the fault plane of 8.826 MPa, while the normal stress decreases by 31.523 MPa. The maximum normal stress decrease is precisely recorded where the thermal front reaches the fault surface, and this decrease then propagates from that point. For the best-case scenario, we see a similar decrease in normal stress of 31.523 MPa, but with a shear stress reduction of 5.849 MPa. This combination results in a higher slip tendency of 0.339, suggesting a potentially less stable condition compared to the most plausible scenario. In the worst-case scenario, the maximum change in normal stress is recorded as 9.771 MPa, with a shear stress change of 3.747 MPa. These variations across different scenarios indicate the complex interplay between thermal effects, fluid injection, convective flow, and stress redistribution in the reservoir. Despite these dynamic changes, when comparing the maximum slip tendency values (0.152 for the most plausible, 0.339 for the best case, and 0.117 for the most plausible stress state scenario) to the coefficient of static friction stated by Byerlee, (1978), it can be concluded that the fault does not initiate slippage in any of the stress state scenarios over the 100-year operational period.

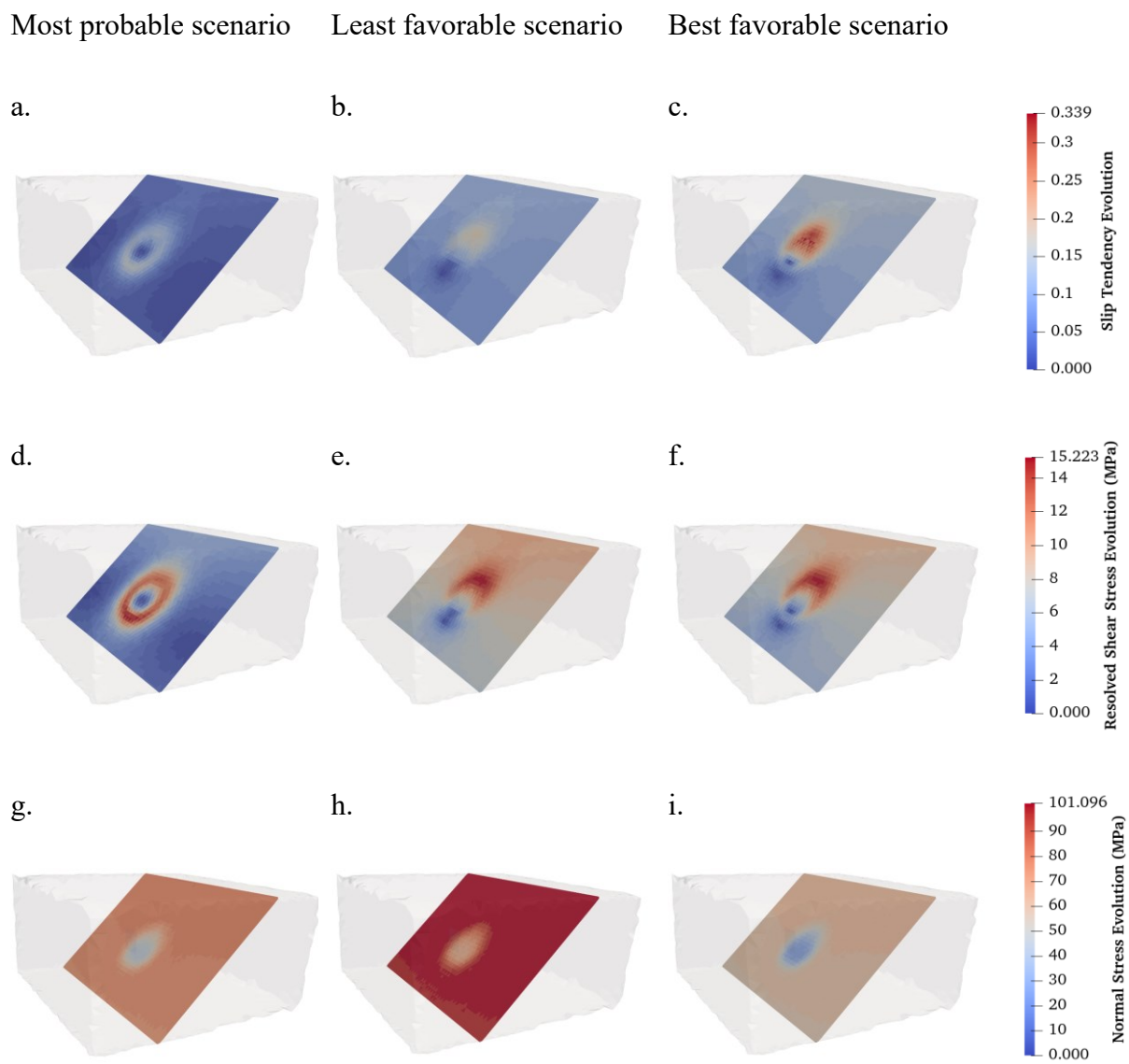

Fig. 10. Initial and evolution of slip tendency results calibrated after Miranda et al. (2023a) for the in-situ stress state in three possible stress state scenarios.

3.7. Discussions

Induced seismicity, a phenomenon of paramount concern in deep geothermal exploitation, is governed by two concurrent mechanisms: pore pressure diffusion and thermal effects. The former, pore pressure diffusion, is intrinsically linked to the pore pressure gradient established between the injection and production wells. This gradient drives the fluid front through the reservoir rock matrix, potentially destabilizing faults by reducing the effective normal stress acting on the fault surface and shifting the Mohr circle towards the failure envelope (Kivi et al., 2022). Concurrently,

cold fluid injection induces thermal contraction along the fluid flow path, primarily propagated through advection as the cooling front advances toward the production well **(Fig. 9(e))**.

The modeled deep geothermal doublet system in northern Quebec have a centrally located fault and equidistantly positioned injection and production wells, the pore pressure diffusion primarily manifests as alterations to fault stability in short term as the fluid front advances through the domain at significantly higher rates than the cooling front. The symmetrical well configuration results in a more uniform pressure distribution, with the fault acting as a conduit for pressure transmission rather than a flow barrier. Furthermore, continuous injection of cold water causes thermal contraction of the reservoir rock, leading to changes in the stress field that can extend far beyond the cooled region. This thermal contraction can induce tensile stresses along the fluid flow path, potentially reactivating the fault that was initially considered stable.

3.7.1. The impact of hydraulic properties

The complex interplay of various mechanisms in geothermal systems presents the critical importance of understanding reservoir hydraulic properties for predicting fault reactivation dynamics. These properties, particularly fluid density and viscosity, play a pivotal role in determining fault stability and governing fluid flow characteristics within the reservoir. Temperature variations in geothermal reservoirs lead to significant changes in fluid density and viscosity, which in turn affect pressure distribution, create buoyancy effects, and contribute to stress changes through thermal contraction. This process typically unfolds with the denser, cold reinjected water initially moving downward due to gravitational forces. As the water heats up, it becomes less dense and rises, driven by buoyancy forces. Over time, this movement tends to establish a pseudo-steady state where fluid pressure within the reservoir balances the hydrostatic pressure gradient.

Our simulation results demonstrate a clear gradient in the magnitude of changes to fluid properties and reservoir conditions from the injection well to the production well in **Fig. 11**. The most significant alterations in fluid density, viscosity, pore pressure, and temperature are observed in the vicinity of the injection well. As we move towards production well, these changes become progressively less pronounced. Near the injection well, the introduction of colder, more viscous fluid leads to substantial increases in pore pressure (**Fig. 11(a))** and marked changes in fluid

properties (**Fig. 11(c)** and **Fig. 11(d)**). This is primarily due to the localized cooling effect and the higher viscosity of the injected fluid, which impedes its movement through the reservoir matrix. In contrast, the area surrounding the production well initially experiences moderate changes. Here, the warmer, less viscous geothermal fluid moves more readily towards the well, driven by the extraction-induced pressure gradient. This results in a noticeable, but comparatively smaller, decrease in pore pressure and less dramatic changes in fluid properties.

It's important to note that the distribution of these changes is not static but evolves over time as the cold front advances through the reservoir. Our simulation reveals that as the cooled fluid front progresses towards the production well, it carries with it significant changes in fluid properties. Initially, the most dramatic alterations are confined to the area near the injection well. However, as time passes and the cold front advances, these changes in fluid density, viscosity, and temperature begin to manifest at increasing distances from the injection point. When the cold front eventually reaches the vicinity of the production well, we observe a marked shift in fluid properties in this region as well. This progression leads to a dynamic, time-dependent alteration of the reservoir's characteristics. The contrast in viscosity between the injected cold water and the reservoir fluid creates an asymmetry in pressure distribution between injection and production wells, which becomes more pronounced over time. Importantly, these fluid properties related effects can extend well beyond the immediate cooled region, potentially triggering the reactivation of distant faults previously considered stable.

The intricate interactions between fluid properties, pressure propagation, and thermal gradients necessitate the use of comprehensive, coupled thermo-hydro-mechanical modeling to accurately predict the long-term behavior and stability of geothermal doublet systems with central faults. Several factors contribute to this complexity, including stress-sensitive porosity changes, long-term alterations in fluid properties due to the advancing thermal front, varying rates of pressure propagation influenced by fluid viscosity, and far-reaching effects of density-driven flow. To address these complexities, our simulation employs the IAPWS-IF97 formulation (Cooper and Dooley, 2007), which provides highly accurate representations of water and steam properties across the range of temperatures and pressures typical in geothermal systems.

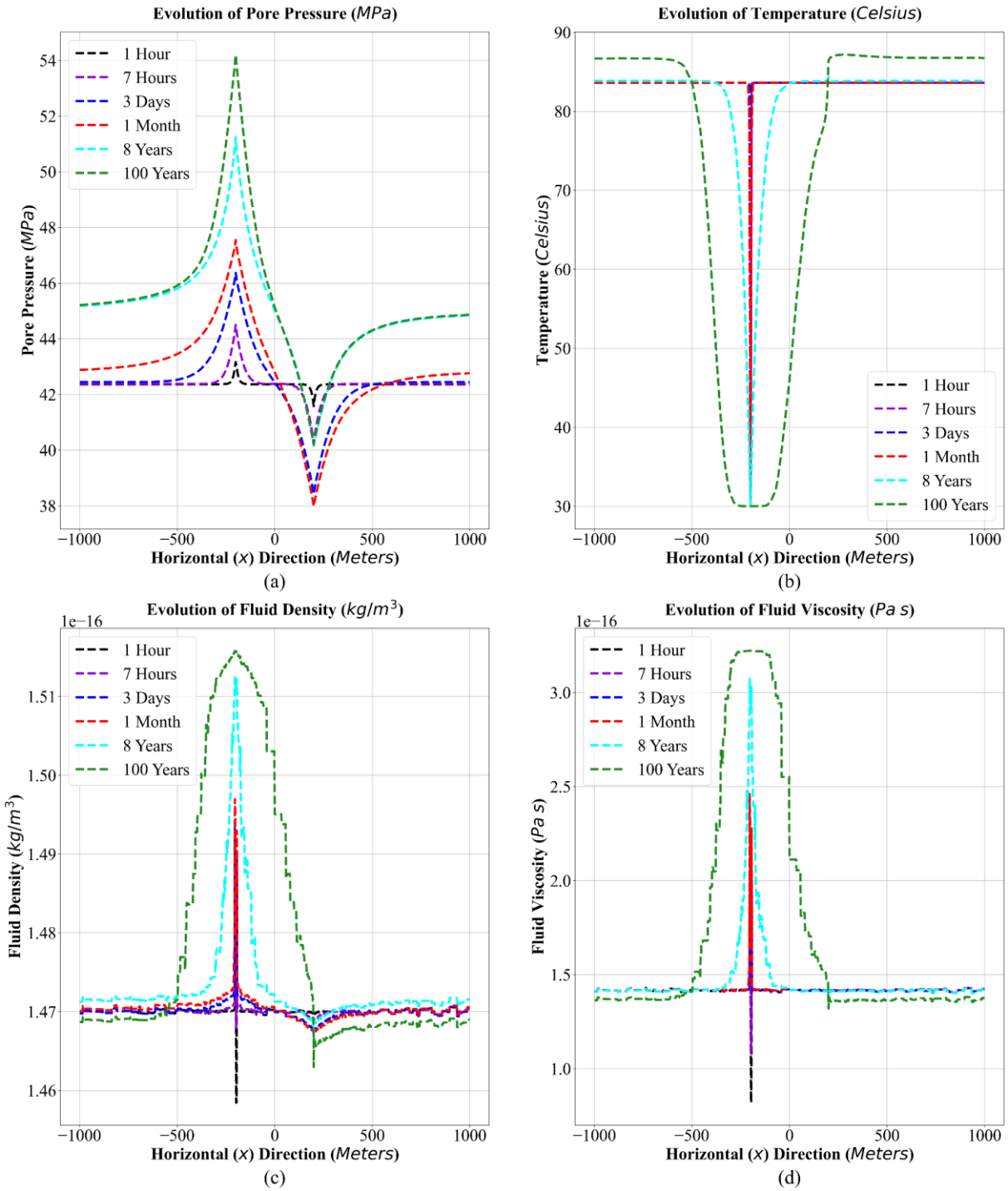

Fig. 11. Plots showing the evolution of pore pressure, temperature, fluid properties (Density and viscosity) of the most probable case over 100 years of operational activity. The injection fracture is located in -200 m, and the prodcution fracture is located in +200 meters. The injection and production fractures are located equidistantly from the fault plane which is located in 0 m in X direction.

Incorporating the rigorous IAPWS-IF97 equations, particularly those for the liquid Region 1, significantly enhances the accuracy of reservoir simulations. This approach allows for precise accounting of pressure and temperature-dependent changes in fluid density and viscosity, which govern the heterogeneous pressure field distributions driving slip tendency along faults and fractures during injection/production operations. In order to demonstrate the effectiveness of applying IAPWS formulation, we also carried out modeling of cases using constant fluid properties. Our simulations reveal substantial differences between models using the IAPWS formulation and those assuming constant fluid properties. As shown in **Fig. 12(a)** and **(b)**, the IAPWS formulation yielded a maximum slip tendency value 18.75% higher than the constant fluid property case. This significant increase indicates the importance of accounting for dynamic fluid behavior. In the case of temperature and pressure-dependent fluid properties, we observed a 19.9% increase in the maximum resolved shear stress on the fault plane (**Fig. 12(c)** and **(d)**), while the normal stress remained constant (Approximately 1.1% increase was seen) (**Fig. 12(e)** and **(f)**). This substantial increase in shear stress directly contributes to higher slip tendency on the fault plane. The change in stresses can also be reflected by notable differences in pressure changes near the injection and production wells (**Fig. 13)**. Near the injection well, the IAPWS formulation resulted in a maximum pressure increase of 11.03 MPa, compared to 10.65 MPa in the constant fluid property case. This represents a 3.57% higher pressure increase when using the IAPWS formulation. Conversely, near the production fracture, we observed a pressure reduction of 1.48 MPa with the IAPWS formulation, in contrast to a much larger reduction of 11.02 MPa in the constant fluid property case.

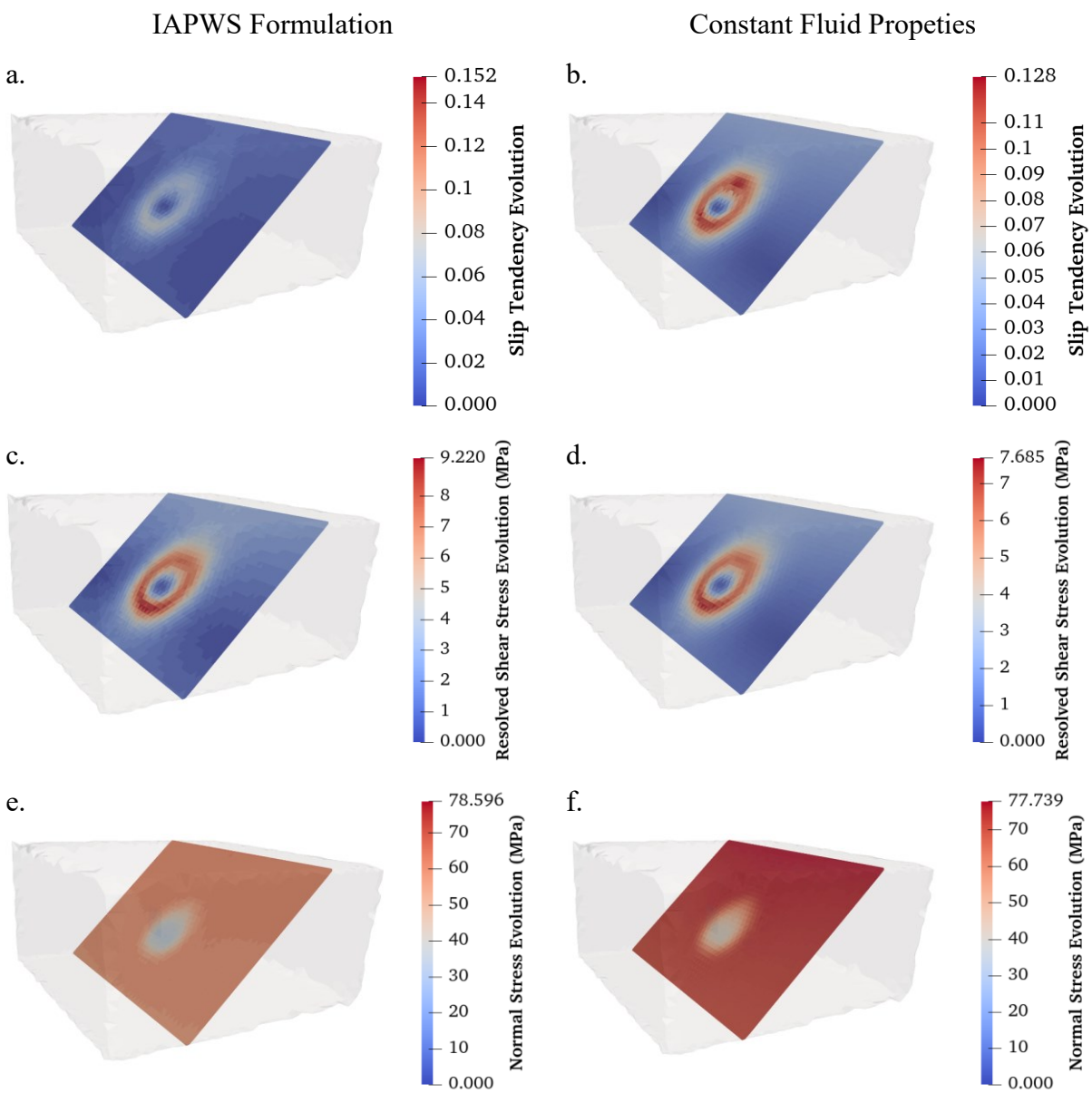

Fig. 12. Graphs showing the slip tendency and stress distribution results for the cases with and without IAPWS formulation.

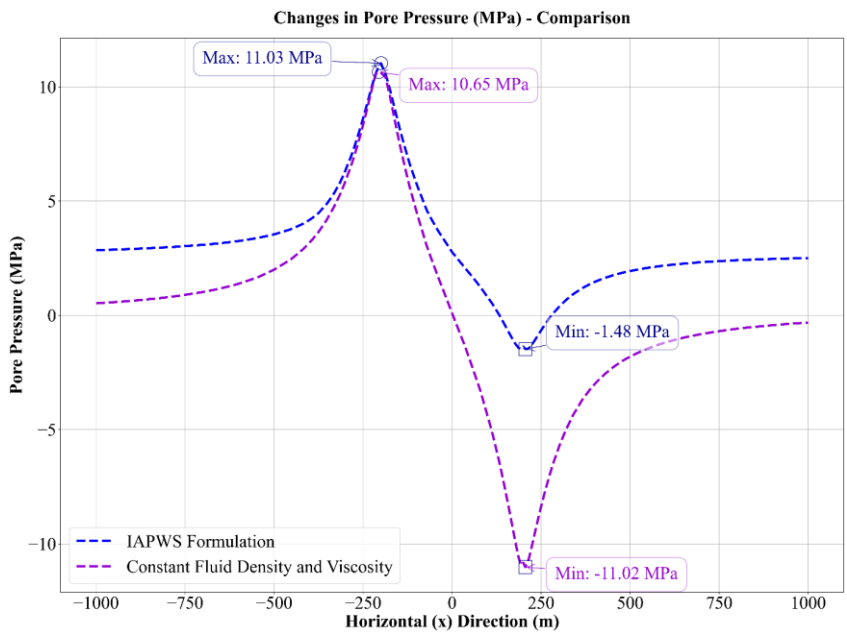

Fig. 13. Plots showing the pore pressure changes for the cases with and without IAPWS formulation.

3.7.2. Evaluating slip tendency results against Mohr-Coulomb predictions

In our numerical modeling, there is no noticeable plastic strain developed in the fault zone even though the reduced strength of rock mass (GSI = 70) is used. To ensure the robustness of our slip tendency results and to see whether the failure would occur in our fault plane or not, we extracted stress data from the fault plane and examined the changes in stress values to identify the region where the most significant stress changes occur. The position is coinciding with locations where the thermal front first reaches the fault. We then constructed Mohr circles for these critical areas to assess their proximity to the failure state. The Mohr circle line was determined based on our laboratory data with reduced strength values (GSI = 70).

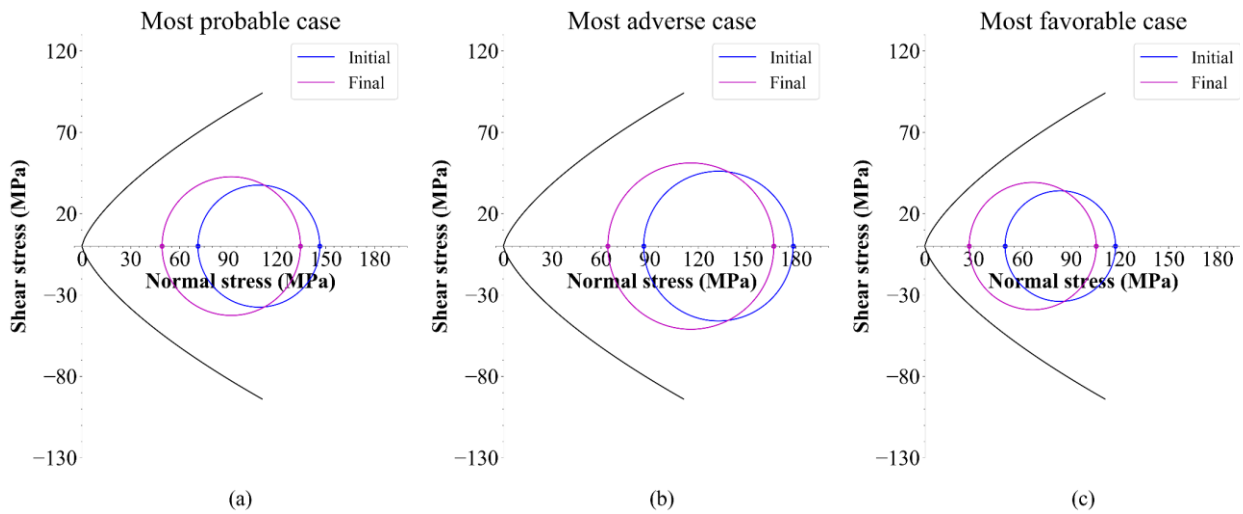

Fig. 14. Mohr circle diagrams illustrating stress conditions during geothermal energy productions.

Fig. 14 reveals that even after extended periods of continuous operation, the system remains far from a failure state at these critical points. Substantial changes in pore pressure and temperature would be required to induce failure. These findings show the inherent stability of the geological formations, confirming their ability to endure additional stress induced by injected fluids. The slip tendency values imply that stress levels generated by the injected fluid remain within the geological formations' tolerance limits. This stability confirms the reservoir's mechanical integrity, indicating its capacity to withstand pressure changes without compromising overall structural stability. However, there remains a possibility that the fault zone could degrade to a lower strength state, potentially leading to injection-induced plastic deformation. Further field investigations, such as image logs, are needed to assess the integrity of the fault zone more thoroughly.

3.8. Conclusions

In this study, we present a comprehensive framework for analyzing efficient geothermal energy extraction systems and predicting the long-term sustainability of a potential geothermal energy reservoir in northern Quebec. Several conclusions can be drawn as the following:

- This differential stress component plays a pivotal role in determining the shear stress resolved on the fault plane, directly influencing the likelihood of fault slippage. A larger differential between $\sigma_{H,max}$ and $\sigma_{h,min}$ increases the resolved shear stress on the fault

plane, thereby enhancing slip tendency and reactivation potential. Our investigation highlights the roles of pore pressure diffusion and thermal stresses in fault reactivation potential. Initially, pore pressure significantly alters the stress state of the fault due to the rapid advance of the fluid front toward the production well compared to the cooling front. However, as the system reaches a pseudo-steady state, the influence of pore pressure diminishes, and thermal stresses become the dominant factor affecting fault behavior.

- The research also highlights the importance of using the IAPWS formulation for determining fluid properties when calculating the slip tendency. In scenarios where fluid properties, such as density and viscosity, vary with temperature and pore pressure, a higher slip tendency value is estimated. This insight emphasizes the necessity of considering variable fluid properties in reservoir simulations for accurate predictions of fault behavior and seismic activity, which is crucial for the design and management of geothermal reservoirs and other subsurface operations.
- Our numerical findings indicate that geothermal reservoirs influenced by thermo-poromechanical effects demonstrate mechanical stability, supporting sustained production and injection activities within the given geological and operational conditions. This study offers some valuable insights into the long-term behavior and safety of geothermal reservoirs, which can provide guidance for future geothermal energy development and management strategies.

4. Chapter 4: Conclusions, limitations, and recommendations for future work

4.1. Additional Discussion

Induced seismicity, a critical consideration in the exploitation of deep geothermal resources, arises due to two main mechanisms: pore pressure diffusion and thermal effects. Pore pressure diffusion occurs when a gradient in pore pressure is created between injection and production wells, driving the movement of fluid through the reservoir's porous rock matrix. This process can destabilize faults by lowering the effective normal stress on the fault planes, a reduction that may lead to fault slip if the stress becomes too low to counteract shear forces. The diffusion mechanism, therefore, poses a potential risk for fault reactivation and seismic events, especially in faulted or fractured reservoirs.

In addition to pore pressure effects, thermal contraction from fluid injection also contributes to induced seismicity. Injected fluid is typically cooler than the reservoir's native fluid, and as it migrates through the reservoir, it induces thermal contraction along its flow path. This contraction effect, which primarily advances through advection with the cooling front, can further contribute to stress redistribution and may prompt fault movement. The combined action of pore pressure changes and thermal contraction highlights the significance of understanding the hydraulic characteristics of the reservoir to anticipate fault reactivation dynamics.

Key hydraulic properties, such as fluid density and viscosity, play a vital role in shaping fluid flow characteristics within the reservoir. These properties directly impact the propagation of pressure waves and temperature changes throughout the rock matrix, dictating the intensity and reach of hydraulic and thermal gradients. Consequently, accurately characterizing these properties is essential for predicting how these gradients will influence the reservoir's stress regime and for mitigating risks associated with induced seismicity in geothermal projects.

4.1.1. The role of hydraulic properties of the (re)injected fluid into the reservoir

The hydraulic properties of the fluid (re)injected into a geothermal reservoir, specifically, its density and viscosity. play a crucial role in shaping the hydraulic and thermal gradients within the system. These fluid properties influence the movement of fluid through the reservoir, affecting interactions with the reservoir rock and subsequently influencing the distribution of pressure and

temperature. Accurate characterization of these parameters is therefore essential for understanding reservoir behavior under variable operational conditions.

To enhance simulation accuracy, precise correlations from the IAPWS-IF97 (International Association for the Properties of Water and Steam Industrial Formulation 1997) standard are used for calculating fluid density (Wagner et al., 2000) and viscosity (Huber et al., 2009) as functions of temperature and pressure. These correlations account for a broad range of temperature and pressure conditions, where deviations from constant fluid properties can lead to significant changes in the reservoir's response.

Monitoring nodes are placed at the injection and production points to track variations in pore pressure and temperature. These nodes, located centrally within the injection and production fractures, allow for real-time data on the evolving pressure conditions over the timeline of reservoir operations. **Fig. 15 (a)** and **(b)** demonstrate these variations in pore pressure, influenced initially by the mass flow rates of injected and extracted fluids, which determine pressure shifts near the injection and production wells.

In simulations where fluid density and viscosity vary with temperature and pressure, pore pressure at the injection well drops significantly over a 12-year fluid circulation period, declining from 55.72 MPa to 48.25 MPa. This pressure reduction results from increased fluid density and viscosity as the injected water cools, causing denser fluid to descend within the reservoir. The cooler water occupies less pore volume per unit mass compared to warmer water, thus creating a localized decrease in pore pressure.

As the injection continues beyond 12.5 years, the density contrast between injected and reservoir fluids begins to diminish as the cold and hot fluids gradually mix, reducing temperature (and thus density) disparities. Over time, continued cold fluid injection further reduces this density contrast across the doublet system.

On the other hand, for simulations with constant viscosity and density, pore pressure increases progressively, reaching a pseudo-steady state after 12.5 years of sustained injection. Here, the pore pressure stabilizes as the changes around the injection wells become constant over time, reflecting a balance in injection and production rates.

At the production well, both cases, variable and constant fluid properties, show an initial drop in pore pressure, followed by stabilization at a pseudo-steady state. This behavior suggests a consistent difference between the flowing wellbore pressure and average reservoir pressure, which persists through the 100-year simulation period, indicating the absence of thermal breakthrough under these operating conditions. This stability underscores the long-term viability of reservoir operation when thermal and hydraulic parameters are effectively managed.

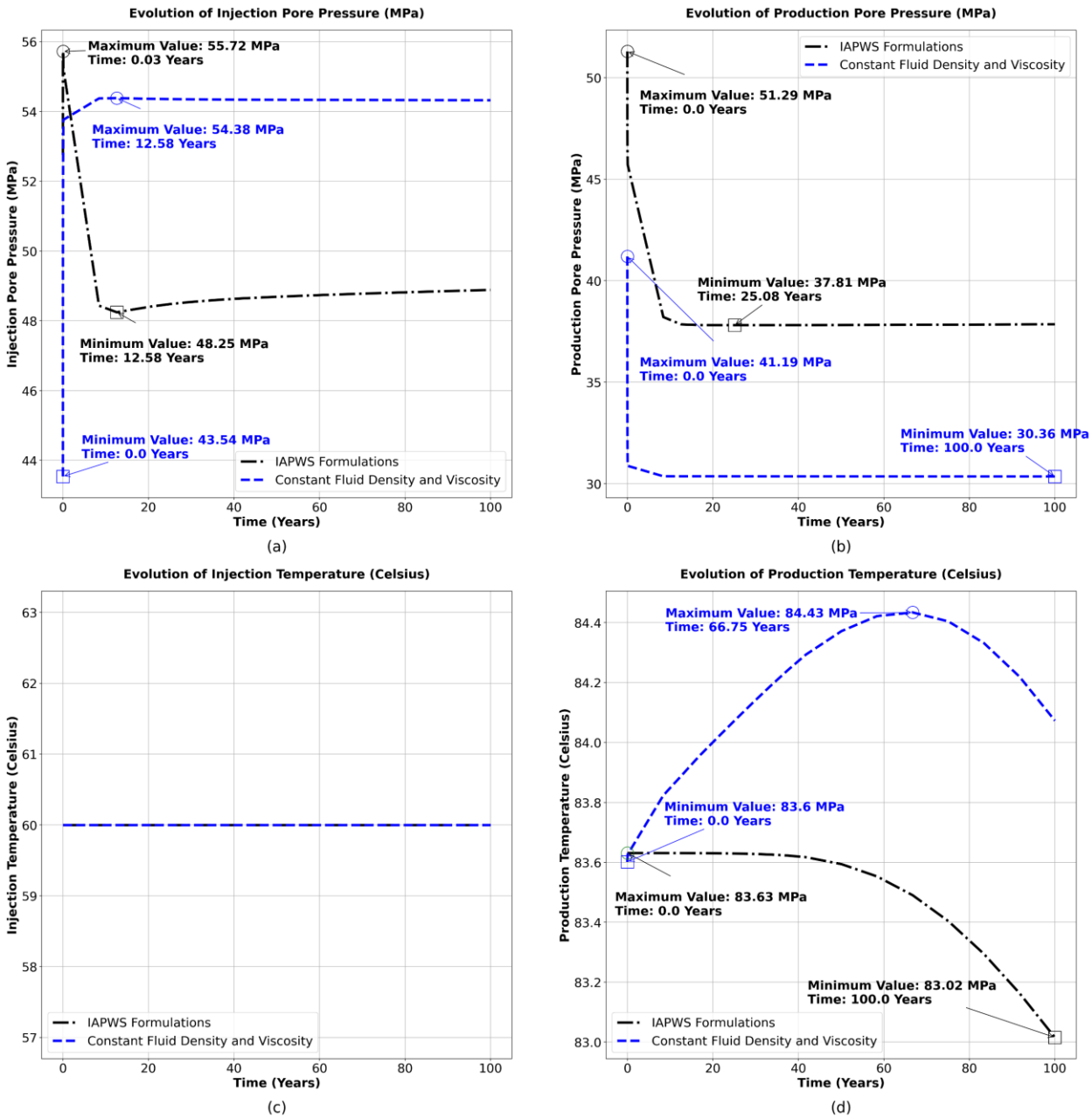

Fig. 15. Temperature and pressure evolutions with time at injection and prediction wells

4.2. Limitations

Slip tendency analysis is a valuable tool for identifying critically stressed faults that may be prone to reactivation. However, the method has inherent uncertainties that limit its predictive accuracy. One significant challenge arises from the difficulty of precisely determining in-situ stress states, particularly the maximum horizontal stress $S_{H,max}$ (Blöcher et al., 2018). This stress component plays a crucial role in slip tendency calculations, yet its estimation remains challenging. Various methods, such as borehole breakout tests, hydraulic fracturing, and focal mechanism solutions from earthquakes, are commonly used to infer stress states. However, each approach carries uncertainties, especially in complex geological settings where stress conditions may be highly variable.

Another key limitation is the uncertainty in defining the friction coefficients of faults. Frictional properties can vary considerably due to differences in fault rock composition, fault gouge characteristics, and the presence of fluids. While laboratory experiments provide useful insights, they often rely on intact rock samples and may not fully capture in-situ conditions. In natural settings, fault zones may exhibit spatially variable friction coefficients along their length and depth, further complicating slip tendency assessments.

Additionally, spatial variations in stress orientation and localized stress rotations around faults introduce further complexity. These factors can lead to deviations in estimated slip tendency values, affecting the overall accuracy of fault reactivation predictions.

Other sources of uncertainty in slip tendency analysis stem from geological and environmental complexities. Fault geometry, including variations in dip, strike, and continuity, significantly influences slip tendency calculations. Moreover, accurate pore pressure data is essential, yet obtaining reliable measurements—particularly at great depths—remains a challenge. Scale effects further contribute to uncertainties, as small-scale heterogeneities in the rock mass, which may influence fault behavior, are often not fully captured in numerical models. Additionally, slip tendency analysis provides a static assessment of fault stability, whereas in reality, stability evolves over time due to factors such as stress corrosion, fluid migration, and ongoing reservoir operations. These dynamic processes introduce further uncertainties into fault reactivation predictions.

While slip tendency analysis offers valuable insights into fault behavior, it is more effective for relative comparisons between faults rather than for making absolute predictions about fault movement. To enhance the reliability of results, slip tendency assessments should be interpreted in conjunction with additional geological and geophysical data. Despite its limitations, this method remains a useful tool for assessing the likelihood of fault reactivation and associated seismic risks.

Another limitation of this study is the assumption that the localized reduction in rock strength around hydraulic fractures is negligible. It is assumed that hydraulic fractures have already formed, the system has stabilized, and geothermal operations proceed under these conditions. This simplification neglects potential long-term weakening effects that may influence reservoirs behavior.

Additionally, fracture aperture is considered constant throughout the simulation. While this assumption could be a limiting factor in certain cases, it is justified here by the continuous operational activity modeled in this study. In reality, fracture aperture may evolve due to stress changes, mineral precipitation, or mechanical deformation, potentially influencing permeability and fluid flow behavior over time.

Finally, the mesh used in this study is first-order tetrahedral elements (4-noded elements). First-order tetrahedral elements are simple and computationally lightweight but suffer from significant limitations in accuracy, geometric fidelity, and efficiency. They are best suited for coarse meshes in problems with mild gradients or where computational cost is critical. For complex geometries, bending, or incompressible materials, second-order tetrahedrons or hexahedral elements are preferred to mitigate locking and improve convergence. These second-order elements should be used alongside with the second-order shape function.

4.3. Concluding remarks

This thesis presents a comprehensive framework for assessing the long-term sustainability and mechanical stability of geothermal reservoirs under the combined influences of thermo-poromechanical effects. By leveraging finite element modeling with realistic variable fluid properties from the IAPWS formulation, this study offers a nuanced understanding of the interplay between pore pressure diffusion, thermal stresses, and reservoir stability in a faulted geothermal system in northern Quebec.

The findings emphasize the critical role of differential stress in determining the resolved shear stress on fault planes. A greater contrast between the principal horizontal stresses ($\sigma_{H,max}$) and ($\sigma_{h,min}$) correlates with increased slip tendency and a higher risk of fault reactivation. During the initial stages of geothermal production, stress changes within fault zones are primarily influenced by pore pressure variations, driven by the rapid movement of the fluid front toward production wells. However, as the system transitions into a pseudo-steady state, the influence of pore pressure diminishes, and thermal stresses, propagated by the advancing cooling front, become the dominant factor governing stress distribution and fault behavior. This shift underscores the long-term significance of thermal effects in shaping reservoir stability, as thermal contraction along fluid pathways alters the shear stress environment.

Additionally, this study highlights the importance of incorporating temperature- and pressure-dependent fluid properties, such as density and viscosity, in reservoir simulations. The use of the IAPWS equations enhances the accuracy of slip tendency predictions, demonstrating that neglecting these variations may lead to an underestimation of fault slip potential and an incomplete assessment of seismic risk. This insight is particularly relevant for subsurface operations, where precise fault behavior forecasting is essential for optimizing geothermal reservoir management and ensuring operational safety.

The numerical results indicate that, under the specified geological and operational conditions, the geothermal reservoir maintains mechanical stability throughout a 100-year operational lifespan. Using a doublet configuration within a faulted reservoir zone, this analysis demonstrates that sustained production and injection can occur without triggering fault reactivation. Even when considering the Hoek-Brown reduction in mechanical properties, slip tendency remains below critical levels. Minimal pore pressure variations further support the conclusion that thermal stresses, rather than fluid pressure, play a predominant role in reservoir stability, particularly in the absence of thermal breakthrough.

Ultimately, this thesis contributes valuable insights into the thermo-poromechanical stability of geothermal reservoirs, with implications for optimizing long-term energy extraction and improving safety in subsurface engineering. The findings and methodologies presented here serve as a reference for future geothermal energy projects, supporting the development of more resilient,

efficient, and sustainable geothermal systems. Furthermore, this work advocates for integrating coupled modeling techniques in subsurface reservoir studies to achieve a more holistic understanding of complex reservoir dynamics. By advancing numerical modeling approaches, this research lays a foundation for future improvements in geothermal energy management and policy development, contributing to the broader goal of sustainable energy transition.

4.4. Recommendations for future work

Currently, the model utilizes the Drucker-Prager plasticity model, where the failure envelope forms a smooth, conical surface in principal stress space. Future studies could explore more complex plasticity models, such as the Mohr-Coulomb model, which features a hexagonal pyramid-shaped failure envelope in principal stress space, or the Hoek-Brown plasticity model, which adopts a non-linear, parabolic failure envelope. This non-linear behavior in the Hoek-Brown model is particularly beneficial for representing rock behavior over a broader range of confining stresses. Notably, while the smooth nature of the Drucker-Prager model can be advantageous for numerical stability, the Hoek-Brown model's non-linearity generally provides a more accurate depiction of rock behavior across varying stress levels (Saiang et al., 2014)

An additional recommendation is the integration of a more detailed mechanical representation of geological discontinuities, such as faults and fractures, using either a discrete approach (e.g., XFEM) or a continuous approach (e.g., phase field modeling). In the model employed in this study, the faults and fractures are modelled as zero thickness elements in which the local fracture mechanics is neglected. Incorporating these advanced descriptions would enable a more precise characterization of deformation dynamics within heterogeneous rocks, particularly the localization and evolution along fault zones. This enhancement would also allow for quantifying feedback mechanisms that affect hydraulic and thermal behaviors within these geological structures. Accurately modeling these processes could improve the ability to forecast environmental impacts, such as induced seismicity, which may result from dynamic fault reactivation during reservoir operations.

In the current study, only a single working fluid, pure water, formulation has been implemented, which is based on (Cooper and Dooley, 2007). However, actual subsurface environments often involve complex fluids, such as gas mixtures or saline water. In particular, CO_2-rich fluids and brine are two common working fluids in geothermal and other subsurface regimes. Future work

could expand the fluid formulation to capture these more realistic fluid compositions, allowing for a more accurate simulation of subsurface thermodynamics.

Finally, adding chemical feedbacks to the model to enable a comprehensive Thermo-Hydro-Mechanical-Chemical (THMC) simulation is recommended. This integration would support more robust modeling of interactions between chemical reactions and the physical processes within the reservoir, enhancing the predictive capabilities of the model in real-world applications.

References

Automatic citation updates are disabled. To see the bibliography, click Refresh in the Zotero tab.

Appendices

Appendix A: Full derivation of the main governing equations

By describing the equation of continuity in terms of the volumetric average for the fluid and solid phase, flow in a porous medium can be described as:

$$\frac{\partial(n\rho_f)}{\partial t} + \nabla \cdot \left(n\rho_f v_f\right) = Q_f \tag{A1}$$

where ρ_f is the density of the fluid phase, n is the porosity, v_f the fluid velocity, Q_f is a sink/source. In a similar way, from the mass balance equation, the following relation is yielded for the solid phase:

$$\frac{\partial((1-n)\rho_S)}{\partial t} + \nabla \cdot \left((1-n)\rho_s v_s\right) = Q_s \tag{A2}$$

where ρ_s is the density of the solid phase, v_s is the solid velocity, an Qs is a sink/source term. For simplicity, the source/sink term for solid (Qs) and fluid phase (Q_f) is considered null hereafter. Form the conservation of momentum of the fluid phase, Darcy's law can be defined in terms of the fluid's velocity relative to the solid's velocity as

$$q_D = n\left(v_f - v_s\right) = -\frac{\kappa}{\mu_f} \cdot \left(\nabla\rho_f - \rho_f g\right) \tag{A3}$$

where q_D is the volumetric flow rate per unit of surface area (Darcy velocity), κ is the permeability tensor, μ_f is the fluid viscosity and g is the gravity vector.

By substituting Eq. (A3) into Equation (A1), the following equation is yielded:

$$\frac{\partial(n\rho_f)}{\partial t} + \nabla.\left(\rho_f q_D\right) + \nabla.\left(n\rho_f v_s\right) = 0 \tag{A4}$$

Eq. (A4), can be reworked by applying the concept of Lagrangian (total) derivative with respect to time for moving fluid[2] and solid[3] while considering $\nabla.\left[(*)v_f\right] = (*)\,\nabla.v_f + \nabla(*).v_f$

$$\frac{n}{\rho_f}\frac{D^f\rho_f}{Dt} + \frac{D^s n}{Dt} + n\nabla \cdot v_s + \nabla \cdot \mathrm{q_D} = 0 \tag{A5}$$

---

[2] $\frac{D^f(*)}{Dt} \equiv \frac{\partial(*)}{\partial t} + \nabla(*) \cdot v_f$

[3] $\frac{D^S(*)}{Dt} \equiv \frac{\partial(*)}{\partial t} + \nabla(*) \cdot v_s$

In a similar way, reworking solid mass balance (Eq. (A2)) the following relation will be obtained:

$$\frac{1-n}{\rho_s}\frac{D^s\rho_s}{Dt} - \frac{D^s n}{Dt} + (1-n)\nabla \cdot v_s = 0 \tag{A6}$$

From Eq. (A6), it can be inferred that when the fluid is injected into or ejected from the pore space, the rock material deforms (contract or dilate). This relation is true if solid skeleton and the pore fluid is considered incompressible.

Reworking Eq. (A6) gives us the evolution of porosity in terms of the Lagrangian derivative with respect to the solid deformation velocity:

$$\frac{D^s n}{Dt} = \frac{(1-n)}{\rho_s}\frac{D^s\rho_s}{Dt} + (1-n)\nabla \cdot v_s \tag{A7}$$

By substituting Eq. (A7) into Eq. (A5), the following relation is derived: (Gao and Ghassemi, 2020)

$$\frac{n}{\rho_f}\frac{D^f\rho_f}{Dt} + \frac{(1-n)}{\rho_s}\frac{D^s\rho_s}{Dt} + \nabla \cdot v_s + \nabla \cdot q_D = 0. \tag{A8}$$

With the use of thermodynamic differentiation, the first term in Eq. (A8) left-hand side can be expressed as the function of fluid pore pressure and temperature as follows:

$$\frac{D^f\rho_f}{Dt} = n\left(\frac{1}{K_f}\frac{D^f\rho_f}{Dt} - \beta_f\frac{D^f T}{Dt}\right), \tag{A9}$$

where $\frac{1}{K_f} = \frac{1}{\rho_f}\left(\frac{\partial(\rho_f)}{\partial P_f}\right)_T$ is the inverse of fluid bulk modulus, and $\beta_f = -\frac{1}{\rho_f}\left(\frac{\partial\rho_f}{\partial T}\right)_{\rho_f}$ is the fluid volumetric thermal expansion coefficient.

The second term in Eq. (A8) can also be reformulated in relation to the problem variables, pore pressure, temperature, and solid skeleton displacements, through the establishment of an appropriate constitutive mechanical model. The linear momentum balance equation for the mixture, expressed in terms of the effective Cauchy stress tensor $\sigma'(x,t)$, is represented as follows:

$$\nabla.\left(\sigma' - \alpha\rho_f\mathbb{I}\right) + \rho_b g = 0 \tag{A10}$$

where $\mathbb{I}$ represents the rank-two identity tensor, $\rho_b = n\rho_f + (1-n)\rho_s$ stands for the bulk density of the fluid-solid mixture, and $\alpha = 1 - k/k_s$ represents the Biot coefficient, where K is the drain

bulk modulus, and K_s is the bulk modulus of the solid grains. The geometrical compatibility condition yields the subsequent strain-displacement relation.

$$\epsilon = \frac{1}{2}(\nabla u + \nabla^T u) = \nabla^s u \tag{A11}$$

The deformation of the solid skeleton is elucidated through thermo-poroelastic response, following Biot's consolidation theory, along with dissipative plastic behavior. For simplification, we focus on small strain conditions in the presentation of the constitutive mechanical model, although the theory has been extended to accommodate finite deformations. Furthermore, considering strain history dependence, the formulation is detailed in an incremental manner. According to Biot's theory, the (effective) stresses are interconnected with elastic strains through the following relationship:

$$\dot{\sigma}' = \dot{\sigma}'_{ij} = \mathbb{C}_{ijkl}\dot{\epsilon}^e_{kl} = \mathbb{C}:\dot{\epsilon}^e. \tag{A12}$$

where $\mathbb{C} = \mathbb{C}_{ijkl} = \lambda\delta_{ij}\delta_{kl} + 2G\delta_{ik}\delta_{jl}$ is a rank-four elastic stiffness tensor with λ and G being the first (volumetric) and second (shear) Lamé moduli, respectively

The stress-strain constitutive relation, Eq. (A12), can be employed to derive an expression for the material derivative of solid density concerning the problem variables, denoted as the second term in Eq. (A8).

$$\frac{(1-n)}{\rho_s}\frac{D^s\rho_s}{Dt} = \frac{(\alpha-n)}{K_s}\frac{D^s p_f}{Dt} - (1-n)\beta_s\frac{D^s T}{Dt} - \frac{1}{K_s}\frac{D^s\bar{\sigma}'}{Dt} \tag{A13}$$

Where $\bar{\sigma}'$ represent mean effective stress, and β_s volumetric thermal expansion coefficient of the solid grain. By substituting Eq. (A9) and Eq. (A13) into Eq. (A8), the gradient of solid deformation velocity can be expressed in terms of the volumetric component of the total strain tensor ($\nabla.v_s = \nabla.\dot{u} = \dot{\epsilon}_{kk}$) as:

$$\frac{n}{K_f}\frac{D^f\rho_f}{Dt} - n\beta_f\frac{D^f T}{Dt} + \frac{(\sigma-n)}{K_s}\frac{D^s\rho_f}{Dt} - (1-n)\beta_s\frac{D^s T}{Dt} - \frac{1}{K_s}\frac{D^s\bar{\sigma}'}{Dt} - \dot{\epsilon}_{kk} + \nabla.q_D = 0 \tag{A14}$$

Utilizing the definition of the total derivative and considering the stress-strain constitutive equation (Eq. (A12)), Eq. (A14) can be reformulated as follows:

$$\frac{1}{M_\mathrm{b}}\frac{\partial p_\mathrm{f}}{\partial t} - \beta_\mathrm{b}\frac{\partial T}{\partial t} - (1-\alpha)\dot{\epsilon}^\mathrm{e}_{kk} + \dot{\epsilon}_{kk} + \nabla\cdot\boldsymbol{q}_\mathrm{D} + \frac{n}{K_\mathrm{f}}\nabla p_\mathrm{f}\cdot\boldsymbol{v}_\mathrm{f} + \frac{(\alpha-n)}{K_\mathrm{s}}\nabla p_\mathrm{f}\cdot\boldsymbol{v}_\mathrm{s} - (n\beta_\mathrm{f}\nabla T\cdot\boldsymbol{v}_\mathrm{f} + (1-n)\beta_\mathrm{s}\nabla T\cdot \boldsymbol{v}_\mathrm{s}) - \frac{1}{K_\mathrm{s}}\nabla\bar{\sigma}'\cdot\boldsymbol{v}_\mathrm{s} = 0 \tag{A15}$$

where $\frac{1}{M_b} = \frac{n}{K_f} + \frac{(\sigma-n)}{K_s}$ represents the specific storage of the porous medium (the reciprocal of the Biot modulus M_b), and $\beta_b = n\beta_f + (1-n)\beta_s$ stands for the bulk volumetric thermal expansion coefficient. Eq. (A15) can be rewritten solely in terms of solid velocity by integrating the momentum balance equation (Eq. (A3)) as follows:

$$\frac{1}{M_\mathrm{b}}\frac{\partial p_\mathrm{f}}{\partial t} - \beta_\mathrm{b}\frac{\partial T}{\partial t} - (1-\alpha)\dot{\epsilon}^\mathrm{e}_{kk} + \dot{\epsilon}_{kk}$$

$$+\nabla\cdot\boldsymbol{q}_\mathrm{D} + \boldsymbol{q}_\mathrm{D}\cdot\left(\frac{1}{K_\mathrm{f}}\nabla p_\mathrm{f} - \beta_\mathrm{f}\nabla T\right)$$

$$+\boldsymbol{v}_\mathrm{s}\cdot\left(\frac{1}{M_\mathrm{b}}\nabla p_\mathrm{f} - \beta_\mathrm{b}\nabla T - \frac{1}{K_\mathrm{s}}\nabla\bar{\sigma}'\right) = 0 \tag{A16}$$

where the final two terms can be regarded as second-order correction terms, accounting for nonlinear advective effects.

To measure permanent (irreversible) material deformation caused by inelastic processes, we employ the concept of eigenstrain (ϵ^*) derived from micromechanics (Mura, 2013). Under the assumption of small strain approximation, the total strain of the material (ϵ) can be decomposed into elastic strain (ϵ^e) and eigenstrain components (ϵ^*) , represented as:

$$\epsilon = \epsilon^e + \epsilon^* \tag{A17}$$

Hence, Eq. (A16) can be expressed as follows:

$$\frac{1}{M_\mathrm{b}}\frac{\partial p_\mathrm{f}}{\partial t} - \beta_\mathrm{b}\frac{\partial T}{\partial t} + \alpha\dot{\epsilon}_{kk} + (1-\alpha)\dot{\epsilon}^*_{kk} + \nabla\cdot\boldsymbol{q}_\mathrm{D} + \boldsymbol{q}_\mathrm{D}\cdot\left(\frac{1}{K_\mathrm{f}}\nabla p_\mathrm{f} - \beta_\mathrm{f}\nabla T\right) + \boldsymbol{v}_\mathrm{s}\cdot\left(\frac{1}{M_\mathrm{b}}\nabla p_\mathrm{f} - \beta_\mathrm{b}\nabla T - \frac{1}{K_\mathrm{s}}\nabla\bar{\sigma}'\right) = 0 \tag{A18}$$

In this study, we specifically address two primary types of residual deformation: thermal expansion and plastic flow, denoted as $\epsilon^* = \epsilon^*_{ij} = \epsilon^{*T}_{ij} + \epsilon^{*p}_{ij} = \epsilon^{*T} + \epsilon^{*p}$. It's worth noting that additional processes such as swelling, fatigue, or phase transformations can be readily integrated into the current formulation.

Thermal strains are linked to deformations caused by temperature variations within the material and can be expressed as follows:

$$\dot{\epsilon}^{*T} = \frac{1}{3}\beta_b \dot{T}\mathbb{I} \tag{A19}$$

where $\dot{T}$ represent the relative temperature rate.

The plastic component of the strain tensor (as defined in Eq. (A17)) is determined by applying the normality rule, represented as:

$$\dot{\boldsymbol{\epsilon}}^{*p} = \dot{\gamma}\frac{\partial \mathcal{Q}}{\partial \boldsymbol{\sigma}'} \tag{A20}$$

where $\dot{\Upsilon} = \dot{\Upsilon}(\sigma', \kappa)$ represents the plastic multiplier, satisfying the classical Kuhn-Tucker conditions ($\dot{\Upsilon} \geq 0,\ F \leq 0,\ \dot{\Upsilon}F = 0$), where $F(\sigma', \kappa)$ is the yield surface. $\mathcal{Q} = \mathcal{Q}(\sigma', \kappa)$ is the plastic potential function indicating the direction of the plastic strain increment, and κ signifies the vector of internal variables influencing the evolution of the yield surface during loading and unloading of the material. Consequently, Eq. (A18) can be expressed for thermal and plastic eigenstrains as follows:

$$\frac{1}{M_\mathrm{b}}\frac{\partial p_\mathrm{f}}{\partial t} - \alpha\beta_\mathrm{b}\frac{\partial T}{\partial t} + \alpha\dot{\epsilon}_{kk} + (1-\alpha)\dot{\epsilon}_{kk}^{*p} + \nabla\cdot\boldsymbol{q}_\mathrm{D} + \boldsymbol{q}_\mathrm{D}\cdot\left(\frac{1}{K_\mathrm{f}}\nabla p_\mathrm{f} - \beta_\mathrm{f}\nabla T\right) + \boldsymbol{v}_\mathrm{s}\cdot\left(\frac{1}{M_\mathrm{b}}\nabla p_\mathrm{f} - \beta_\mathrm{b}\nabla T - \frac{1}{K_\mathrm{S}}\nabla\bar{\sigma}'\right) = 0 \tag{A21}$$

Likewise, the evolution of porosity can be expressed utilizing Eq. (A7) and Eq. (A13) in conjunction with the strain decomposition, stated as:

$$\frac{\partial n}{\partial t} = \frac{(\alpha - n)}{K_\mathrm{s}}\frac{\partial p_\mathrm{f}}{\partial t} - \beta_n\frac{\partial T}{\partial t} + (\alpha - n)\dot{\epsilon}_{kk}$$

$$+(1-\alpha)\dot{\epsilon}_{kk}^{*p} + \boldsymbol{v}_\mathrm{s}\cdot\left(\frac{(\alpha-n)}{K_\mathrm{s}}\nabla p_\mathrm{f} - (1-n)\beta_\mathrm{s}\nabla T - \frac{1}{K_\mathrm{s}}\nabla\bar{\sigma}' - \nabla n\right) \tag{A22}$$

Where $\beta_n = (1-n)\beta_s - (1-\alpha)\beta_b$ represents the volumetric thermal expansion coefficient of the pores, and the final term can be regarded as a second-order effect.

Up to now, constitutive rules for fluid flow and deformation have been derived. The equation for heat transfer within the medium is the final one left. The PDE, explaining heat transfer, is derived from the energy balance equation for the fluid-rock mixture, considering local thermal equilibrium

between the phases and neglecting the dissipation of mechanical energy due to solid phase deformation:

$$T\frac{\partial(\rho c)_b}{\partial t} + (\rho c)_b\frac{\partial T}{\partial t} + \nabla\cdot\left(\rho_f c_f q_D T - \lambda_b \nabla T\right) - \dot{H} = 0 \tag{A23}$$

Where $(\rho c)_b = n\rho_f c_f + (1-n)\rho_s c_s$ represents the bulk specific heat of the porous medium, $\lambda_b = n\lambda_f + (1-n)\lambda_s$ stands for the bulk thermal conductivity, and $\dot{H}$ signifies the rate of energy production. The first term on the left-hand side of Eq. (A23) accounts for secondary, non-Boussinesq dissipative effects linked to the pressure-temperature dependence of bulk storage. Typically, these effects are expressed considering variable fluid and solid density.

$$T\frac{\partial(\rho c)_\mathrm{b}}{\partial t} = (1-n)c_\mathrm{s}T\left(\frac{\rho_\mathrm{s}}{K_\mathrm{s}}\frac{\partial p_\mathrm{f}}{\partial t} - \rho_\mathrm{s}\beta_\mathrm{s}\frac{\partial T}{\partial t}\right) + nc_\mathrm{f}T\left(\frac{\rho_\mathrm{f}}{K_\mathrm{f}}\frac{\partial p_\mathrm{f}}{\partial t} - \rho_\mathrm{f}\beta_\mathrm{f}\frac{\partial T}{\partial t}\right). \tag{A24}$$

Utilizing a conservative finite-element formulation in Eq. (A23) ensures the preservation of fluid enthalpy $(\rho_f c_f T)$ at both element and node levels. This approach guarantees the prevention of accumulating unbalances in intercell fluxes over time, a common issue in non-conservative formulations for convective-type problems (Giudice et al., 1992). The energy conservation equation provided by Eq. (A23) holds for a porous medium in the absence of any thermoelastic coupling. By following Biot's consolidation theory, it becomes feasible to incorporate the effects of solid elastic deformation on the temperature distribution by augmenting Eq. (A23) with a thermoelastic dissipation rate term, as follows:

$$T\frac{\partial(\rho c)_\mathrm{b}}{\partial t} + (\rho c)_\mathrm{b}\frac{\partial T}{\partial t} + T_0\beta_\mathrm{b}\dot{\epsilon}^\mathrm{e}_{kk} + \nabla\cdot(\rho_\mathrm{f}c_\mathrm{f}\boldsymbol{q}_\mathrm{D}T - \lambda_\mathrm{b}\nabla T) - \dot{H} = 0 \tag{A25}$$

where T_0 denotes the absolute temperature of the stress-free porous medium. This equation can be readily adjusted to incorporate additional thermal effects arising from fluid dilation and shear heating stresses.